TESIS DE LA UNIVERSIDAD DE ZARAGOZA

2021 244

Diego Alastruey López

# Towards Functional Preoperative Planning in Orthopaedic Surgery



Director/es
Pérez Ansón, María Ángeles

ISSN 2254-7606

Prensas de la Universidad
Universidad Zaragoza

ISSN 2254-7606

Universidad Zaragoza
1542

Tesis Doctoral

# TOWARDS FUNCTIONAL PREOPERATIVE PLANNING IN ORTHOPAEDIC SURGERY


Autor

Diego Alastruey López

Director/es

Pérez Ansón, María Ángeles

**UNIVERSIDAD DE ZARAGOZA**
**Escuela de Doctorado**


2021

University of Zaragoza

Doctoral Degree in Biomedical Engineering

# Towards Functional Preoperative Planning in Orthopaedic Surgery

*Diego Alastruey López*

Supervisor
Dr. Mª Ángeles Pérez Ansón

# Abstract

Locomotor system surgeries represents more the 20 million interventions per year for the correction of injuries that affect muscles, joints, ligaments, tendons, bones or nerves; elements that form the musculoskeletal system. This kind of biomechanical affections may have several sources, being the main ones traumas, bones and soft tissues degenerative injuries, poor postural or motor habits and those of congenital source.

The use of current technologies in the correction process for these injuries is part of the day-to-day in the operating rooms and the monitoring of patients. However, the use of computational tools that allow preoperative planning is still far from being part of the preoperative evaluation process in this kind of injuries. For this reason, the main goal of this thesis consists in demonstrating the viability of the use of computational tools in the preoperative planning of different orthopaedic surgeries.

Among the most common surgeries, most of them focus in the lower body joints of the human anatomy. For this reason, this work will focus in the analysis of different surgeries whose purpose is to solve injuries in the main joints of the lower body: lumbosacral region, hip, knee and ankle.

Some of the most commonly used computational tools, and whose capability in different fields has been widely proven, were used in order to be able of performing the analysis of these surgeries. 3D reconstruction has been used for obtaining anatomical models in which the viability of the surgeries could be verified. These reconstructions are based on the medical images obtained through Computerized Tomography (CT) or Magnetic Resonance Imaging (RMI). Images from RMI allow differentiating all the tissues of the anatomy, including soft ones such as tendons and cartilages; while CT scans make easier the bones differentiation. This last procedure is the most commonly used in diagnoses. For their analysis and reconstruction software Mimics v 20.0 and 3-Matic 11.0 (Materialise NV, Leuven, Belgium) were used. As alternative for the models generation when the necessary images for the reconstruction are not available or when flexibility is required for these models, modelling in the Finite Element Analysis software Abaqus/CAE v.6.14 (Dassault Syst'emes, Suresnes, France) was used. This software was also used for the simulation of the effects of the different surgeries in the interest region. In order to perform the simulations, those parameters, elements and conditions necessary to represent the characteristics of each surgery were included. Finally, for those situations requiring data analysis, *machine learning* technologies were used. The selected solution for these cases were Artificial Neural Networks (ANN). These networks were developed using the software MATLAB R2018b (MathWorks, Massachusetts, USA).

The study of the knee joint focuses in one of the key ligaments for the patellar stability and which, however, is one of the least analysed so far, the medial patellofemoral ligament. The reconstruction of this ligament is the main clinical solution for solving this instability and different surgeries used for that purpose have

been analysed through the development of a finite element parametric model that allows their simulation. In this model adapting knee geometry is possible so that those conditions that can affect the stability of the patella, such as trochlear dysplasia or patella alta, can be simulated.

The study of the lumbosacral region focuses in the analysis of different possible configurations for spine fusion surgeries. The analyses focused in the pedicle screws fixation and the influence of polymethyl methacrylate (PMMA) as fixation element in the vertebrae. To do this, osseous models for different patients that required this kind of intervention were reconstructed. The different configurations considered were simulated on these models through finite element analysis comparing their behaviour.

In the case of the hip, the study focuses in the analysis of the total hip arthroplasty, which implies replacing the anatomical joint by a prosthesis, usually made of titanium. When this kind of surgery is performed, it is common for later issues arising from the arrangement of the prosthesis and which can lead to impingement between its components and, on some occasions, their dislocation. This happens when the range of movement of the joint is limited. This kind of events are more common when the external extension (EE) or internal rotation (IR) movements of the leg are performed. The study was developed with the goal of elaborating a computational tool able to predict the impingement and dislocation based on the diameter of the head of the femur and the anteversion and abduction angles. To do this, artificial neural networks (ANN) were used. An independent network was configured for each movement (EE and IR) and for each possible event (impingement and dislocation), so that four completely independent networks. For the training and the first testing of the networks, a parametric finite element model of the hip was used; with which different simulations were performed determining the range of movement for each case. Finally, the networks were validated again with the use of data proceeding from patients that suffered dislocation after going through this kind of surgery.

Finally, the study of the ankle region focused in the ankle syndesmosis injury. This kind of injuries implies the tear of some ligaments that connect the main bones of the joint (tibia, fibula and talus) together with part of the intraosseous membrane, which extends along the tibia and fibula linking both bones. When this kind of injuries happens, it is necessary to resort to the inclusion of elements that fix the joint and prevent the bones distance. The most common methods, which focus this analysis, include the screws fixation and the suture button fixation. In order to carry out an analysis that allows comparing the effectiveness and incidence of this kind of surgeries, a 3D reconstruction of the joint from a patient that suffered this kind of injury was used. With this geometrical model, different finite element models including each of the considered alternatives were developed. The simulations of these models, together with the injured and anatomical situations, allowed an approximation of the surgical solution that better restores the initial healthy state of the affected region.

# Resumen

Las cirugías del aparato locomotor suponen más de 20 millones de intervenciones anuales para la corrección de lesiones que afectan a músculos, articulaciones, ligamentos, tendones, huesos o nervios; elementos que conforman el sistema musculoesquelético. Este tipo de afecciones de la biomecánica pueden tener diversos orígenes; siendo los principales los traumatismos, las lesiones degenerativas en huesos y tejidos blandos, los malos hábitos posturales o motores, y los de origen congénito.

El uso de las tecnologías actuales en los procesos de corrección de estas afecciones forma parte del día a día en los quirófanos y en la monitorización de los pacientes. Sin embargo, el uso de técnicas computacionales que permitan la preparación de las intervenciones quirúrgicas antes de proceder con la cirugía están todavía lejos de formar parte del proceso de evaluación preoperatoria en este tipo de lesiones. Por este motivo, el objetivo principal de esta tesis consiste en demostrar la viabilidad del uso de herramientas computacionales en la planificación preoperatoria de diferentes cirugías ortopédicas.

Entre los tipos de cirugías más comunes, la mayor parte de ellas se centran en las articulaciones del tren inferior de la anatomía humana. Por este motivo, este trabajo se centrará en el análisis de diferentes cirugías cuya finalidad es solucionar lesiones en las principales articulaciones del tren inferior: región sacrolumbar, cadera, rodilla y tobillo.

Para poder realizar el análisis de estas cirugías se hizo uso de algunas de las herramientas computacionales más usadas habitualmente y cuya capacidad en diversos ámbitos ha sido comprobada. Se ha utilizado la reconstrucción 3D para la obtención de modelos anatómicos sobre los que comprobar la viabilidad de las cirugías. Estas reconstrucciones se basan en las imágenes médicas obtenidas mediante Tomografia Axial Computerizada (TAC) o Resonancia Magnética (RM). Las imágenes procedentes de RM permiten diferenciar todos los tejidos de la anatomía, incluyendo los blandos tales como tendones o cartílagos; mientras que los TAC facilitan la diferenciación de los huesos. Esta última es la prueba más habitual en los diagnósticos. Para su análisis y reconstrucción se hizo uso de los software Mimics v 20.0 y 3-matic 11.0 (Materialise NV, Leuven, Belgium). Como alternativa para la generación de los modelos cuando no se dispone de las imágenes necesarias para realizar la reconstrucción o cuando se requiere dotar de flexibilidad a estos modelos, se recurrió al modelado en el software de análisis por elementos finitos Abaqus/CAE v.6.14 (Dassault Systèmes, Suresnes, France). Dicho software fue además utilizado para la simulación del efecto de las diferentes cirugías sobre la región de interés. Para resalizar las simulaciones, se incluyeron en los modelos aquellos parámetros, elementos y condiciones necesarios para poder representar las caraterísticas propias de cada cirugía. Finalmente, para aquellas situaciones que requerían del análisis de datos se hizo uso de tecnologías de *machine learning*. La solución seleccionada para estos casos fueron las redes neuronales artificiales (ANN). Dichas redes se desarrollaron

haciendo uso del software MATLAB R2018b (MathWorks, Massachusetts, USA).

El estudio de la rodilla se centra en uno de los ligamentos clave en la estabilidad de la rótula y que, sin embargo, es uno de los menos analizados hasta ahora, el ligamento medial patelofemoral. La reconstrucción de este ligamento es la principal solución clínica para solventar esta inestabilidad y diferentes cirugías utilizadas para dicho fin han sido analizadas mediante el desarrollo de un modelo paramétrico en elementos finitos que permita su simulación. En este modelo es posible adaptar la geometría de la rodilla de forma que se puedan simular diferentes condiciones que pueden afectar a la estabilidad de la rótula, tales como la displasia troclear y la patella alta.

El estudio de la región sacrolumbar se centra en el análisis de diferentes posibles configuraciones para las cirugías de fusión vertebral. El análisis se centró en la fijación con tornillos y la influencia del Polimetimetacrilato (PMMA) como elemento de fijación en las vértebras. Para ello, se reconstruyó el modelo óseo de diferentes pacientes que necesitaron este tipo de intervención. Sobre estos modelos se simularon mediante elementos finitos las diferentes configuraciones consideradas de forma que se pudiera comparar su comportamiento en diferentes casos.

En el caso de la cadera, el estudio se centra en el análisis de la artroplastia total de cadera, que implica el reemplazo de la articulación anatómica por una prótesis habitualmente de titanio. Cuando este tipo de cirugías es realizado, es común que surjan posteriormente problemas derivados de la disposición de la prótesis y que pueden llevar al pinzamiento entre sus componentes y, en algunas ocasiones, su dislocación. Esto ocurre cuando el rango de movimiento de la articulación es reducido. Este tipo de sucesos son más comunes cuando se realizan los movimientos de extensión externa (EE) o de rotación interna (RI) de la extremidad. El estudio se desarrolló con el objetivo de elaborar una herramienta computacional capaz de predecir este choque y dislocación basándose en el diámetro de la cabeza del femur y de los ángulos de abducción y anteversión. Para ello, se recurrió al uso de redes neuronales artificales (ANN). Se configuró una red independiente para cada movimiento (EE y RI) y cada posible evento (pinzamiento y dislocación), de forma que se obtuvieron cuatro redes completamente independientes. Para el entrenamiento y primer testeo de las redes se recurrió a un modelo paramétrico en elementos finitos de la prótesis con el que se realizaron diferentes simulaciones determinando el rango de movimiento para cada caso. Finalmente, las redes fueron de nuevo validadas con el uso de datos procedentes de pacientes que sufrieron dislocación tras ser sometidos a este tipo de cirugías.

Finalmente, el estudio de la región del tobillo se centró en la lesión de la sindesmosis del tobillo. Este tipo de lesiones implica la rotura de algunos de los ligamentos que unen los principales huesos de esta articulación (tibia, peroné y astrágalo) junto con parte de la membrana intraósea, que se extiende a lo largo de la tibia y el peroné ligando ambos huesos. Cuando se produce este tipo de lesiones, es necesario recurrir a la inclusión de elementos que fijen la articulación y prevengan la separación de los huesos. Los métodos más comunes y que centran este análisis comprenden la fijación con tornillos y la fijación mediante botón de sutura. Para poder realizar un análisis que permita comparar la efectividad y incidencia de este tipo de cirugías se recurrió a la reconstruccción 3D de la articulación de un paciente que sufrió este tipo de lesión. Con este modelo geométrico, se procedió al desarrollo de diferentes modelos en elementos finitos que incluyeran cada una de las alternativas consideradas. Las simulaciones de estos modelos junto a las situaciones anatómicas y lesionadas, permitió hacer una aproximación sobre la solución quirúrgica que mejor restablece el estado incial sano de la región afectada.

# Contents

# List of Figures

# List of Tables

# Chapter 1

# Introduction

Orthopaedic surgeries are one of the most common type of surgeries performed annually worldwide. These surgeries try to solve biomechanical issues or injuries caused as a consequence of a wide variety of sources such as ageing, trauma impacts, physical efforts, repetitive movements or malformations among others. Approximately 22.3 millions of these kind of surgeries were performed in 2017 [9], being the most common procedures:

- Anterior Cruciate Ligament (ACL) Repair
- Knee Replacement
- Hip Replacement
- Shoulder Replacement
- Spinal Surgeries
- Knee/Shoulder Arthroscopy
- Ankle Repair
- Joint Fusion
- Trigger Finger Release

Due to the continuous evolution of medical resources and technologies, surgical procedures are susceptible of changing and include alternative techniques or new elements. Usually, most common surgeries have a *gold standard* procedure which has been assumed as the most suitable technique for those situations. On the other hand, procedures that are not so common use to present different accepted alternatives but without a clear consensus about the most suitable one.

However, in both cases, specially in the less common injuries, it is very difficult to evaluate the effects of a surgical procedure in the medium or long term after the surgery. This situation can cause difficulties to implement new procedures or technologies due to the lack of evidences and the doubts that this can cause about their real effectiveness. Also, in most orthopaedic cases not only the region where the surgery was performed is affected, but the rest of the structure of the joint, close areas or even the whole biomechanical structure of the body can suffer any alteration that leads to injuries only perceptible long time after the procedure. To all these variables it is necessary to add the fact that patients daily activities, once the recovery

time is finished, can cause additional injuries that may be or not related with the surgery they went through.

To avoid the latest and improve the surgery success, preoperative planning should be considered, defining personalised guidelines for every patient, attending to their unique conditions. Computational tools may potentially help clinicians in the design and planning phases of the most adequate procedure.

## 1.1. Computational biomechanics in surgery preoperative planning

Computational simulations have shown to be a powerful tool for the analysis of different situations prior to developing any kind of project. Computational models can provide information of very different situations depending on the kind of tool implied. Finite Element Analyses (FEA), artificial networks (ANN), mathematical models and a large etcetera of technologies are well known for their high performance in developing predictions of behaviours and providing reliable information at low economical cost when simulation conditions are well defined [10, 13, 162] .

This kind of analyses are widely required and are an essential part in the main fields of industry such as the aerodynamic or high impact simulation for vehicles [173, 177], the computational simulation of fluids behaviour [85, 96], the different factors affecting buildings constructions [14, 15, 110] or improving manufacturing processes [25] among others. Even these tools are also widely known by their performance in some medical fields as the image analysis for disease diagnosis [90, 166], biomechanical analyses and bone remodelling studies [60, 117] or cell migration studies [66, 151].

Surgeries involving biomechanical injuries that commonly affect the structural basis of the human anatomy, generally bones and ligaments, imply two key factors that require accuracy and effectiveness. The first of them is the need for solving an injury that influences the daily life of the patient and requires a speedy recovery. The second one is that in most cases, the long-term effects of the surgical procedure cannot be analysed until several years later. At this point, if the surgery has failed and the patient has not reported any issue, it is very difficult to perform another surgery that can solve this condition, specially when tissue degeneration or articular instability has been induced. However, the use of computational biomechanics for orthopaedic preoperative planning is not yet established as part of the daily methodology in the preparation of clinical interventions.

## 1.2. Aim

As it could be observed in the list of the common orthopaedic surgeries, most of these surgical procedures are performed in the lower body, that is, the region of the human body that goes from the lumbar region to the feet and whose main joints include lumbosacral union, hip, knee and ankle. Only shoulder replacement and trigger finger release (usually made in hands) are out of this region (joint fusion is also common in lumbosacral region and toes).

From a biomechanical point of view these joints are the ones that suffer more efforts in the daily life of any person. They bear the weight of the body in different steps and provide stability to the whole anatomical structure. Also, postural habits have a critical influence in the appearance of injuries derived from a load unbalance unwittingly maintained that can cause deviations or tissue degradations among others.

**The main goal of this thesis is to demonstrate the viability of using computational tools in preoperative planning of different orthopaedic surgeries**. For that purpose, this work will analyse surgeries performed to solve different orthopaedic medical conditions in the lower body joints (Lumbosacral spine, hip, knee and ankle) making use of some of the main technologies available nowadays.

Real patients conditions solved by clinicians without the use of computational tools will be used for the reconstruction of the issue and analysed with the help of different techniques in order to show the benefits of these powerful tools in the criteria selection for surgical procedures.

Following previous motivation, four specific objectives are defined depending on unsolved problems in preoperative planning of orthopaedic surgeries of the lower extremities joints. The motivations and the goals related to each of these specific objectives are presented below.

### 1.2.1. Preoperative planning for Medial Patellofemoral Ligament (MPFL) reconstruction

Clinical interest in comparing different surgical techniques for the reconstruction of one of the key elements in the lateral patellar stability, the Medial Patellofemoral ligament (MPFL), will focus this first analysis. Finite Element Analysis (FEA) will be used for the simulation of the loads distribution in one of the most complex joints in the human body, the knee.

For this aim, a FE parametric model will be developed in order to be able of adapting its geometry to each unique patient anatomy. The model will be created based in a real patient 3D reconstruction and ligaments will be included based in clinical previous studies. The model will be validated using real patients and the results will focus in those considered key points by the surgeons: patellar contact pressure and ligaments stress.

### 1.2.2. Preoperative planning for spine fusion

The comparison of different spine fusion techniques used to correct injuries affecting the lumbosacral regions will be the main motivation of this second objective. Surgical alternatives for cements and screws inclusion in spine fusion will be analysed in different anatomical geometric models. Continuing with the technology of the previous objective, FEA will be used for analysing the anatomy of patients that required surgical treatment and compare the solution proposed by the clinicians

with other similar alternatives. In this case, real patient 3D reconstructions of their lumbosacral regions will be modelled including some assumptions for the rest of anatomical elements.

### 1.2.3. Preoperative planning for preventing hip prosthesis dislocation

Due to the reported cases of dislocation after Total Hip Arthroplasty (THA) procedures, the next objective will be to develop a computational tool able to predict the Range of Movement (ROM) for dislocation and impingement in THA.

Artificial Neural Networks (ANNs) will be used for developing a preoperative computational tool able to predict this ROM based on three main parameters in the THA: prosthesis head size, adduction angle and abduction angle. These variables will be the input of this tool. In order to obtain the data required for the ANNs configuration, a parametric FE model of the proximal femur is created and multiple FE simulations are performed defining the ROM for different situations and creating an initial database. The use of this kind of tool may help in making a decision about the positioning of the prosthesis prior to the surgical procedure. Also, this computational tool could help in predicting what patients of those who already had their hip replaced are susceptible of suffering future dislocation. The computational tool created will be validated with few real cases that had undergone hip dislocation.

### 1.2.4. Preoperative planning for syndesmotic injury correction

Nowadays, syndesmotic injuries are one of the most under-diagnosed injuries [22, 168]. They are normally hidden by other more important injuries. However, it is an injury that requires specific surgery for its adequate correction and avoidance of future issues in the affected region.

The specific objective here is the simulation of the main surgical techniques for syndesmosis recovery (screws and suture button inclusion) and its comparison with the healthy and injured states when a patient gives a step forward. For that purpose, the simulations will be performed using FEA on an anatomical ankle joint reconstruction. This way, the behaviour of this joint will be analysed with the application of the loads involved in this movement over the tibial bone.

## 1.3. Thesis Outline

Chapter 2 includes the development of a parametric finite element model of the knee, the simulation and comparison of different static and dynamic MPFL reconstruction techniques, and the validation of the model with real patients. Furthermore, MPFL graft alternatives and knee geometry influence in the success of the surgeries are also analysed.

Chapter 3 presents the finite element analysis and the comparison of different cement and screws inclusion alternatives in lumbosacral spine fusion. This work shows the 3D reconstruction of the low back anatomy of five patients and their finite elements simulations were the surgical alternatives are analysed.

Chapter 4 describes the process for configuring, training and testing Artificial Neural Networks (ANNs) that may help in predicting the Range of Movement (ROM) after Total Hip Arthroplasty (THA) for two main movements: external extension and internal rotation. Two ANNs are included for each movement, predicting the ROM until impingement and dislocation.

Chapter 5 analyses different surgical solutions, screws fixation or suture button inclusion, for the ankle syndesmosis injury based in the anatomical 3D reconstruction of a patient. The surgical alternatives as well as the healthy and injury state of the joint are simulated using finite elements analyses.

Chapter 6 summarises the global conclusions of the thesis, the original contributions and the future lines for the different works developed in the previous chapters.

# Chapter 2

# Preoperative planning for Medial Patellofemoral Ligament (MPFL) reconstruction

This first chapter will focus in the study of the reconstruction of the Medial Patellofemoral Ligament (MPFL), one of the least studied ligaments in the knee joint that, when damaged, causes instability in the patellar bone and can lead to its dislocation.

Due to clinicians interest in analysing the mid-long term effect on the knee of different techniques for the reconstruction of this ligament, the main objective of the study will be the analysis of different reconstruction techniques and their comparison. The study will consider three static and two dynamic surgical alternatives, as well as the native state of the knee for be taken as a reference. The surgical techniques will need to be analysed in those positions of clinical interest following clinicians previous studies [132].

This work will also include other objectives for its completion. Surgical techniques can be performed using different kinds of graft whose properties are supposed to be relevant in the surgery success. Some of the graft material alternatives will need to be analysed. Also, the geometry of the knee is extremely irregular and it significantly changes between patients. Thus, the work requires a tool able to simulate different geometries without high computational cost. For this reason, finite element analysis (FEA) will be used for the modelling and simulation of the different techniques. In order to obtain a tool that can be adapted to different surgeries and patient characteristics, this work will include developing a functional FE parametric model of the knee. The analysis will focus in the patellar cartilage contact pressure and the main ligaments stress. This model will need to be validated, so some real patients clinical cases will be also analysed in order to compare the information provided by the model and the real situation of each case.

Finally, anatomical abnormalities affecting the knee joint in terms of geometry (as trochlear dysplasia) and relative bone positioning (as occurs in patella alta) will be also analysed as a source of symptomatology that can lead to the injury in the knee joint. The parametric model will need to be able of adapting its geometry to these circumstances.

## 2.1. Biomechanics of the knee joint

Before describing the injury of this ligament and the surgical techniques that will be analysed for its reconstruction, it is necessary to define the anatomy of the knee joint along with the main elements that must be considered for these analyses.

Knee joint is one of the most complex and important joints inside the human body. This joint does not only have a main role in the motion of our body, but also stabilising the whole biomechanical structure and bearing our body weight. For this reason, knees are joints susceptible for suffering a wide range of injuries.

This joint is mainly composed by three bones: femur, tibia and patella (*Figure 2.1*); and stabilised in the contact between femur and tibia by the menisci. Thus, this joint can be described as the union of two different joints: the tibiofemoral joint (joint between femur and tibia) and the patellofemoral joint (joint between patella and femur).

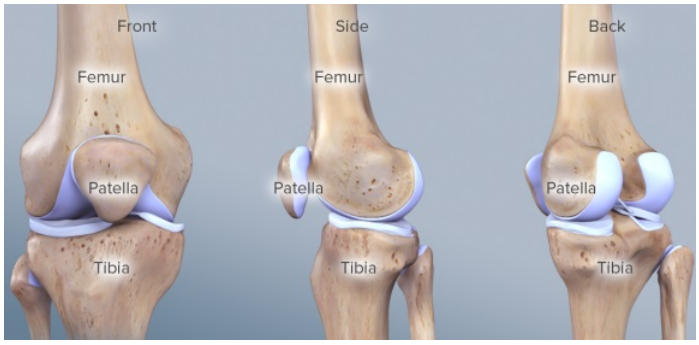


Figure 2.1: Main structure of the knee joint [1].

*Tibiofemoral joint (Figure 2.1)*: This joint forms the main structure of the knee. It is the responsible of the loads transmission thanks to the contact of the femoral condyles and the tibia through the menisci. Both bones are attached by two groups of ligaments, the lateral ligaments (Lateral Collateral Ligament and Medial Collateral Ligament) and the internal ligaments (Anterior Cruciate Ligament and Posterior Cruciate Ligament. These ligaments are responsible of avoiding the dislocation of this joint (*Figure 2.2*).

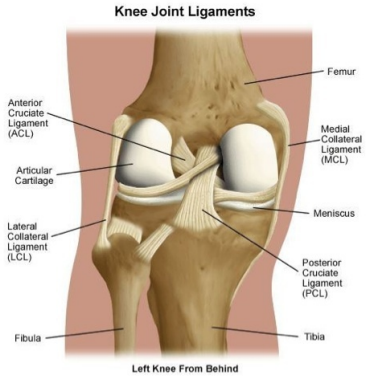


Figure 2.2: Tibiofemoral joint structure [2].

*Patellofemoral joint (Figure 2.1)*: this joint is defined by the contact between the patella and the femur, specifically in the throclear region. When in leg extended situation, petella position is mainly fixed by the action of the Quadriceps Femoris (QF) and its insertion in the tibia through the Patellar Tendon (PT). While the joint tilts, the lateral displacement and the rotation are stabilised by the Lateral Retinaculum (LR), the Medial Patellofemoral Ligament (MPFL) and, to a lesser extent, by the Medial Patellomeniscal Ligament (MPML), the Medial Patellotibial Ligament (MPTL) and the Lateral Patellotibial Ligament (LPTL). (*Figure 2.3*)

**Patellofemoral Joint**

In the Patellofemoral Joint (PFJ), patella position and stability is determined by the action of the different ligaments and muscles (through their tendons) that have an insertion point in this bone (*Figure 2.3*).

The muscles with insertion in this joint are the group that form the quadriceps femoris, responsible of the leg extension. Quadriceps femoris consists of four muscles: the rectus femoris (RF), the only muscle of this group that goes through two joints (hip and knee) and the vastus muscles: vastus medialis (VM), vastus lateralis (VL) and vastus intermedius (VI). Its insertion is located in the top of the patella and follows until the tibia through the Patellar Tendon (PT) (*Figure 2.3*).

Lateral position of the patella is determined by the action of the lateral ligaments. The MPFL and the LR connect the patella and the femoral trochlea through the medial and the lateral section, while the MPML connects the bottom of the patella and the tibia (*Figure 2.3*).

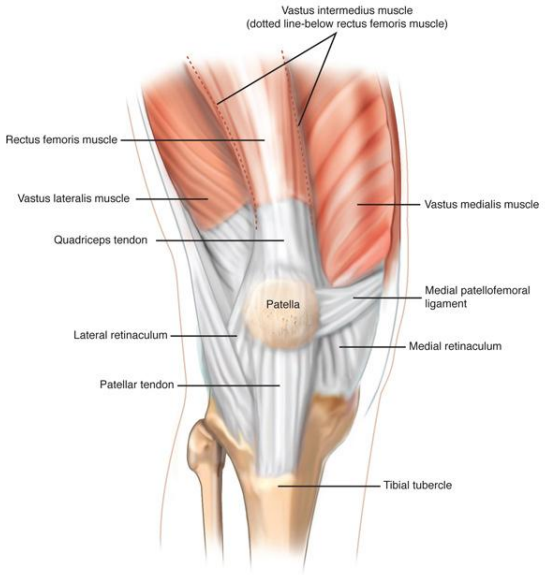


Figure 2.3: Superficial knee joint muscles and ligaments [3].

## 2.2. Clinical Interest

Currently, medial patellofemoral ligament reconstruction (MPFLr) is the *gold standard* in chronic lateral patellar instability (CLPI) surgery. It is typically performed whenever there have been at least two previous episodes of lateral patellar dislocation [131, 132]. Different surgical techniques with different attachment points, different types of grafts and different configurations for the reconstruction have been described for MPFLr. Each one has good short-term clinical results [53, 57, 131, 156, 172]. However, there is uncertainty regarding the long-term outcome of these MPFL reconstructions techniques. To classify a surgical technique for MPFLr as being effective, it is not enough for the instability and pain to disappear. For a surgical technique to be considered effective, new problems like chondropathy or patellofemoral osteoarthritis (PFOA), should never be caused. These problems might be the consequence of the increase in the patellofemoral contact pressure secondary to an inadequate MPFLr [42, 130, 148, 149], which is clinically relevant because surgery for lateral patellar instability is generally performed in young individuals. Moreover, the development of symptomatic PFOA in young persons does not currently have a good solution. In an ideal MPFLr, the graft should be tense at 0–30° of knee flexion. Beyond 30°, the graft should be loose [132]. All the other parameters should be considered inadequate [132]. Given that in the daily clinical practice many MPFL reconstructions with a clearly incorrect femoral fixation point can be seen, we must evaluate not only the correct reconstructions but also the clearly incorrect ones.

Many surgical techniques using various types of grafts (autografts, allografts, or synthetic) and fixation techniques have so far been described. Based on the fixation technique used, there are two types of MPFLr, static and dynamic [11, 12, 57, 87, 100, 118, 131]. A static MPFLr, which involves an anatomic femoral bone attachment and a patellar bone attachment, is currently more common [131]. In the less used dynamic reconstruction, only one of the graft's extremities is fixed to bone, while the other one is fixed to soft tissues. This type of reconstruction is therefore a less rigid reconstruction [11, 12, 57, 87, 100, 118]. Static and dynamic reconstructions show MPFL isometry between 0º and 90º [118, 132]. In a static/anatomic MPFLr, the graft is isometric in all the cases between 0º and 30º of knee flexion [132]. In 83% of cases, the graft is isometric from 0º to 60º [132]. Beyond 60º of knee flexion, the MPFL becomes progressively lax and isometry is lost [132]. Regarding isometry, a ligament is considered isometric when there is less than 5 mm of length change throughout the entire range of motion [147].

Both static and dynamic reconstruction techniques have been shown to yield satisfactory clinical results in the short and intermediate terms [12, 57, 100, 131]. However, what is not known is whether one type of MPFLr is more likely than the other to lead to the development of patellofemoral osteoarthritis (PFOA) in the long term. We hypothesized that a static anatomic reconstruction might generate greater patellar contact pressure than a dynamic reconstruction and would therefore increase the risk of PFOA in the long term. Nevertheless, from a functional standpoint, a dynamic reconstruction would enable behaviour that is more like that of a native MPFL than a static reconstruction. In a dynamic MPFLr, the fixation point gives a bit before the graft starts to stretch when the patella moves laterally. Therefore, the dynamic MPFLr allows for patellar contact pressures that are closer to those generated in a native knee. After the fixation of the MPFLr, it is important to verify that the patella can still be manually lateralized in full extension some 10 mm, to avoid any over-constraint, but with a firm endpoint. To avoid excessive tension on the

graft when anatomic/static MPFLr is performed, the graft has to be fixed at 30º of knee flexion as it is at this angle that the distance between the femoral and patellar attachments points is the largest [132].

An effective way to evaluate patellofemoral contact pressure throughout the range of motion of the knee after MPFLr is by using the finite element methodology (FEM) [42, 171, 41, 42, 143]. Moreover, this technology also enables us to evaluate the kinematic behaviour of the MPFL graft and maximum MPFL-graft stress, that is, the tension that the graft can withstand before breaking, in all knee flexion-extension positions. Therefore, the first objective was to create a parametric model of the patellofemoral joint (PFJ) where the joint geometry is simplified and can be meshed by means of automatic mesh generation programs with suitable finite element aspect ratios for all meshes. Additionally, another objective was that the parametric model would enable a surgeon to simulate different types of surgical techniques for MPFLr. It is hypothesized that this model would allow to evaluate patellofemoral contact pressure and the maximum MPFL-graft stress in each specific reconstruction at different knee flexion-extension angles. And finally, the last objective was to determine the negative theoretical effects (patellofemoral contact pressure and the maximum MPFL-graft stress) on the PFJ in each type of MPFLr. This negative effect could be related to long-term deterioration of the PFJ.

## 2.3. Material and Methods

### 2.3.1. Parametric finite element model of the patellofemoral joint

From a previous study [132], high spatial resolution Computerized Tomography (CT) data were available from 24 knees of patients with chronic lateral patellar instability. Images were acquired with a 64-detector Multi-Detector CT system (Philips Medical Systems, Best, the Netherlands) at the highest spatial resolution, without slice interpolation ($0.255 \times 0.255 \times 0.672$ mm$^3$). An iterative thresholding scheme was used to extract bones from the imaging data, and triangulated surfaces were defined to describe the outer surfaces (Mimics v. 20, Materialise NV, Leuven, Belgium). The main characteristics and dimensions considered for the parametric model were measured as a reference (femur and patella bone dimensions) from the 24 knees [132].

| Femoral geometrical characteristics | | | | | | | | |
|---|---|---|---|---|---|---|---|---|
| Width | Width 2 | Width 3 | Length | Length 2 | Length 3 | Medial radius | Lateral radius | Posterior radius |
| 72.28 ± 8.92 | 54.00 ± 5.83 | 39.01 ± 3.85 | 47.71 ± 5.21 | 33.99 ± 3.40 | 28.44 ± 3.00 | 28.91 ± 4.75 | 26.09 ± 4.21 | 13.84 ± 2.71 |
| Patella geometrical characteristics | | | | | | | | |
| Radius | | Curvature radius | | Height | | | | |
| 20.26 ± 6.24 | | 45.49 ± 3.31 | | 19.09 ± 2.46 | | | | |

Table 2.1: Mean values (mm) and standard deviation (±) (mm) of the geometrical parameters defining the parametric PFJ measured on the 24 knees [132].

Knee geometry was simplified to construct a 3D parametric model that achieved nearly anatomical geometry with variable parameters (i.e., trochlear dysplasia, patellar width, patellar diameters, geometry of the patella). The parameters were measured from CT scans both on the axial plane and by using a multi-planar reformatting (MPR) technique. Patients were pathological. Therefore, the parametric geometry also considered their particular geometry. The main parts of the PFJ parametric model were the bones of the femur (femoral condyle) and patella as rigid parts as well as the femoral and patellar cartilages as hexahedral deformable components (*Figure 2.4 a-d*). As previously stated, each part was simplified to obtain nearly anatomical geometry with variable parameters [43]. The patellar bone was modelled starting from a concave-revolution-solid shape, with the parametric radius, height and radius curvature (*Figure 2.4 e*). Several revolution cuts were performed on the solid part, and its final geometry was obtained (*Figure 2.4 b*). The patellar cartilage was created following the same procedure while maintaining the patellar dimensions (*Figure 2.4 a*). The femoral bone was the most complex part of the model. It was defined as a discrete rigid part that had four main elements: a revolution shape that defined the bottom geometry, with a parametric width and radius (lateral and medial); a solid loft for the irregular section, with different width and length parametric sections (width, width 2, width 3, length, length 2, length 3); a revolution shape in the posterior geometry, where the radius can be modified; and two revolution shapes (*Figure 2.4 f*) that represent the femoral epicondyles (*Figure 2.4 c*). Width and length parameters corresponded to the maximum distance between both femoral epicondyles. Width 2 and length 2 were taken at the point where the medial epicondyle joins the main femoral bone. Width 3 and length 3 were measured at the same point as the highest position of the patella (0° knee flexion angle). The posterior radius defined the contact region between the patellar and femoral cartilages. The femoral cartilage was defined as deformable, and its generation was based on femur geometry and consisted of a revolution shape for the bottom geometry and a combination of elements that defined the upper region (*Figure 2.4 d*). The PFJ parametric model was developed using the Abaqus/CAE v.6.14 software (Dassault

Systemes, Suresnes, France). Measuring previous geometrical characteristics on the 24 knees, a mean parametric model was generated (*Table 2.1*).

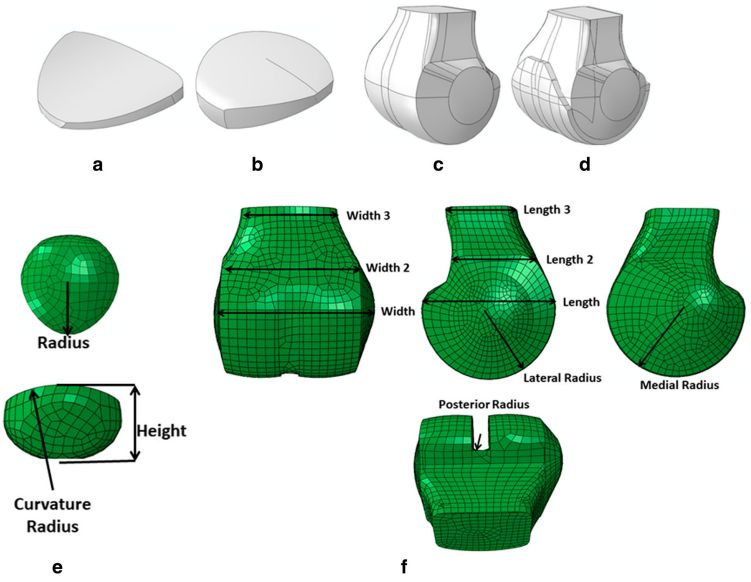


Figure 2.4: Parametric geometry of the four main parts of the PFJ model: *a* Patellar cartilage; *b* patellar bone; *c* femoral bone; *d* femoral cartilage; *e* geometric parameters of the patellar bone; *f* geometric parameters of the femoral bone

As cartilages cannot be reconstructed correctly from a CT, a fixed thickness of 3mm was assumed [32]. Tendons and ligaments were also included since they help to stabilize the patella and better distribute patellofemoral pressures (*Figure 2.5*). The quadriceps tendon (QT), which consists of the vastus medialis (VM), vastus lateralis (VL), vastus intermedius (VI), and the rectus femoris (RF) tendons and the patellar tendon (PT) were modelled as a group of four and two truss elements, respectively (*Figure 2.5*) whilst the MPFL and the lateral retinaculum (LR) were defined as beam elements (B33) (*Figure 2.5*). The QT was oriented from the insertion site on the patella to the muscle origin or the most distal wrapping point on the femur. The PT was oriented from the distal patella to the tibia [40, 41, 42]. The tendon and ligament properties were taken from previous studies [29, 38, 42] and are summarized in Table 2.2. A radius of 1mm was assumed for the beam elements. A mesh convergence analysis was performed for the deformable parts, which determined that an element size should be 1 mm, so that the cartilages would have at least three elements along their thickness. Finally, the patellar cartilage was compounded by 5756 nodes and 4125 elements, while the femoral cartilage was defined by 24,918 nodes and 18,201 elements. The cartilages were modelled with an elastic modulus of 10 MPa and Poisson's ratio of 0.45 [21, 51, 143]).

Bone-cartilage interactions, i.e., femoral bone with femoral cartilage and patellar bone with patellar cartilage, were defined as a tie constraint. The contact between both was defined as a surface-to-surface standard contact with a contact adjustment of 0.1, a hard contact for the normal behaviour and a penalty friction formulation with a friction coefficient of 0.02 for the tangential behaviour [17]. A sensitivity analysis was performed changing the friction coefficient.

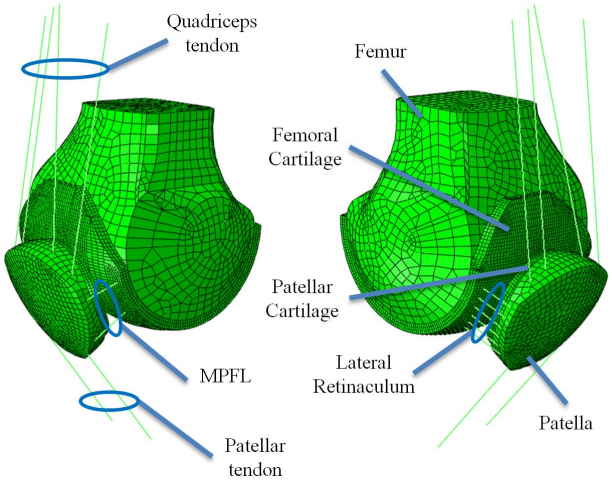


Figure 2.5: General view of the model

| | Stiffness (N/mm) | Poisson Ratio |
|---|---|---|
| Quadriceps Tendon (QT) | 1350 | 0.3 |
| Patellar Tendon (PT) | 2000 | 0.3 |
| Lateral Retinaculum (LR) | 2 | 0.3 |
| Intact Medial Patellofemoral Ligament (MPFL) | 12 | 0.3 |
| MPFL Reconstruction (Semitendinosus Graft) | 100 | 0.3 |
| MPFL Reconstruction (Gracilis Graft) | 80 | 0.3 |
| MPFL Reconstruction (Quadriceps Tendon Graft) | 33.6 | 0.3 |
| MPFL Reconstruction (Posterior Tibial Graft) | 513 | 0.3 |

Table 2.2: Material properties considered for ligaments and tendons in the FE model simulation

### 2.3.2. MPFL reconstruction techniques

Five types of MPFL double-bundle reconstruction techniques were simulated, three static reconstructions and two dynamic ones. Static reconstructions included anatomic reconstruction, meaning a reconstruction with a femoral anatomic fixation point (*Figure 2.6 a*); non-anatomic but physiometric reconstruction, meaning the femoral fixation point is not anatomic, but behaves kinematically like a native MPFL (*Figure 2.6 b*); and non-anatomic and non-physiometric reconstruction (*Figure 2.6 c*). For this last type of reconstruction, the femoral fixation point is too anterior, which means the ligament is too short and that it behaves kinematically, the opposite of a native ligament [132]. Dynamic reconstructions were the dynamic reconstruction using the adductor magnus (AM) tendon as the femoral fixation (*Figure 2.6 d*); and the dynamic reconstruction using the quadriceps tendon (QT) as the attachment point (medial quadriceps tendon-femoral ligament (MQTFL) reconstruction) (*Figure 2.6 e*). Static non-anatomical reconstructions were simulated using semitendinosus graft. Two types of grafts were used for both the anatomic and dynamic reconstructions using the AM tendon as a pulley. They were the semitendinosus autograft and gracilis autograft (*Table 2.2*). These are the most frequently used grafts during MPFLr surgery. Two types of grafts were also used in the original MQTFL reconstruction (MQTFLr) technique described by Fulkerson and Edgar [57]. Those were

the semitendinosus autograft and posterior tibial tendon allograft. For that reason, two simulations were performed during MQTFLr, using a semitendinosus autograft in one of them and a posterior tibial tendon allograft in the other. For the anatomic reconstruction, the native ligament was also simulated for results comparison (intact knee).

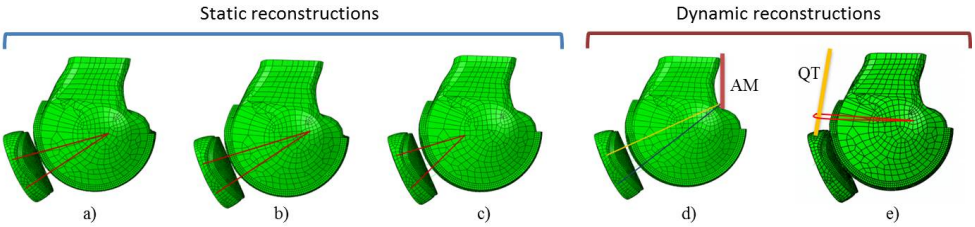


Figure 2.6: *a*) Reconstruction with a patellar bone fixation point and an anatomic femoral fixation point. *b*) Reconstruction with a patellar bone fixation point and a non-anatomic femoral fixation point that has physiometric behaviour. *c*) Reconstruction with a patellar bone fixation point and a femoral fixation point that is too far anterior and without physiometric behaviour. *d*) Dynamic reconstruction using AM tendon as the femoral fixation. *e*) Dynamic reconstruction using the quadriceps tendon (QT) as one of the attachment points.

The length of a normal MPFL increases during flexion from 0 to 30° and decreases from 30 to 120° [132]. This pattern is considered as the *in vivo* MPFL standard dynamic length change. In a normal (anatomic) MPFL reconstruction, the graft is isometric in all the cases between 0 and 30° of knee flexion [132]. In 83% of cases, it is isometric from 0 to 60° of knee flexion [132]. Beyond 60° of knee flexion, the MPFL becomes progressively lax and isometry is lost [132]. Regarding isometry, a ligament is considered isometric when there is less than 5mm of length change throughout the range-of-motion [147].

### 2.3.3. Simulation of the different surgical techniques

The surgical techniques were analysed for five knee flexion positions: 0, 30, 60, 90 and 120°, as in a previous existing dynamic CT scan study [132]. The parametric FE model and the simulations were carried out using the software Abaqus/CAE v.6.14 (Dassault Systèmes, Suresnes, France). Models were generated for each degree of knee flexion. Initially, for all of the surgical techniques, the patellar group (bone and cartilage) was not in contact with the femoral group (bone and cartilage) to avoid nondesirable initial contact problems. The patella was initially aligned with the trochlear groove using the CT images. A perpendicular displacement (approximately 0.5 mm) to the femoral cartilage surface was imposed upon the patella. Once the contact between both cartilages was generated, initial contact pressures were stored. Then, the ligaments and tendons were included and the three surgical MPFLr techniques were analysed. The elements representing the QT and PT were then fixed so that the model was in equilibrium and no forces were applied through them. The initial contact pressures were subtracted from the ones generated with the ligaments and tendons inclusions. Therefore, the results are presented in terms of relative contact pressures, which we subsequently refer to as the contact pressure, to compare the different surgical techniques under the same conditions. The femur position was fixed once every knee flexion position was simulated. Maximum

patellar contact pressures at each degree of knee flexion were evaluated. Maximum MPFL graft stress at each degree of knee flexion was then evaluated for the different positions of the knee.

The data considered for the MPFL inclusion were taken from existing studies [132, 57]. *Table 2.3* summarizes the mean distance between the patella and femoral insertion points for the different MPFL reconstructions. Based on that data, the insertion nodes for each technique and the elongation suffered by the ligaments were determined. The reference position, where the ligaments did not experience any strain was considered knee flexion at 40°. The average MPFL lengths were considered, in this part of the study, to compare the performance of the different surgical techniques over the mean parametric FEM of the PFJ. LR lengths were assumed to be the same as the MPFL length to preserve the equilibrium on both sides of the joint.

The average length of the MPFL for each surgical technique was analysed (*Table 2.3*), indicating that the distance between the femur and patella insertion points was smaller than the reference distance (40°) in some knee flexion positions. That means that the ligament is not experiencing any type of stress. Thus, analysis of certain positions was not necessary (*Table 2.3*, cases indicated by $*$). In the remaining positions, two different types of simulations were performed. First, in certain positions, the MPFL undergoes an elongation, which is simulated by applying a pretension force, $\Delta l \cdot K$, where Δl is the length increment and $K$ is the stiffness of the ligament (*Table 2.3*, cases indicated by *a*). Second, several positions showed an MPFL length that was only possible if the cartilage was compressed because the distance between the patella and femoral insertion point was further than in the reference position (40°). As only-tension elements can be compressed, only working under tension, this relative position change was simulated with a temperature reduction (*Equation 2.1* , where Δl is the length increment, $L_{0_{MPFL}}$ is the initial length of the MPFL and $\alpha$ MPFL is the assumed thermal dilatation coefficient of the MPFL (0.0005 $°C^{-1}$).

$$\Delta T = \frac{\Delta L}{L_{0_{MPFL}} \cdot \alpha_{MPFL}} \tag{2.1}$$

This type of simulation allows cartilages to be modelled in a compressed state. Equilibrium on both sides of the joint was preserved assuming the same Δl for the LR ligament and with the inclusion of the $\alpha_{LR}$ coefficient for the LR, calculated as shown in equation 2.2 (*Table 2.3*, cases indicated by *b*), because ΔT was the same for the entire model. This was an iterative process in which ΔT was recalculated until the desired length of the MPFL was achieved.

$$\alpha_{LR} = \frac{\Delta L}{L_{0_{LR}} \cdot \Delta T} \tag{2.2}$$

| Flexion Angle (°) | Anatomical Insertion w/ Osseous Tunnel | | Posterior Non-Anatomical Insertion w/ Osseous Tunnel | | Anterior Non-Anatomical Insertion w/ Osseous Tunnel | | Posterior Non-Anatomical Insertion w/o Osseous Tunnel (Superior Bundle) | | Posterior Non-Anatomical Insertion w/o Osseous Tunnel (Inferior Bundle) | | Medial Quadriceps Tendon-Femoral Ligament Insertion | |
|---|---|---|---|---|---|---|---|---|---|---|---|---|
| | Length (mm) | SD (mm) | Length (mm) | SD (mm) | Length (mm) | SD (mm) | Length (mm) | SD (mm) | Length (mm) | SD (mm) | Length (mm) | SD (mm) |
| 0 | 60.2[a] | ± 6.1 | 51.6[a] | ± 4.6 | 37.5[a] | ± 7.8 | 61.1[a] | ± 6 | 58.3[a] | ± 6.3 | 65[a] | - |
| 30 | 57.9[a] | ± 6.8 | 50.8[a] | ± 5.4 | 36.5[a] | ± 9.2 | 60.9[a] | ± 5.9 | 60.1[a] | ± 5.9 | 63[a] | - |
| 40 | 57.7 | ± 6.0 | 48.8 | ± 5.0 | 36.2 | ± 8.1 | 60.8 | ± 5.9 | 60.8 | ± 6.0 | 62.7 | - |
| 60 | 57.3* | ± 6.4 | 44.9* | ± 5.2 | 35.7[b] | ± 10.1 | 60.7* | ± 6.3 | 62.1* | ± 6.6 | 62* | - |
| 90 | 55.6* | ± 5.7 | 38.3* | ± 4.9 | 35.6[b] | ± 7.9 | 60.4* | ± 6.4 | 62.2* | ± 6.1 | 62* | - |
| 120 | 50.7* | ± 4.9 | 33.7* | ± 4.8 | 35.4[b] | ± 5.6 | 55.8* | ± 5 | 57* | ± 5.3 | 62* | - |

Table 2.3: Distance between the patellar and femoral insertion points for the MPFL reconstruction techniques analysed. *a*, tension type 1; *b*, tension type 2; $*$, no tension.

### 2.3.4. Clinical validation of the parametric model

Five patient-specific cases were used for clinical validation of our parametric model. The geometry of each patient was generated by modifying the main knee parameters of the parametric model (femur and patella dimensions - see parametric finite element model of the patella femoral joint section-*Figure 2.4*). Patient-specific geometrical data is indicated in Table 2.4. MPFLr was simulated depending on patient-specific data.

| | **Case 1** | **Case 2** | **Case 3** | **Case 4** | **Case 5** |
|---|---|---|---|---|---|
| *Width* | 71.6 | 89.55 | 66 | 65.03 | 70.5 |
| *Width 2* | 49.71 | 60.13 | 50.2 | 46 | 53.48 |
| *Width 3* | 41.38 | 41.97 | 38.78 | 31.9 | 40.72 |
| *Length* | 52.74 | 48.28 | 51.25 | 39.09 | 47.01 |
| *Length 2* | 32.42 | 40.16 | 31.3 | 30.95 | 33.05 |
| *Length 3* | 28.75 | 33.47 | 25.35 | 28.66 | 25.4 |
| *Medial radius* | 27.43 | 36.94 | 29.56 | 27.57 | 22.28 |
| *Lateral radius* | 27.12 | 33.47 | 22.09 | 23.79 | 23.18 |
| *Posterior radius* | 14.07 | 11.2 | 12.43 | 14.73 | 12.09 |
| *Radius* | 19.01 | 20.32 | 17.12 | 16.54 | 32.23 |
| *Curvarture radius* | 44.94 | 51.24 | 42.41 | 43.51 | 43.17 |
| *Height* | 19.61 | 23.02 | 17.94 | 20.72 | 16.22 |

Table 2.4: Patient-specific geometrical data (*Figure 2.4*). Measurements in mm

The graft insertion points were based on each patient's geometry with the help of the corresponding CT data. Each patient underwent a different type of MPFLr. Each specific case was simulated bearing the surgeon's MPFL measurements in mind, as indicated in Table 2.5.

| **Patient** | **Reconstruction** | **Graft material** | **Meassured length for each position (mm)** | | | | | |
|---|---|---|---|---|---|---|---|---|
| | | | ***0º*** | ***30º*** | ***40º*** | ***60º*** | ***90º*** | ***120º*** |
| *1* | 1st | Semitendinosus | 36.3* | 35.9* | 36.83 | 38.7$^{b}$ | 43.7$^{b}$ | 46.3$^{b}$ |
| | 2nd | Semitendinosus | 63.2* | 63.9$^{a}$ | 63.37 | 62.3* | 53* | 46.3* |
| *2* | 1st | Semitendinosus (Proximal) | 23.1* | 33.3* | 36.33 | 42.4$^{b}$ | 46.6$^{b}$ | 48.6$^{b}$ |
| | | Semitendinosus (Distal) | 25.4* | 39.7* | 42.77 | 48.9$^{b}$ | 54.3$^{b}$ | 54.8$^{b}$ |
| | 2nd | Semitendinosus (Proximal) | 43.1* | 46.8$^{a}$ | 46.73 | 46.6* | 41.1* | 37.9* |
| | | Semitendinosus (Distal) | 41.5* | 47.8$^{a}$ | 47.77 | 47.7* | 41.6* | 40.3* |
| *3* | 1st | Quadriceps Tendon | 56.2$^{a}$ | 46.8$^{a}$ | 43.03 | 35.5* | 24.2* | 22.4* |
| | 2nd | Semitendinosus | 51.3$^{a}$ | 49$^{a}$ | 47.87 | 45.6* | 40.5* | 38.2* |
| *4* | 1st (Unique) | Semitendinosus (Proximal) | 52.2$^{a}$ | 51.1$^{a}$ | 50.17 | 48.3* | 41.3* | 35* |
| | | Semitendinosus (Distal) | 49.9$^{a}$ | 49.7$^{a}$ | 48.37 | 45.7* | 39.7* | 35.1* |
| *5* | 1st (Unique) | Semitendinosus (Proximal) | 56.4$^{a}$ | 57$^{a}$ | 55.07 | 51.2* | 46.9* | 42.3* |
| | | Semitendinosus (Distal) | 55.1$^{a}$ | 56$^{a}$ | 54.17 | 50.5* | 45.8* | 41.9* |

Table 2.5: MPFL patient-specific surgical data for the model validation. *a*, tension type 1; *b*, tension type 2; $*$, no tension.

## 2.4. Results

### 2.4.1. Simulation of the different surgical techniques

In a knee with a virtual intact MPFL, which was used as a reference for the comparison among different reconstruction techniques, the maximum patellar cartilage contact pressures at 60, 90 and 120° were very low compared to the pressures at 0 and 30°. Anatomic reconstruction increased the pressure in all of the knee angles, but the amount of pressure increase was only relevant at 0°. In non-anatomic reconstructions with a physiometric behaviour, an increase in all of the positions was found, but the amount of pressure was relevant only at 0 and 30°. In non-anatomic reconstruction without physiometric behaviour the pressure increased in all the knee positions and with a relevant amount of pressure. In the dynamic reconstruction using AM tendon as pulley only were relevant the 0º and 30º knee flexion position, showing a behaviour very similar to those observed in the intact knee. In the dynamic MQTFL reconstruction the variation in the attachment point (QT) is clearly observed showing a different type of pressure map than the rest of situations analysed. The maximum patellar cartilage contact pressures are displayed in *Figure 2.7*.

In a native knee, both the MPFL and LR are under tension at 0 and 30° of knee flexion. At 60, 90 and 120°, both the MPFL and LR were loose. In both the anatomic and a non-anatomic MPFLr with physiometric behaviour, the ligament was tense between 0 and 30° of knee flexion, but it had no tension at 60, 90 and 120°. The same situation is observed for both dynamic reconstructions, AM tendon as a pulley and MQTFLr. In the nonanatomic with non-physiometric behaviour reconstruction, the MPFL was tense at 60, 90 and 120° of knee flexion and and so it does for 0 and 30° of knee flexion too. The MPFL and LR maximum stresses are displayed in *Table 2.6*. The following cases demonstrate the sensitivity and possible clinical implications of the use of a parametric model of the PFJ using FEM to evaluate MPFL reconstructions.

| Ligament Status | Flexion Angle (∘) | Maximum MPFL Stress (MPa) | Maximum LR Stress (MPa) |
|---|---|---|---|
| *INTACT MPFL* | 0 | 8.85 | 1.52 |
| | 30 | 0.78 | 0.15 |
| *ANATOMIC MPFLr* | 0 | 74.72 | 1.51 |
| *Semitendinosus autograft* | 30 | 6.55 | 0.14 |
| *ANATOMIC MPFLr* | 0 | 58.78 | 1.51 |
| *Gracilis autograf*t | 30 | 5.12 | 0.14 |
| *Non-anatomic MPFL reconstruction with a physiometric behavior* | 0 | 97.02 | 1.66 |
| *Semitendinosus autograft* | 30 | 69.6 | 1.1 |
| *Non-anatomic MPFL reconstruction* | 0 | 63.44 | 0.78 |
| *with a femoral fixation that is too* | 30 | 14.74 | 0.17 |
| *anterior and without* | 60 | 46.71 | 1.24 |
| *a physiometric behavior* | 90 | 77.57 | 2.09 |
| *Semitendinosus autograft* | 120 | 92.7 | 2.51 |
| *MPFLr with AMT as a Pulley* | 0 | 7.11 | 0.15 |
| *Semitendinosus autograft* | 30 | 2.53 | 0.05 |
| *MPFLr with AMT as a Pulley* | 0 | 6.35 | 0.15 |
| *Gracilis autograft* | 30 | 2.1 | 0.05 |
| *MQTFLr with AMT as a Pulley* | 0 | 66.7 | 1.42 |
| *Semitendinosus autograft* | 30 | 9.36 | 0.23 |
| *MQTFLr with AMT as a Pulley* | 0 | 100.8 | 1.42 |
| *Posterior Tibial allograft* | 30 | 49.76 | 0.23 |

Table 2.6: MPFL and LR maximum stress (MPa) values for each case analyzed.

**Static MPFLr Techniques**

With the static anatomical technique, the patellar contact pressures at 0º and 30º of knee flexion were greater than those of the native knee regardless of whether semitendinosus or gracilis autografts were used (*Figure 2.7 A, B.1 and B.2*). As in a native knee, the patellar contact pressures at 60º, 90º, and 120º were very low. The maximum patellar cartilage contact pressures are displayed in *Figure 2.7 B.1 and B.2*. The maximum MPFL graft stress at 0º and 30º was greater than in a native knee regardless of whether semitendinosus or gracilis autografts were used (*Table 2.6*). As in a native knee, at 60º, 90º, and 120º the MPFL graft was loose, meaning that it had no tension (*Figure 2.7 A, B.1 and B.2*). The MPFL and LR maximum stresses are displayed in *Table 2.6*.

In the non-anatomic MPFLr with physiometric behaviour, performed using semitendinosus autograft, a significant increase of relative contact pressure was observed for 0º and 30º knee flexion positions, 2.77MPa and 1.91MPa respectively (*Figure 2.7 C*). As in the previous cases, contact pressures at 60º, 90º and 120º were low. This surgery shows the highest pressure. The maximum MPFL stress was also higher than those found for the intact knee and the anatomical reconstruction for both 0º and 30º positions (*Table 2.6*). LR maximum stress shows similar values for the 0º position and increases for the 30º to 1.1 MPa (*Table 2.6*). As in the previous surgeries, for 60º, 90º and 120º the graft was loose.

In the non-anatomic with non-physiometric behaviour reconstruction performed with semitendinosus the relative contact pressure is significant in all five positions analysed (0º, 30º, 60º, 90º and 120º), being specially high for 0º and 120º: 2.42MPa and 1.75 MPa respectively. MPFL does also show significant stress in all the positions (*Table 2.6*). LR shows a similar behaviour than the previous simulations for 0º, 30º and 60º, while substantially increases for 90º and 120º positions (*Table 2.6*). This surgery shows continuous stress in the graft and compression in the cartilage.

**Dynamic MPFLr Techniques**

In the dynamic MPFLr using the AMT as a pulley (*Figure 2.7 E.1 and E.2*), the patellar contact pressures were very similar to those of a native knee through the entire range of knee motion regardless of whether semitendinosus or gracilis autografts were used. The maximum patellar cartilage contact pressures are displayed in *Figure 2.7 E.1 and E.2*. The maximum MPFL graft stress was less at 0º than that of a native ligament when a gracilis autograft was used (*Table 2.6*). However, the maximum MPFL graft stress was greater at 30º than in a native ligament, regardless of whether a semitendinosus or gracilis autograft was used. After 30º of flexion, the MPFL graft loosened like in a native knee. The MPFL and LR maximum stresses are displayed in *Table 2.6*.

In the dynamic MQTFLr, using either a semitendinosus autograft or posterior tibial tendon allograft, the maximum patellar contact pressure was slightly greater than in a normal knee but lower than with the static anatomical technique (*Figure 2.7 F.1 and F.2*). The maximum patellar cartilage contact pressures are displayed in *Figure 2.7 F.1 and F.2*. The maximum stress of the MPFL graft using a semitendinosus autograft was much greater at 0º and 30º than that of a native MPFL (*Table 2.6*). With a posterior tibial tendon allograft, the maximum MPFL graft stress was greater than with a semitendinosus autograft. In all cases, after 30º of flexion, the MQPFL graft loosened like the native ligament. The MPFL and LR maximum stresses are displayed in *Table 2.6*.

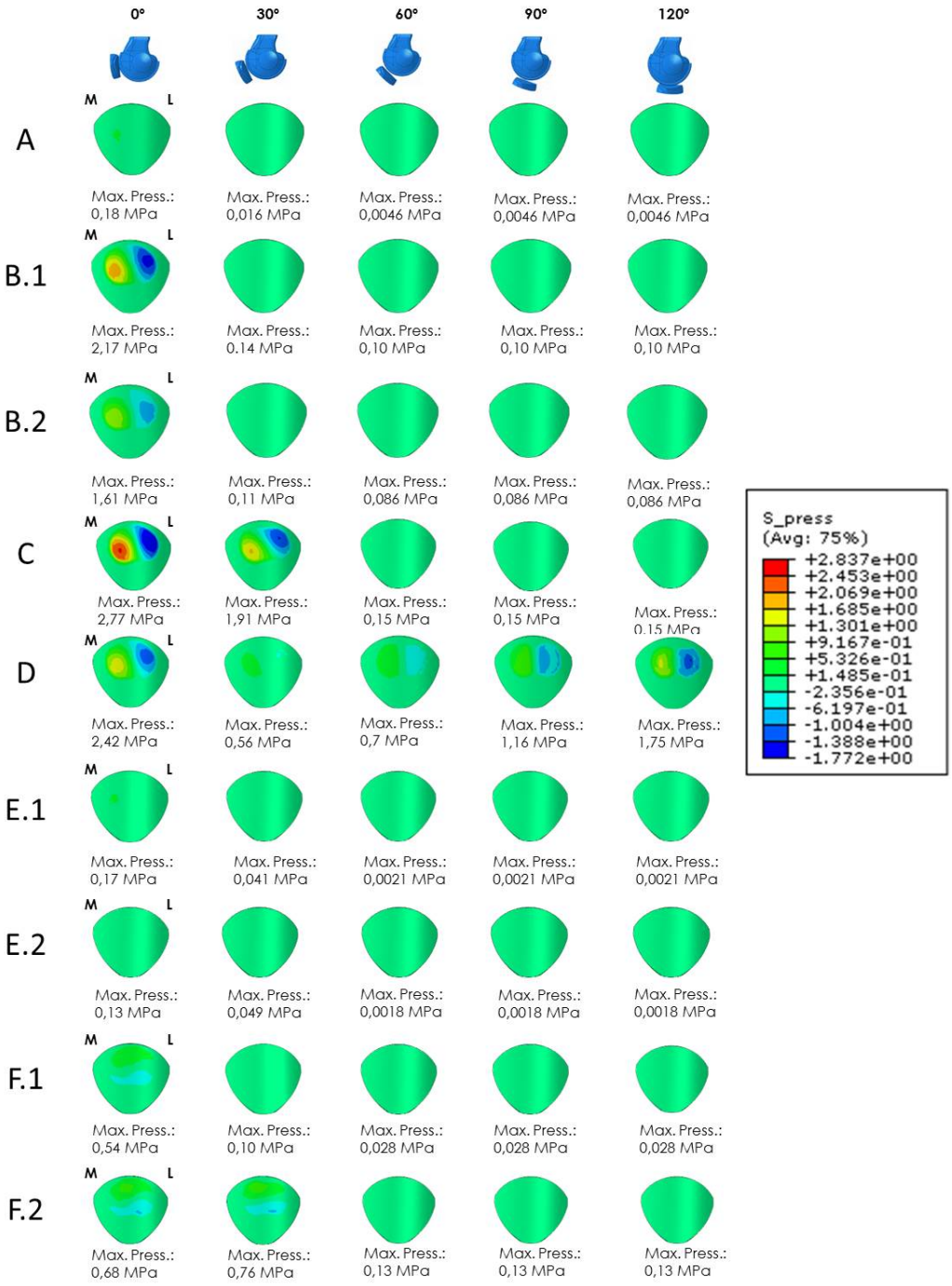


Figure 2.7: Contact pressure (MPa) on the patellar cartilage: (A) intact knee, (B.1) anatomic MPFLr with semitendinosus autograft, (B.2) anatomic MPFLr with gracilis autograft, (C) Non-anatomic MPFL reconstruction with physiometric behaviour, (D) Non-anatomic MPFL reconstruction with a femoral fixation that is too far anterior and without physiometric behaviour,(E.1) MPFLr with semitendinosus autograft using the AMT as a pulley, (E.2) MPFLr with gracilis autograft using the AMT as a pulley, (F.1) MQTFLr with semitendinosus autograft, and (F.2) MQTFLr with posterior tibial tendon allograft (M: Medial; L: Lateral).

### 2.4.2. Clinical validation of the parametric model

**Case 1**

A 17-year-old man was operated on for lateral patellar instability using a single semitendinosus bundle MPFL graft. The patient expressed persistent lateral patellar instability and severe pain. The simulation predicted a contact pressure on the patellar cartilage of 1.19MPa for 60° of knee flexion, 2.25MPa for the 90° position and an important contact pressure of 5.84MPa for 120° of knee flexion (*Figure 2.8*). The maximum MPFL stress at 60° was 59.03 MPa. At 90°, it was 119.2 MPa and 252 MPa at 120°. At 0 and 30°, the MPFL was loose (*Table 2.7*). The maximum lateral retinaculum (LR) stress at 60° was 1.62MPa, 5.38MPa at 90° and 7.06 MPa at 120° (*Table 2.7*). At 0 and 30°, the LR was loose. From that data, we predicted that the patient would develop patellar chondropathy, which was in fact seen during the arthroscopy performed during the MPFL revision surgery (*Figure 2.8 D*). The tension pattern of the MPFL graft is typically seen in a non-anatomic femoral fixation point that is too far anterior in which the graft exhibits non-physiometric behaviour. This can very clearly be seen in the last preoperative 3D CT scan (*Figure 2.8 C*).

The simulation for the second reconstruction, a non-anatomic MPFL reconstruction with a physiometric behaviour, predicted a contact pressure on the patellar cartilage of 0.76MPa for 30° of knee flexion (*Figure 2.8 A*). The maximum MPFL stress at 30° was 26.51 MPa (*Table 2.7*). The maximum lateral retinaculum (LR) stress at 60° was 1.67MPa (*Table 2.7*). In the other positions the ligament was loose. This data predict a good performing of the surgical reconstruction for the patient.

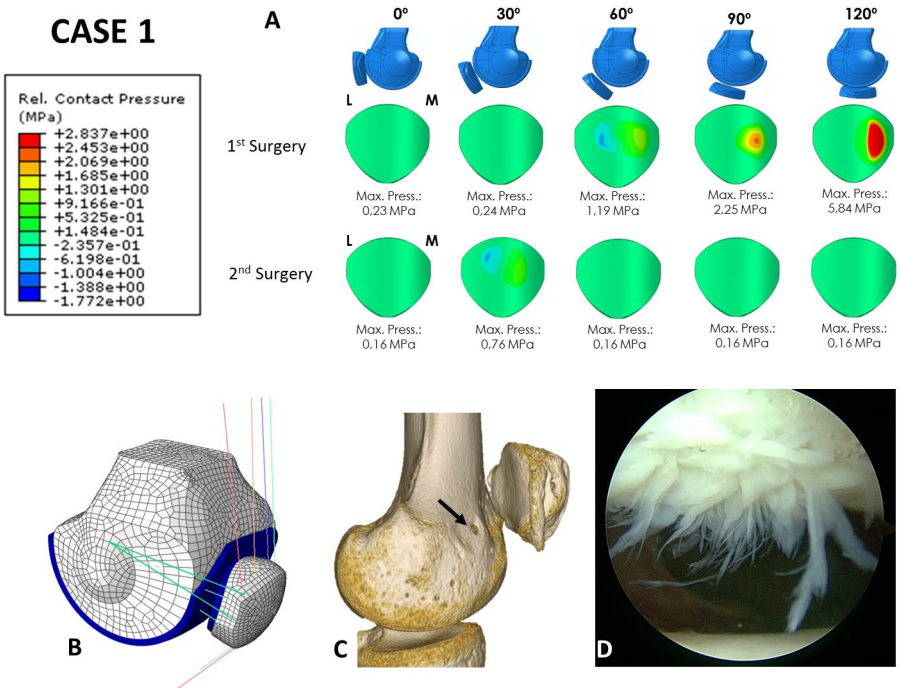


Figure 2.8: **Case 1**: **A** Contact pressure (MPa) on the patellar cartilage for the two performed reconstructions: L=lateral, M= Medial. **B** Parametric model of patient 1. **C** Femoral attachment point is too far anterior (black arrow). **D** Visible patellar chondropathy during arthroscopy.

**Case 2**

A 28-year-old woman operated on for lateral patellar instability with a double-bundle MPFL plasty, using the semitendinosus. The patient complained of severe pain and incapacitating lateral patellar instability. The simulation predicted high contact pressures: 6.17 MPa for the 60° knee flexion position, 5.18 MPa for the 90° knee flexion position and 7.13 MPa for the 120° knee flexion position (*Figure 2.9*). The maximum MPFL stress at 60° was 19.51 MPa, 29.52 MPa at 90° and 34.7 MPa at 120° (*Table 2.7*). At 0 and 30°, the MPFL was loose. The maximum LR stress at 60° was 4.56 MPa, 7.54 MPa at 90° and 8.37 MPa at 120° (*Table 2.7*). At 0 and 30°, the LR was loose. The MPFL was tense at 60, 90 and 120° of knee flexion and was completely loose at 0 and 30° of knee flexion. Clinically, this tension pattern will lead to PFOA, which was in fact seen during surgery (*Figure 2.9 D*). This tension pattern is typical of a non-anatomic femoral fixation point that is far too anterior, as clearly seen in the 3D CT scan in which the graft exhibits nonphysiometric behaviour (*Figure 2.9 C*).

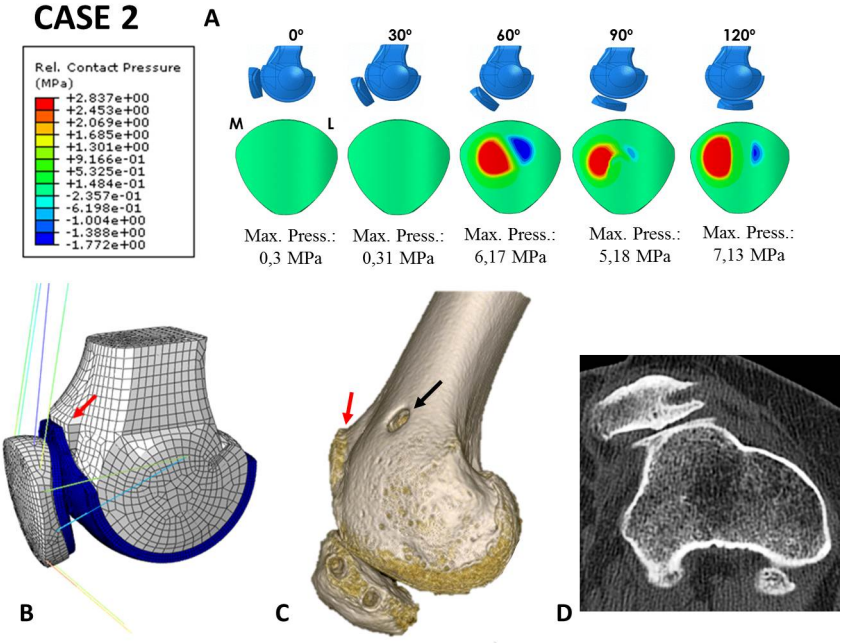


Figure 2.9: **Case 2**: **A** Contact pressure (MPa) on the patellar cartilage for the two performed reconstructions: L=lateral, M= Medial. **B** Parametric model of patient 2. Trochlear dysplasia type D (red arrow). **C** Superior femoral attachment point is too far anterior (black arrow) Trochlear dysplasia (red arrow). **D** Visible patellofemoral osteoarthritis.

**Case 3**

A 38-year-old woman was operated on for lateral patellar instability with an MPFL single-bundle reconstruction using the quadriceps tendon. The patient complained of severe pain and incapacitating lateral patellar instability. The simulation performed with our FEM showed patellofemoral contact pressures far below those found in a native knee (*Figure 2.10 A*). The maximum MPFL and LR stresses predicted for the 0° knee flexion position were 12.28 MPa and 8.22 MPa, respectively. They were 3.93 MPa and 2.68 MPa for 30°, respectively (*Table 2.7*). The prediction fulfils the requirements for an effective MPFLr: a tense graft at 0 and 30° of knee flexion, with greater stress than a native MPFL, and the patellofemoral pressure was below the normal values that could cause symptomatic PFOA. In fact, no chondropathy was seen in this patient during the arthroscopy performed in the revision surgery (*Figure 2.10 D*).

The second reconstruction performed to solve the pain and instability suffered by the patient shows a significant change in the pressure region of the cartilage. The simulation predicted again contact pressures below those found in a native knee (*Figure 2.10 A*). The maximum MPFL and LR stresses predicted for the 30° knee flexion position were 35.71 MPa and 0.76 MPa, respectively (*Table 2.7*). At 0° of knee flexion, they were 103.9 MPa and 2.24 MPa, respectively. Despite the higher tension, affectation to the cartilages is not expected.

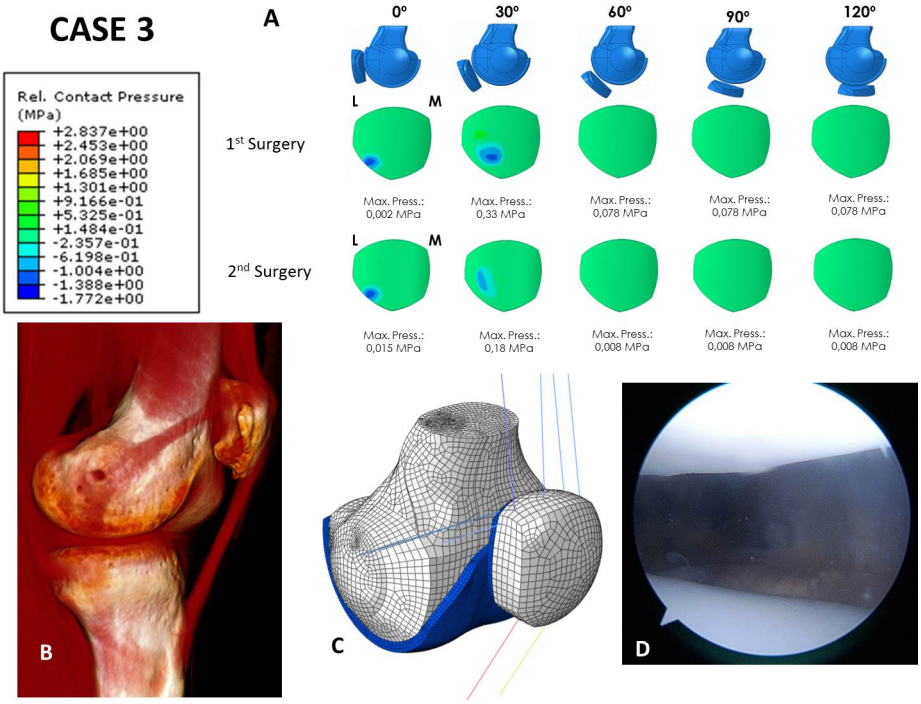


Figure 2.10: **Case 3**: **A** Contact pressure (MPa) on the patellar cartilage for the two performed reconstructions: L=lateral, M= Medial. **B** One can see that the graft is preserved; however, the orientation is too oblique and extremely vertical. **C** Parametric model of patient 3 **D** Arthroscopy at the time of the revision surgery shows normal patellofemoral cartilage.

**Case 4**

An 18-year-old woman was operated on for lateral patellar instability with an anatomic MPFL reconstruction using a double-bundle semitendinosus autograft, with an excellent clinical result at 5 years of follow up. The simulation predicted a contact pressure of 0.2 MPa at 0° of knee flexion and 0.91 MPa at 30° of knee flexion. The maximum MPFL and LR stresses predicted for the 30° of knee flexion position were 29.47 MPa and 0.79 MPa, respectively. For 0° of knee flexion, they were 60.02 MPa and 1.15 MPa, respectively (*Table 2.7*). The prediction fulfils the requirements for an ideal MPFLr; a tense graft at 0 and 30° of knee flexion with far greater stress to failure than a native ligament. The patellofemoral pressures were kept below the values that could cause symptomatic PFOA. This tension pattern is typical of an anatomic femoral fixation point as is clearly seen in the 3D CT scan (*Figure 2.11 C*).

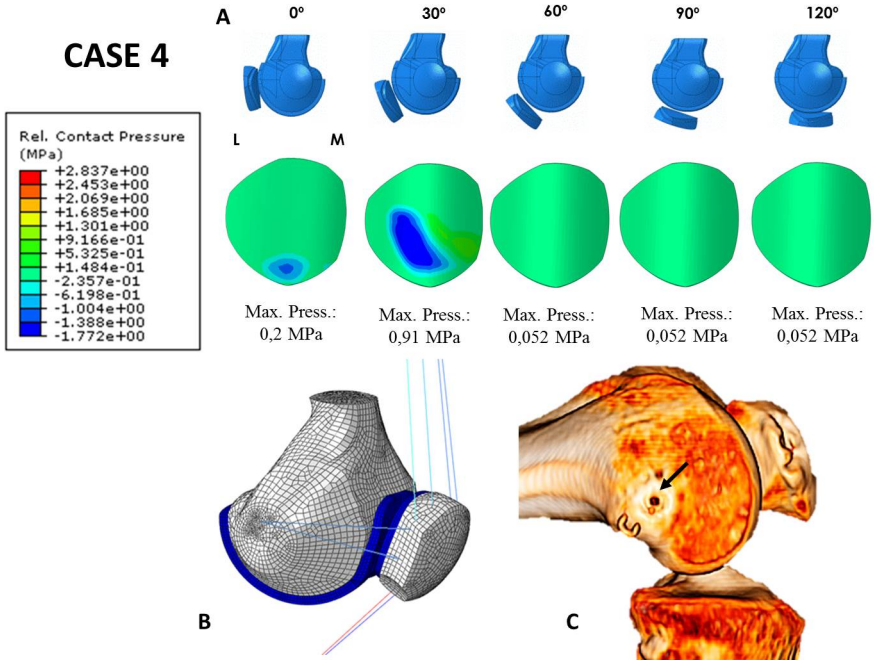


Figure 2.11: **Case 4**: **A** Contact pressure (MPa) on the patellar cartilage for the two performed reconstructions: L=lateral, M= Medial. **B** Parametric model of patient 4. **C** Anatomic femoral attachment point (black arrow).

**Case 5**

A 15-year-old woman was operated on for lateral patellar instability with an anatomic MPFL reconstruction using a double-bundle semitendinosus autograft, with an excellent clinical result at 5 years of follow up. The simulation predicted a contact pressure of 1.57 MPa for 0° of knee flexion position and 1.63 MPa for 30° of knee flexion position. The maximum MPFL and LR stresses predicted for the 30° knee flexion position were 70.3 MPa and 1.27 MPa, respectively. At 0° of knee flexion, they were 40.24 MPa and 0.53 MPa, respectively (*Table 2.7*). The prediction fulfils the requirements for an ideal MPFLr; a tense graft at 0 and 30° of knee flexion with a far higher stress to failure than a native ligament. The patellofemoral pressure values were below those thought to cause a symptomatic PFOA. This tension pattern is typical of an anatomic femoral fixation point as is clearly seen in the 3D CT scan (*Figure 2.12 C*).

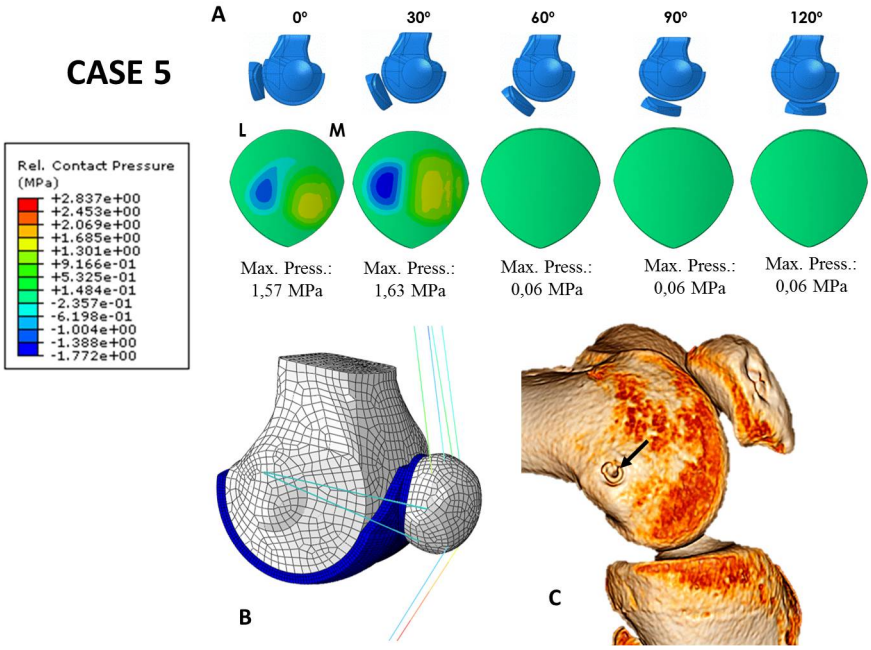


Figure 2.12: **Case 5**: **A** Contact pressure (MPa) on the patellar cartilage for the two performed reconstructions: L=lateral, M= Medial. **B** Parametric model of patient 5. **C** Anatomic femoral attachment point (black arrow).

**Model's accuracy**

FEM was very accurate in cases 1, 2, 4 and 5, but not in case 3. Case 3 fulfilled the requirement for a correct plasty relative to the maximum stress and patellofemoral pressure. However, the patient had pain and instability after surgery. The instability could be explained by the single-bundle configuration of the graft, the vertical direction of the graft because of the non-anatomic femoral fixation point (*Figure 2.10*) and the patella alta. All of them make this graft non-functional. All these factors can contribute to instability and therefore to pain. This reason lead to the second MPFL reconstruction.

| Patient | Surgery | Flexion Angle (°) | MPFL stress (MPa) | LR stress (MPa) |
|---|---|---|---|---|
| *1* | 1st surgery | 60 | 59.03 | 1.62 |
| | | 90 | 119.2 | 5.38 |
| | | 120 | 252 | 7.06 |
| | 2nd surgery | 30 | 26.51 | 1.67 |
| *2* | Only surgery | 60 | 19.51 | 4.56 |
| | | 90 | 29.52 | 7.54 |
| | | 120 | 34.7 | 8.37 |
| *3* | 1st surgery | 0 | 12.28 | 8.22 |
| | | 30 | 3.93 | 2.68 |
| | 2nd surgery | 0 | 103.9 | 2.24 |
| | | 30 | 35.71 | 0.76 |
| *4* | Unique surgery | 0 | 60.02 | 1.15 |
| | | 30 | 29.47 | 0.79 |
| *5* | Unique surgery | 0 | 40.24 | 0.53 |
| | | 30 | 70.3 | 1.27 |

Table 2.7: MPFL and LR ligaments stress obtained for each reconstruction and position analyzed.

## 2.5. Discussion

This model is the first parametric 3D FEM of the PFJ that analyses the effect of different MPFL reconstructions on the patella contact pressure as well as on the kinematic behaviour of the MPFL-graft and MPFL-graft stress along the total range-of-motion of the knee.

Generation of a patient-specific FEM (i.e., a real FEM) of the PFJ requires CT images to be processed, segmented and then converted into a 3D finite element model. This process is complex, expensive and very time-consuming. However, the parametric model is the opposite. Segmentation is a process that requires manual correction to eliminate undesired tissues, and the computational burden makes the real model unsuitable for clinical integration as a tool for MPFLr planning. A parametric model is a generic model, that is a simplified model valid for any knee that could have direct clinical application.

The difference between the current work and previous ones is that in this study the contact pressures for all the angles of knee flexion (from 0 to 120°) in both anatomical and non-anatomical (physiometric and nonphysiometric) MPFL reconstructions are analysed. Since this is a novel method, the study was focused on clinical validation. In this way, five clinical cases are presented to demonstrate the accuracy of the model and to show its versatility for predicting challenging clinical cases. An extrapolation of the computational results was performed to provide a qualitative comparison to the clinical outcomes. The contribution of these results is the introduction of FEM in daily clinical practice to optimize surgical procedures by using personalized treatments.

Findings using the FEM are in agreement with those reported in previous computational studies [41, 42, 143] and could have meaningful potential implications for clinicians performing MPFLr surgery [33, 36, 42, 132, 142]. Elias et al. evaluated medial patellofemoral cartilage overload in cases with technical errors during MPFLr estimating contact pressures between 3 and 6 MPa [42, 43]. Shah et al. also obtained very similar values to previous computational studies. Various authors have demonstrated that the changes in the length of a ligament that occur during joint flexion-extension show changes in the tension of that ligament [67, 101, 132, 141, 152]. Based on this observation, in a previous study using a dynamic CT scan, it has been concluded that the native MPFL was tense during the first 30° of knee flexion in all cases and progressively loosened after 30° [132]. The explanation behind this conclusion lies in the fact that the attachment points of the MPFL are separated further during the first 30° of knee flexion and become progressively closer from 30° onwards. It is called the physiometric behaviour of the ligament. The current study enabled us to directly confirm these findings. The ligament is tense between 0 and 30° of knee flexion, but at 60, 90 and 120°, it has no tension. This fact has clinical relevance as the MPFL is a structure that is only involved in the lateral stability of the patella during the first 30° of knee flexion. After 30°, the ligament loosens and the patellofemoral contact pressure, which also contributes somewhat to patellofemoral stability and is already low during the first 30° (0.23 MPa), decrease considerably (0.0046 MPa). This finding is in agreement with several anatomic and biomechanical studies that show that the MPFL is the most important restraint to lateral patellar displacement from 0 to 30° of knee flexion [33, 36, 70]. After 30° of knee flexion, lateral patella stability depends on the femoral trochlea. Additionally, this study confirms previous findings that show that the location of the femoral attachment point is of utmost importance to obtain satisfactory clinical results [132]. The femoral attachment point is related to the patellofemoral contact pressure, tension of the

MPFL-graft and physiometry of the reconstruction.

The ideal MPFLr technique must combine a precise balance between an optimal patellofemoral pressure with maximum graft stress. It makes a new tear less likely. The patellofemoral contact pressure of a virgin knee must be reproduced, and a maximum MPFL-graft stress greater than that of the native MPFL must be created with the intention to compensate for the anatomic factors (increased tibial tuberosity – trochlear groove (TTTG) distance, patella alta and trochlear dysplasia) that predispose to lateral patellar dislocation [131]. However, it is very important not to increase maximum MPFL-graft stress with a subsequent increase in the patellofemoral pressure because the technique will have a suitable result in the short term but will have a deleterious effect and will lead to degenerative changes in the long term. MPFLr evaluation by means of the FEM is more sensitive than evaluations using only clinical or radiological tests. The FEM can demonstrate the validity of a surgical technique in the long term since it enables one to determine whether a specific technique will lead to an increase in the patellofemoral pressure, which is closely related to future development of PFOA. The elevated MPFL graft tension or an incorrect femoral tunnel position will increase the pressure applied to patellofemoral cartilage [148, 149], and this increase in PFJ contact pressure might result in joint degeneration [130, 148]. Rood et al. in 2015 [130] have shown that static MPFL reconstructions (i.e., reconstruction with both femoral and patellar osseous attachments) result in higher patellofemoral pressures compared with those in the intact situation and thus increase the chance of PFOA in the long term. While Rood et al. showed elevated contact pressures with MPFLr, Stephen et al. in 2014 [148] did not show a pressure increase. In this way Stephen et al., in 2014 and 2016 [148, 149], found that an anatomic MPFLr with a tension of 2N and fixed at 0, 30 or 60° of knee flexion, regardless of the type of graft used, restores PFJ contact pressures to the intact state. However, graft overtensioning and/or non-anatomic positioning of the femoral attachment increases PFJ contact pressures [43, 148, 149]. A broad variability in patellofemoral anatomy, graft tension and non-anatomic femoral attachment could explain these different findings. The current tendency is to perform MPFL reconstructions with an anatomic femoral bone attachment and patellar bone attachment. In this study, we observed an increase in the patellofemoral contact pressures at 0 and 30° of knee flexion after an MPFL reconstruction (2.17 MPa at 0° and 0.14 MPa at 30° when using the semitendinosus as a graft) compared to the pressure found in a normal non-operated knee (0.18 MPa at 0° and 0.016 MPa at 30°). This leads us to consider the possible long-term effects from a slightly greater patellofemoral contact pressures. However, in theory, the patellofemoral contact pressures found in the anatomic reconstructions are not great enough to cause symptomatic PFOA since they are lower than those causing knee osteoarthritis [139]. The objective would be not to exceed safe levels of patellofemoral pressure to induce patellofemoral chondropathy and ultimately PFOA. It should also be remembered that the increase in patellofemoral contact pressures helps to stabilize the PFJ. Therefore, this factor would be beneficial in the classical anatomic reconstruction. Thus, a discrete increase in contact pressure, as observed, is desirable.

Currently, what is being discussed is the precise consequences of the clinical results for the MPFLr of the dynamic techniques and the static non-anatomical techniques, in which the MPFL-graft behaves like a native MPFL (physiometric behaviour) from the physiological point of view. For the static reconstructions, Servien et al. in 2011 [142] and Sanchis-Alfonso et al. in 2017 [132] found no negative clinical effects after 2 years when using these reconstructions, which could be due to the short follow-up in both cases. In this type of reconstruction, the FEM shows an increase in

patellofemoral contact pressure at 0 and 30° of knee flexion in comparison to these pressures in the native knee (2.77 MPa at 0° and 1.91 MPa at 30° vs 0.18 MPa at 0° and 0.016 MPa at 30°). This pressure increase mainly occurs on the medial patellar facet. According to Jones et al. [74], the average contact stress at 30° is 1.7 ± 0.6 MPa, with a peak of 3.2 ± 0.6 on the surface of the patellar cartilage and of 2.8 ± 0.7 MPa at the deepest point. The differences found between this study and the one by Jones et al. [74] can be explained by the fact that Jones uses a laboratory controlled study with cadaver knees using a different method than us. What is not known is whether this pressure increase will result in chondropathy in the long-term and ultimately result in symptomatic PFOA. As far as we know, there is no study of the PFJ that has determined the contact stress threshold that is predictive of symptomatic PFOA. Segal et al. [139] observed that a threshold of 3.42 to 3.61 MPa had a 73.3% sensitivity with specificity ranging from 46.7% to 66.7% for the prediction of symptomatic knee osteoarthritis. Obviously, these values cannot be extrapolated to the PFJ, which is the joint with the thickest cartilage in the human body. It is logical to think that the pressures causing symptomatic PFOA would be greater. In non-anatomical MPFL reconstructions, the maximum patellofemoral contact pressures are on the order of 2.77 MPa, values that are considerably below the cut-off point mentioned above. Therefore, it is likely that a non-anatomical but physiometric reconstruction would not have long-term negative effects on the PFJ. Consequently, it would seem more important for the ligament to be *physiometric* rather than perfectly anatomical.

On the other hand, and becoming one of the most important finding of this study, the analysis of dynamic reconstructions showed that the patellar contact pressure from 0º to 30º of knee flexion, the range in which the patella is usually unstable [131, 132], was lower compared to the static reconstructions. In addition, the pressure was similar in dynamic reconstructions compared with an intact knee. This was consistent with the initial hypothesis. These results are different from those found by Rood et al. [130] in a controlled laboratory study using Tekscan pressure-sensitive films. According to these authors, the static MPFLr resulted in greater peak and mean pressures from 60º to 110º of flexion when compared to dynamic reconstructions. Moreover, these authors showed that the static MPFLr results in greater patellofemoral pressures and thus increases the risk of PFOA in the long term, while the dynamic reconstruction results in more normal pressures.

In the most commonly used dynamic MPFLr, the femoral attachment site uses the AM tendon as a pulley [11, 12, 87, 100]. Some authors have tested the validity of this surgical technique, both clinically and radiologically, and found very satisfactory clinical results in the short term [12, 100]. Fulkerson and Edgar [57] described the MQTFLr, another dynamic reconstruction technique. While the soft tissue technique using AM tendon is considered to be a non-anatomic technique, the soft tissue technique using the quadriceps tendon as the soft tissue fixation point is an anatomic technique as it reconstructs the MQTFL [153, 154]. This technique also has good clinical results in the short term, like that of the static anatomic MPFL reconstructions with a patellar attachment point [57]. Moreover, this surgical technique essentially avoids the risk of patella fracture, which is a serious complication after MPFLr [111, 134]. Both dynamic techniques restore the medial patella stabilizer, preventing lateral patella dislocation. Nevertheless, uncertainty currently exists relative to the long-term outcomes associated with these dynamic techniques, particularly with the development of PFOA. MPFLr evaluation by means of the FE parametric model, as done in the present study, is more sensitive than evaluations using clinical and radiological tests alone. It allows for the evaluation of patellar compression forces

whose increment has been associated with the appearance of osteoarthritis in the tibiofemoral joint [139].

In the present study, the results have shown that the dynamic technique using the AM tendon as a pulley with a gracilis tendon autograft (i.e., the most used graft) [100] not only does not increase the patellar contact pressure compared to an intact knee, but also shows a slightly lower resistance to rupture of the graft compared to a native ligament at 0º (*Figure 2.7 E.1 and E.2*, *Table 2.6*). In an ideal MPFLr, the graft should be more resistant than the native ligament to compensate for other instability predisposing factors [131]. Moreover, it is logical to think that if the reconstruction uses a graft with the same or lower maximum stress as the torn ligament, there is risk of leading to a new rupture. If the maximum stress is greater, then a repeat tear is less likely. Therefore, the aim is a stronger graft that will not tear again. However, this increment of the graft's resistance should never be achieved by increasing the patellar contact pressure. Using a graft with the same or lower maximum stress as the ligament that has just tore could explain this technique's failure when performed as an isolated MPFLr in patients with a severe trochlear dysplasia. Lind et al. [87] found that the outcomes after MPFLr with the gracilis tendon looped around the AMT insertion in pediatric patients were inferior to MPFLr using bony femoral fixation in adult patients (20% of the pediatric patients experienced redislocation within the first postoperative year compared with 5% of the adult patients). In this series, 20 out of 24 patients had some degree of trochlear dysplasia (10 cases were grade B and 10 cases were grade C or D, 42%) [87]. However, there was no correlation between high degree of trochlea dysplasia (grade C and D) and redislocations. Of the five redislocations, only two were seen in the 10 high-dysplasia knees. This uncorrected factor may have contributed to the high degree of redislocation observed in this series. Alm et al. [11] also found an elevated redislocation rate after MPFLr in children and adolescents when the adductor sling technique was used. The authors concluded that the adductor sling technique could only be recommended in the absence of additional patellofemoral maltracking, caused by an elevated tibial tuberosity-trochlear groove (TT-TG) distance (>15 mm), patella alta, or especially severe trochlear dysplasia. However, the clinical approach was to treat the associated predisposing factors for CLPI, and MPFLr was associated with realignment surgery in 56% of the cases. This approach could explain their satisfactory clinical results [8]. In their series of isolated MPFLr using the AM tendon as a pulley, the percentage of trochlear dysplasia grade C or D was only 8.5% (unpublished data). The fact that this type of reconstruction does not increase patellar contact pressure is very important because it indicates that it will not be predisposed to the development of a patellar chondropathy or PFOA in the long term.

This study showed that MQTFLr, from a biomechanical point of view, behaves like an anatomic static MPFLr (*Figure 2.7 F.1 and F.2*). The MQTFL graft was under tension during the first 30º of knee flexion, but it loosened after 30º and the already low patellar contact pressure decreased considerably after the first 30º (*Table 2.6*). MQTFLr significantly increased the resistance of the reconstruction without significantly increasing patellar contact pressure. This finding is very important because it indicates that this type of reconstruction is unlikely to contribute to the development of patellar chondropathy or PFOA in the long term. MQTFLr fulfills all the criteria for an ideal MPFLr from a biomechanical point of view. It combines a perfect balance between an optimal patellar contact pressure with the maximum graft stress, making a new tear less likely.

Importantly, from a biomechanical standpoint, a dynamic reconstruction is better than a static one because it enables patellar contact pressure that is like that of an

intact knee. To be able to definitely answer the question as to which reconstruction technique is better, the clinical results regarding the percentage of redislocations and functional results need to be considered. However, there are few clinical studies, and those that exist are of low quality with respect to the scientific evidence. We need well-designed, long-term prospective studies with many patients to answer these questions.

With the FEM, it is possible to predict which MPFLr have an increased risk of severe patellofemoral chondropathy resulting in symptomatic PFOA and requiring active treatment. In the cases in which PFOA occurred, it was because the MPFL-graft was loose, with knee flexion from 0 to 30°, and was tense from 60° onward. In these cases, the patellofemoral contact pressures were over 5 MPa from 60° onward, the femoral attachment point being extremely non-anatomical (too far anterior) and the MPFLr was not physiometric. The predictive value of the parametric model of the PFJ has made its clinical validation possible.

**Clinical Relevance**

These findings have important clinical relevance because they validated the use of MPFLr using the AM tendon as a pulley. The results are relevant not only for adults with a CLPI as a primary surgery, but also in certain situations, such as in revision surgeries with multiple bone tunnels or in children. In children, this method avoids injury to the distal femur growth plate and subsequent risk of developing a deformity of the knee [140]. Moreover, our study validated the use of MQTFLr not only as a primary surgery but also in the revision setting to avoid patellar problems. Another interesting finding of our study was that the type of graft does matter, at least from a biomechanical point of view (*Figure 2.7*, *Table 2.6*). Numerous MPFLr surgical techniques, using autografts as well as allografts, have been described. From a clinical point of view, there seems to be no significant differences between the various types of grafts [97, 172]. However, our FE parametric model study showed significant differences in terms of patellar contact pressure and the maximum MPFL graft stress. For example, the gracilis autograft has been recommended [100] in the MPFLr using the AM tendon as a pulley because the gracilis tendon appears to be long and strong enough to duplicate the MPFL function [69, 102]. However, according to the results found using the FE method, the semitendinosus tendon has greater stress to failure relative to the gracilis, without significantly increasing the patellar contact pressure. In theory, a new tear is therefore less likely with a semitendinosus tendon autograft (*Figure 2.7 E.1 and E.2*, *Table 2.6*).

**Limitations**

This study has several limitations. The patellar and femoral cartilages had a constant thickness of approximately 3 mm. The PFJ was reconstructed from CT data in which soft tissues are not clearly distinguished. However, the gap between both bones was approximately 6mm. Accordingly, the same thickness for both cartilages was assumed. Small differences would have been predicted if other thickness values had been considered. Additionally, the ligament material properties were taken from the literature [29, 38, 42]. In the future, patient-specific material properties should be considered. The inclusion of magnetic resonance (MR) data from the same patients and the use of image registration techniques might combine MR and CT data. It which would not only make it possible to extract cartilage thickness accu-

rately but also to determine patient-specific multi-variate matrix properties, such as the T1 or T2 relaxation times, which are related to proteoglycan and collagen matrix integrity, respectively [92].

Another limitation is that there was no estimation of the amount of error in the patient-specific shape when creating the patient-specific model. There was only qualitative assessment of the global patient-specific shape. Additionally, to preserve equilibrium, the elements representing the QT and PT were fixed and no forces were applied through them. Furthermore, the same LR length changes were assumed as for the MPFL.

Another important limitation of this study is the fact that the patellofemoral pressure values that predict the development of a symptomatic PFOA are not known. Segal et al. [139] observed that a threshold of 3.42 to 3.61 MPa had 73.3% sensitivity, with specificity from 46.7% to 66.7%, regarding the prediction of symptomatic knee osteoarthritis. Obviously, these values cannot be extrapolated to the PFJ, which is the joint with the thickest cartilage in the human body. However, it is logical to think that the pressures causing a symptomatic PFOA would be greater. Several experimental studies have included a certain amount of the quadriceps force applied to the patella [42, 130] to determine the patella femoral spatial relationship and contact pressure. This model did not incorporate this force.

Using the FEM allows to reliably predict the clinical evolution of an MPFL-graft. Logically, in a condition with multifactorial etiopathogeny such as lateral patellar instability, the model fails in some cases because there are additional factors (e.g., patella alta, increased tibial tubercle-trochlear groove distance and trochlear dysplasia) other than the tension of the MPFL-graft and patellofemoral contact pressures that could be responsible for the failed surgery. This is a major limitation of this study. The abovementioned anatomic additional factors are often associated in patients requiring MPFLr and can change the pressures at the PFJ and lead to different outcomes. Although it has not been addressed in the present work, the conditions in which the graft would not prevent post-operative instability could be incorporated [50, 70, 131].

## 2.6. Study Conclusions

The main finding of this study is that **the use of a parametric 3D finite element model of the PFJ allows the evaluation of different types of surgical techniques for MPFLr with regard to the effect on the patellofemoral contact pressure**. That also goes for the kinematic behaviour of the MPFL-graft with flexion-extension of the knee and the maximum MPFL-graft stress based on a previous study which has shown that the graft length variation differs in each type of MPFLr. In this way, from diagnostic images like a CT, for example, it is possible to simulate different surgical treatments and customize the treatment for individual patients.

The patellar contact pressures after dynamic MPFLr were like those of the native knee, whereas static reconstruction resulted in greater pressures and, thus, could eventually increase the risk of PFOA in the long term. Therefore, dynamic MPFLr might be a safer option than static reconstruction from a biomechanical point of view. We need long-term clinical studies with both dynamic and static techniques to corroborate the conclusions that were obtained with our biomechanical study using a FE parametric model.

# Chapter 3

# Preoperative planning for spine fusion

This chapter will focus in the analysis of spine fusion as a surgical procedure for spine fixation when lumbosacral joints suffer damage. This kind of surgery usually implies the fusion of the sacrum, specifically the S1 vertebra, and lumbar vertebrae L5, L4 and, in some occasions L3. In contrast to the previous chapter, this kind of surgery is the most common when trying to solve low back severe injuries; especially in patients with osteoporosis.

This study will simulate different alternatives in the surgical procedure for pedicle screws and cement inclusion, using FEA applied in the 3D reconstructions of patients lumbosacral regions that already suffered injuries and required surgical procedures to solve their condition. This way, the surgical alternatives will be compared in order to obtain a guideline of the influence of each element separately and combined in the loads distribution in the lumbosacral region and their effect in the injury recovery.

## 3.1. Biomechanics of the lumbosacral spine

Main biomechanical structure of the lumbosacral region consists of the lumbar vertebrae (L1 to L5), the sacrum and the intervertebral discs (*Figure 3.1*). Sacrum consists of the fusion of 4 smaller vertebrae forming an unique bone that articulates with the 5th lumbar vertebra through an intervertebral disc in its upper surface; the coccyx bone at the bottom of its structure through the sacrococcygeal symphysis, a fibrocartilaginous joint; and the iliac bones at the sides, forming the sacroiliac joint (SIJ), a semi-mobile joint where bones are connected by ligaments.

Intervertebral discs form every fibrocartilaginous joint between the vertebrae along the spine. These elements consist of an outer ring, the annulus fibrosus, formed by collagen type I and II fibrocartilage layers, and the nucleus pulposus, whose gelatinous characteristics helps in loads distribution and impacts absorption. This structure is closed up and down by cartilage endplates, surfaces that connect the disc with the corresponding vertebrae.

This structure is reinforced by ligaments that keep the union between the bones. Also, most of muscles in the back core are involved in the stability and curvature of the spine (lumbar lordosis).

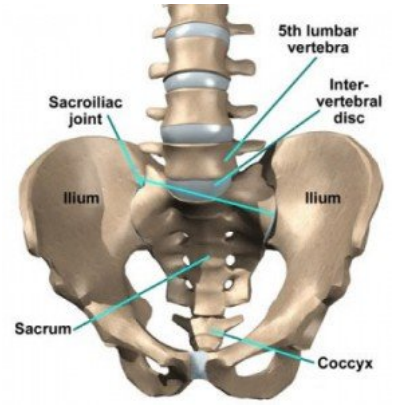


Figure 3.1: Anatomical lumbosacral and iliac region [4].

## 3.2. Clinical Interest

As the population gets old and life expectancy increases, the demand for surgical treatments in older patients with osteoporosis and spinal degenerative diseases becomes progressively more important [54, 163]. Osteoporosis predisposes elderly patients to progressive spinal deformities and potential neurological complications and is subjected to major concern before spine surgery. Therefore, it can complicate spine surgery, especially interventions with bone fusions and instrumentations [58, 163]. Pedicle fixation is widely used for the stabilization of the spine surgery.

Spine fusion is a widely known surgical technique where vertebral region affected is fused using two plates or rods placed along the spine and fixed to every bone, when possible, through the selected option, which usually are pedicle screws (*Figure 3.2*). This surgical solution has several functions. In the first place, it allows the loads transmission from upper vertebrae to the lower ones where fixation is done; this way, if there is any affected area (bones or intervertebral discs) in the upper region most of the loads that this region should bear is shared by the plates and the screws avoiding greater problems. Also, this fixation helps correcting some severe deviations and redistributing the loads transmission. Finally, this kind of fixations restricts the rotation of the fixed bones, this prevents some degenerative issues that can lead to affections in soft tissues or nerves transmissions.

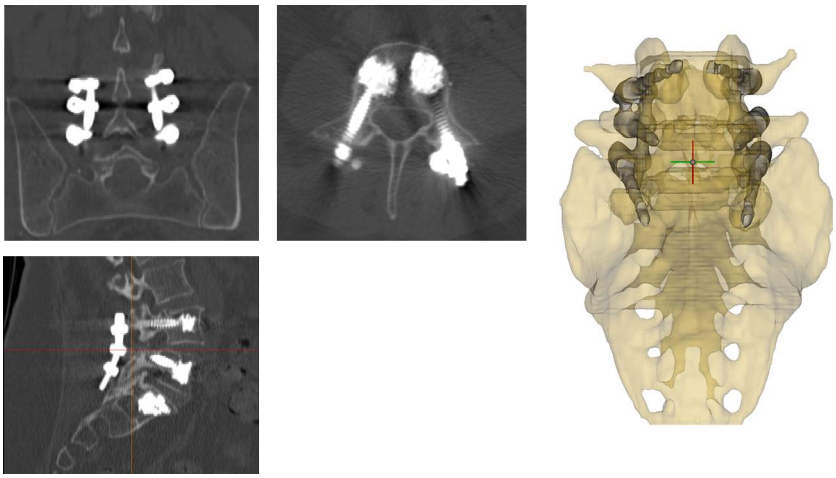

Figure 3.2: Spine fusion example using pedicle screws, rods and cement injection. Model reconstruction developed using Mimics v 20.0 (Materialise NV, Leuven, Belgium).

Loosening of pedicle screws [58] and instrumentation failure has been clinically documented [37, 125, 157]. Many solutions have been proposed to improve the fixation strength of instrumentation and reduce the risk of failure: multiple fixation points [94], four-rod technique [144], expandable screws [83, 94], large diameter screws with bicortical purchase [73, 112] and screw augmentation with polymethylmetacrylate (PMMA) [18, 34, 39, 63, 65, 93]. Augmenting pedicle screw fixation with PMMA appears to be a promising approach [39]. Polymethylmetacrylate (PMMA), hereafter referred to as cement, is an effective material for enhancing pedicle screw fixation. It has been reported that this procedure can increase screw pull out strength by a factor up to 1.5 compared to surgical procedures that employ non-augmented screws [34, 56, 58].

In recent years, the importance of computational modeling for the investigation of research questions in the field of orthopaedics has been continuously increasing [91, 98]. Finite element (FE) analysis is commonly used to study the biomechanics of human lumbar spine [128, 135, 176] developed and validated a lumbar spine model FE model for healthy subjects. There have been many works in the literature that have modelled unilateral, bilateral pedicle screw fixation or other fixation techniques [26, 64, 76, 127, 158, 169]. In 1998, Templier et al. [158], developed the first FE analysis of a spinal fixation devices on a L3-sacrum segment. Later, Rohlmann et al. [127] analysed the effect of using a bilateral dynamic stabilization device. Gong et al. [64] performed a FE analysis on a lumbar spine (L3-L5) model studying the effect of three types of posterior fixation techniques (bilateral pedicle screw, unilateral pedicle screw and unilateral pedicle screw and translaminar facet screw). The three fixation techniques increased the stiffness of the lumbar spine. Wang et al. [170] and Zhou et al. [182] incorporated the effect of cement augmentation in their computational models. Wang et al. [170] performed a biomechanical study using a FE model of one lumbar vertebrae where they compared the effect of cement augmentation of pedicle screw fixation in normal and osteoporotic bone. They demonstrated that cement augmentation increased the fixation strength of pedicle screws. Zhou et al. [182] performed a FE analysis of a conventional pedicle screw and cement-augmented pedicle screw instrumentation in a model of L4-L5 with fusion (cage in the transforaminal lumbar interbody fusion). They showed that both solutions increased the range of movement and disc stresses.

The purpose of the current study is to compare the biomechanical features of different pedicle screw fixation with and without cement augmentation in the lumbosacral region of five patients. We hypothesised that cement augmentation will improve the screw fixation resulting in a stiffen lumbosacral region. We also hypothesised that the same solution (combination of cement and screws, or cement and screws in a different position, etc.) will not be the optimal solution for each patient. To our knowledge, no other patient-specific finite element analysis has been published in the literature.

## 3.3. Material and Methods

### 3.3.1. FE Model development

Lumbosacral reconstructions were obtained using the software Mimics v 20.0 (Materialise NV, Leuven, Belgium). Bones, sacrum and affected vertebrae, were semiautomatically extracted from the CT images, while intervertebral discs were manually segmented based on the intervertebral space between bones (*Figure 3.3*). Once 3D reconstructions were completed, each bone and intervertebral disc was independently imported in a single project created in the software 3-Matic v 11.0 (Materialise NV, Leuven, Belgium).

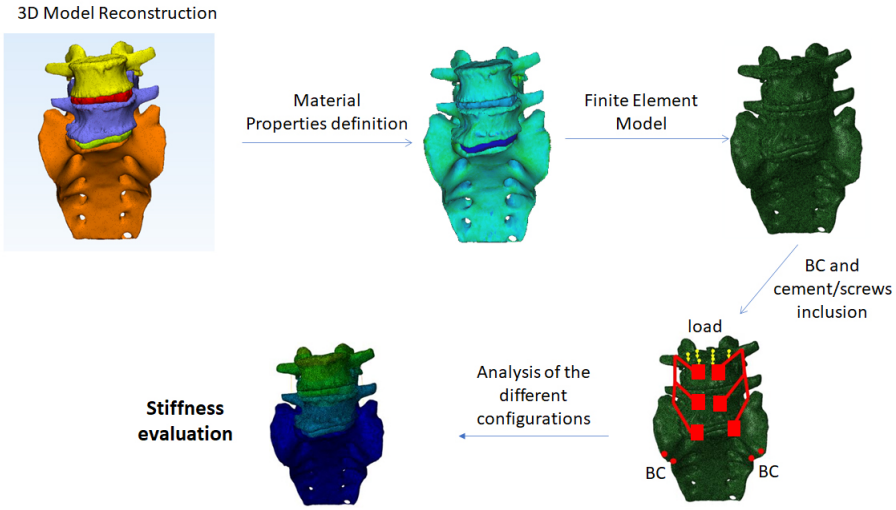


Figure 3.3: Workflow for patient-specific 3D reconstruction.

The surface of each component of the model was meshed as a preliminar step for obtaining the volumetric mesh. To preserve the accuracy of the posterior computational simulations, mesh triangles maximum edge length was set to 2.5 mm for all parts. A sensitivity mesh analysis was performed. Meshes were generated through the adaptive mesh tool; this way, mesh size was smaller and more accurate in the regions with small complex geometries. Once the meshes were completed, volumes were created using quadratic tetrahedral elements and preserving a 2.5 mm maximum edge length (*Figure 3.3*).

Parts were transferred from 3-Matic to Mimics model to assign the material properties. Isotropic bone properties were mapped from the CT images to the mesh (Mimics). Cortical bone was simulated on both the sacrum and vertebrae as a 1.5mm thick shell element. Young's modulus and Poisson's ratio were 18000 MPa and 0.3, respectively [72, 181, 119]. Patient-specific material properties were considered for trabecular bone. Normally, CT calibration phantom is used to obtain radiological density ($\rho$). However, in the present work, as no scanner calibration was available, each Hounsfield unit (HU) was converted to density using the information from the images and the literature [75]. In more detail, equation 3.1 was used to convert HUs to density (kg/m$^3$) for trabecular bone:

$$\rho = 527 + 0.44 * HU \tag{3.1}$$

Finally, Young's modulus and Poisson's ratio for each trabecular element (in MPa) was calculated using the following equation [75]:

$$E = 0.02721 * \rho^{1.44} (MPa) \tag{3.2}$$

Intervertebral discs were assumed as linear elastic with Young's modulus and Poisson's ratio of 10 MPa and 0.45, respectively [169].

Lumbosacral 3D FE model geometry for each patient was completed. Figure 3.4 represented the five patient-specific lumbosacral regions. All patients include the sacrum and L4 and L5. Additionally, patient 2 model incorporated L3.


Figure 3.4: Lumbosacral FE models of the five patient-specific reconstructions

Bones and intervertebral discs were connected through tie constrains in order to avoid the sliding of any part and assure the load transmission from the upper vertebra to the sacral bone. Boundary conditions were applied in the sacral bone restricting its displacement *Figure 3.3*. A follower load was applied on the upper surface of the 1st vertebra of each model with a total value of 600 N distributed in a set of 10 nodes [106, 129, 176, 179]. The models were simulated with the software Abaqus/CAE 6.14 (Dassault Systemes, Suresnes, France).

### 3.3.2. Simulation of fixation techniques and biomechanical evaluation performed

Cement is usually included to fix the screws to prevent the pull as a consequence of region compression in spine fusion surgeries [39]. But cement is also used to reinforce osteoporotic bones [122, 123]. Cement regions were selected among the trabecular bone elements in the vertebrae. Cement was assumed homogeneously distributed within the region and with linear elastic mechanical properties (Young's modulus 2000 MPa; Poisson's ratio 0.3) [116, 115]. The effect of cement volume injected was also analysed. Commercial screws allowed surgeons to change the angle of the screw fixation in the sacrum [108]. Bilateral fixation was simulated. Screws were included as connected beam elements with titanium alloy mechanical properties (Young's modulus 110000 MPa; Poisson's ratio 0.3) [26, 127]. A screw diameter of 7 mm and 50 mm length was considered. Different screw configurations were also simulated for the one positioned in the sacrum (*Figure 3.5*) in the sagittal plane: standard angulation (cement+screws) and ±7° approximately (cement + screw up position and cement + screw down position).

Summarizing, seven configurations were evaluated for each patient (*Figure 3.5*):

a) Cement alone: Cement volume included (approximately 2.5 $cm^3$ per screw fixation)

b) Screws alone: Screws located with a standard angle

c) Cement + Screws: combination of configurations *a)* and *b*)

d) Cement + Screw up position: Configuration *a)* and screws with the insertion points selected with a smaller angle (blue screw *Figure 3.5 h*) than in the configuration *(b)*

e) Cement + Screw down position: Configuration a) and screws with the insertion points selected with a higher angle (yellow screw *Figure 3.5 h*) than in the configuration (b)

f) Screws + High cement volume: Screws of configuration *b)* and a high cement volume included (approximately 3.7 $cm^3$ per screw fixation)

g) Screws + Low cement volume: Screws of configuration *b)* and a low cement volume included (approximately 1.2 $cm^3$ per screw fixation)

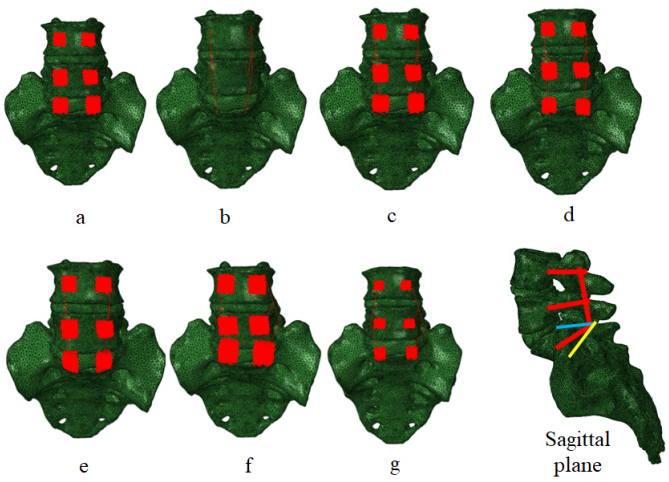


Figure 3.5: Surgical alternatives for stiffness improvement. *a*, cement alone; *b*, screws aone; *c*, Cement + Screws; *d*, Cement + Screw up position; *e*, Cement + Screw down position; *f*, Screws + High cement volume; *g*, Screws + Low cement volume; *h*, screws angle variations.

Detailed amount of cement injected in each screw position for all the configurations and patients can be consulted in *Table 3.1*. The performance of each surgery configuration was evaluated computing the stiffness of the resulting model. Stiffness was calculated based on the mean value of the composition of displacement (measured in mm) for every node selected in the loading region and the load applied (600 N) (*Figure 3.3*) (*Equation 3.3*):

$$Stiffness = \frac{600}{mean\ displacement}(N/mm) \tag{3.3}$$

For each patient, stiffness was computed in the *reference* configuration. *Reference* refers to the anatomical preoperative model considered as the base result for the comparisons. The stiffness variation of each new configuration (*Figure 3.5*) with respect to the reference configuration was calculated following equation 3.4:

$$Stiffness\ variation = \frac{New\ config\ stiffness \quad - \quad Ref\ stiffness}{Ref\ stiffness} \cdot 100(\%) \tag{3.4}$$

| ***Cement volume (cm3)*** | | **L3 right screw** | **L3 left screw** | **L4 right screw** | **L4 left screw** | **L5 right screw** | **L5 left screw** | **Sacrum right screw** | **Sacrum left screw** | **Total cement volume** |
|---|---|---|---|---|---|---|---|---|---|---|
| *Patient 1* | Conf. a) c) d) e) | - | - | 1.68 | 1.84 | 2.36 | 2.57 | 3.54 | 3.69 | 15.68 |
| | Conf. f) High | - | - | 4.51 | 4.13 | 3.26 | 3.03 | 5.56 | 5 | 25.49 |
| | Conf. g) Low | - | - | 0.75 | 0.7 | 0.79 | 0.81 | 2.18 | 2.3 | 7.53 |
| *Patient 2* | Conf. a) c) d) e) | 1.69 | 2.05 | 2.38 | 2.48 | 2.49 | 2.85 | 2.95 | 3.35 | 20.24 |
| | Conf. f) High | 2.57 | 2.29 | 3.98 | 4.00 | 4.17 | 4.45 | 3.27 | 3.34 | 28.07 |
| | Conf. g) Low | 0.95 | 0.92 | 1.39 | 1.54 | 1.28 | 1.22 | 1.96 | 2.16 | 11.42 |
| *Patient 3* | Conf. a) c) d) e) | - | - | 2.15 | 2.03 | 2.37 | 2.38 | 2.28 | 1.92 | 13.13 |
| | Conf. f) High | - | - | 3.51 | 3.26 | 4.9 | 4.55 | 3.28 | 3.31 | 22.81 |
| | Conf. g) Low | - | - | 0.63 | 0.62 | 0.86 | 0.93 | 0.86 | 1 | 4.9 |
| *Patient 4* | Conf. a) c) d) e) | - | - | 2.61 | 2.72 | 2.57 | 2.28 | 3.29 | 3.16 | 16.63 |
| | Conf. f) High | - | - | 1.61 | 1.45 | 1.17 | 1.04 | 7.71 | 7.43 | 20.41 |
| | Conf. g) Low | - | - | 0.51 | 0.58 | 0.51 | 0.49 | 1.24 | 1.29 | 4.62 |
| *Patient 5* | Conf. a) c) d) e) | - | - | 1.62 | 1.67 | 2.48 | 2.04 | 3.86 | 3.81 | 15.48 |
| | Conf. f) High | - | - | 2.96 | 3.47 | 3.38 | 3.23 | 5.55 | 5.26 | 23.85 |
| | Conf. g) Low | - | - | 0.9 | 0.97 | 1.32 | 1.32 | 2.82 | 2.84 | 10.17 |

Table 3.1: Detailed amount of cement ($cm^3$) injected in each screw position for all the configurations and patients.

## 3.4. Results

Stiffness calculated for every patient and every surgical alternative is summarised in *Table 3.2.* All analysed alternatives do show higher stiffness values than the reference situation for each case. The analysis of the reference situations show the lowest estimated stiffness in patient 1 (115.64 N/mm), while the highest value is shown by patient 3 (464.04 N/mm). This discrepancy in the absolute values of the stiffness impedes the direct comparison between cases; thus, the relative variation provided by each surgical alternative will be the main point of evaluation.

| Patient | Reference | Cement (PMMA) alone inclusion | Pedicle screws alone inclusion | Pedicle screws + cement inclusion | Pedicle screws (up position) + cement inclusion | Pedicle screws (down position) + cement inclusion | Pedicle screws + cement inclusion (high volume) | Pedicle screws + cement inclusion (low volume) |
|---|---|---|---|---|---|---|---|---|
| *1* | 115.64 | 115.98 (0.29%) | 124.51 (7.67%) | 124.85 (7.96%) | 128.15 (10.82%) | 121.97 (5.47%) | 125.33 (8.37%) | 124.51 (7.67%) |
| *2* | 286.62 | 287.52 (0.31%) | 288.27 (0.57%) | 299.79 (4.59%) | 309.94 (8.14%) | 303.08 (5.74%) | 313.59 (9.41%) | 297.31 (3.73%) |
| *3* | 464.04 | 466.61 (0.55%) | 563.10 (21.35%) | 575.87 (24.10%) | 583.08 (25.65%) | 694.49 (49.66%) | 590.33 (27.27%) | 519.02 (11.85%) |
| *4* | 432.23 | 439.53 (1.59%) | 490.16 (13.40%) | 533.87 (23.51%) | 517.46 (19.72%) | 496.60 (14.89%) | 527.84 (22.12%) | 507.94 (17.52%) |
| *5* | 429.81 | 432.99 (0.74%) | 536.96 (24.93%) | 543.01 (26.34%) | 509.31 (18.50%) | 575.86 (33.98%) | 544.08 (26.59%) | 536.40 (24.80%) |

Table 3.2: Stiffness calculated for every patient and surgical solution simulated, stiffness units N/mm. Numbers in brackets represented the stiffness variation %.

- Patient 1:

  This patient shows the lowest increase among all the analysed situations for the cement alone inclusion (0.29%). Screws inclusion obtains better results reaching an increase of 7.67% while the inclusion of cement slightly improves the stiffness (7.96%). However, changing the position of the screws to the upper position achieves the maximum surgical improvement with an increase of 10.82%. Cement volume variation does not show influence when reduced but shows a significant increase when higher volume is included (8.37%).

  **Best solution:** *Pedicle screws (up position)+ cement inclusion (10.82%)*

- Patient 2:

  Patient 2 shows a similar increase for cement alone inclusion (0.31%) and also shows the lowest improvement for screws alone inclusion (0.57%). In fact, is the case where surgical alternatives show the lowest stiffness increase (maximum 9.41% for pedicle screws + cement inclusion (high volume)).

  **Best solution:** *Pedicle screws + cement inclusion (high volume) (9.41%)*

- Patient 3:

  Patient 3 is one of the most clear examples of screws capability in this kind of surgeries. Their inclusion gets an increase of 21.35%, increasing until 24.10% when cement is included. This patient does also achieve the highest improvement in all the situations analysed, reaching a maximum of 49.66% increase fr the Pedicle screws (down position)+ cement inclusion. This patient shows the less noticeable damage on its 3D anatomical reconstruction. This could be a reason for the better correction of the injury with this procedures. Also it is the patient where the cement volume shows the highest influence, decreasing the stiffness to 11.85% when the volume reduced.

  **Best solution:** *Pedicle screws (down position) + cement inclusion (49.66%)*

- Patient 4:

  Patient 4 shows the best results for the cement alone inclusion (1.59%), doubling the following better result (0.74% in patient 5). Pedicle screws + cement inclusion reaches the maximum improvement (23.51%) in stiffness. This is the only case where the variation in screws position or cement volume inclusion does not improve the results.

  **Best solution:** *Pedicle screws + cement inclusion (23.51%)*

- Patient 5:

  Patient 5 shows the second best results for the surgical interventions. This case gets the best results for the screws alone inclusion (24.93%) and shows a clear influence of the screws position in its results. Reference screws position obtain 26.34% stiffness increase, but when screws are changed to upper position this values decreases to 18.50%. However, when changed to down position, the results improve until 33.98%. Cement volume variation does not seem to have a significant influence in this case.

  **Best solution:** *Pedicle screws (down position) + cement inclusion (33.98%)*

All five patients predicted an increase of the stiffness after the surgical procedures. Also, all cases showed pedicle screws fixation increasing the model stiffness, and the inclusion of cement augmentation improved the results of the pedicle screws inclusion alone. Variation of the volume of cement included affected differently to each patient. The same was observed for the change in the angle of the screws in the sacral insertion. Nevertheless, changes in the cement volume showed a lower effect on the model stiffness than changes in the screw angle fixation.

## 3.5. Discussion

Cement augmentation of pedicle screws in lumbosacral vertebrae improved screw fixation [39]. The results of the current study support our original hypothesis that cement augmentation increased the stiffness of the lumbosacral region (*Table 3.2*). Cement inclusion reflects a small improvement regarding the reference situation, but away from the substantial increase observed when screws were included in the model, adding cement to the screws fixation also increase the model stiffness (*Table 3.2*). Cement has also shown its relevance in the fixation success not only by helping in screws stability and pull out prevention [34, 56, 58], but also providing an extra stiffness increase which improves the results shown by the screws alone.

Cement volume variation does also show evidence of its direct influence in the stiffness increase (*Table 3.2*). Those cases where cement volume is higher computed high stiffness of the lumbosacral region. Only for patient 4, the estimated stiffness is reduced with respect to the initial cement volume considered. Similarly, configurations with lower cement volume showed a reduction in the lumbosacral stiffness. Wang et al., [170] analysed the effect of injecting 1 or 2.5 $cm^3$ of cement, resulting in an increased fixation strength when using 2.5 $cm^3$. It would be important to determine the optimal amount of cement to be injected not only in terms of improving the screw fixation but also considering associated problems to cement injection. The injection of excessive amounts of cement may result in thermal necrosis of bone tissue or even embolism, the minimum cement volume required to achieve a predefined level of augmentation should be determined [122, 123].

Sacral screw position has also demonstrated to be a key factor for the lumbosacral load distribution when screws and cement are included. In three of the five patients analysed (Patients 1, 3 and 5), the highest stiffness was estimated with the reference cement volume and using different screws positions: up position for patient 1, down position for patients 3 and 5 (*Table 3.2*). Orientation of a pedicle screw may play a role in the risk of screw loosening or screw breakage *in vivo*, and angulations in both the sagittal and axial planes can have an effect [108].

Post-surgical images were used to determine the real solution selected by the surgeons to solve the lumbosacral issue for every patient. In most cases, 4 of the 5 analysed cases, the solution selected was the screws + cement inclusion in reference position. This was the case for patients 1, 2, 3 and 5. However, in patient 4 the surgeon decided to include only one screw in L5 vertebra (and cement in the five screws). It was not clear if the surgical solution adopted for patient 4 was caused by the state of the vertebrae that prevents the usual 6 screws fixation solution.

The results presented here are quite promising. Nevertheless, the proposed methodology presents certain limitations. A reduced number of patients have been analysed. The results are quite interesting and can help the surgeon for the planning of the surgery. The FE model of the lumbosacral region did not consider the presence of the ligaments and muscles. There were no magnetic resonance images (MRI) in order to obtain the exact positioning of each ligament and muscle. These are key elements in the load distribution and stability of the spine, although when screws are included their influence is considerably lower due to the movement restriction imposed to the lumbosacral joints [129]. Another important limitation was the assumption of intervertebral discs as a homogeneous solid with uniform material properties, which affects to the disc behaviour in the simulations [64]. However, the study was focused in the load distribution along the spine to the sacral bone, the analysis of the intervertebral disc was out of the scope of the present work. Additionally, when spine fusion surgery is performed, intervertebral discs influence

is reduced due to the redistribution of the body loads that are mainly transmitted through the screws. Another limitation was that the same load value was considered for the five patients, when each patient had their own weight. Our main goal here was to simplify the boundary conditions and that all the patients were working under the same conditions. Finally, only different positions of the sacrum screws were simulated. In a future, additional screw configuration should be tested and include them in a patient-specific methodology for spinal surgery [108].

## 3.6. Study Conclusions

Summarizing, the main purpose and contribution of this study were to introduce patient-specific planning of lumbosacral surgery using the finite element method. Results can help in obtaining a better understanding on how the lumbosacral region is affected by the inclusion of cement and screws for osteoporotic bones treatment. Also, it can introduce new considerations, as the sacral screws position, amount of cement to be injected, etc. which can be analysed by the surgeon prior to perform a surgery. Thus, this methodology could be used as a pre-operative planning tool for lumbosacral surgery.

# Chapter 4

# Preoperative planning for preventing hip prosthesis dislocation

This third chapter will focus in analysing the parameters affecting hip dislocation after Total Hip Arthroplasty (THA) surgery. When hip is replaced due to bone degradation or failure and a prosthesis is implanted as a substitute of the native joint, the way this prosthesis is placed can affect the mobility of the patient and, in some cases, hip dislocation may happen that will require a new surgery.

For trying to predict the Range of Motion (ROM) of these prosthesis before dislocation, a 3D parametric finite element model will be used. It will be combined with Artificial Neural Networks (ANNs) to predict the moment when impingement and dislocation can occur. The combination of these two technologies (FE modelling and ANN) will be validated with several benchmark simulations and the computational tool will be applied to predict dislocation in several patient that have already suffered from hip dislocation

## 4.1. Biomechanics of the hip joint

Hip joint is located in the union between femur and iliac bone. In this area the head of the femur, with a hemispherical shape, is inserted in the acetabulum, a cup-shaped cavity in the low lateral region of the iliac bone (*Figure 4.1*). Both surfaces, femoral head and acetabulum, are covered by cartilages in order to avoid the bone to bone contact and to ease the joint rotation (*Figure 4.1*).

As occurs with all the joints in the human body, hip joint is reinforced by ligaments. In this case, hip counts with three extracapsular ligaments that cover the region from the acetabulum to the femoral greater trochanter (iliofemoral, ischifemoral and pubofemoral ligaments) and one intracapsular ligament that links the femoral head and the acetabulum. The musculoskeletal region is completed by muscles that cover the structure and are responsible of the rotation movements of the joint and the bones positioning. These muscles are responsible of several movements in the low extremities of the body. Different muscles groups connecting iliac and femoral bones induce external rotation, internal rotation, extension, flexion, adduction or abduction of the legs.

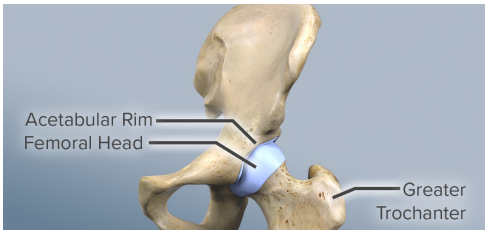


Figure 4.1: Hip joint bone structure [5].

The main function of this joint is to support the weight of the body both when moving (dynamic) and when standing (static). Also, it has a key role in the balance of the whole musculoskeletal structure, and therefore the whole body; and in the pelvic rotation. Hip influence in pelvic rotation is combined with the action of the core muscles, specially abdominal muscles, and the iliopsoas.

When hip joint is affected by some severe degenerative injuries (as cartilages degradation) of bone damages (as femoral neck fractures), the joint is usually replaced by a titanium prosthesis through a total hip arthroplasty (THA) surgical procedure. This way, a prosthesis consisting of two elements is placed in the joint location replacing the femoral neck and head, and covering the acetabular cavity (*Figure 4.2*).

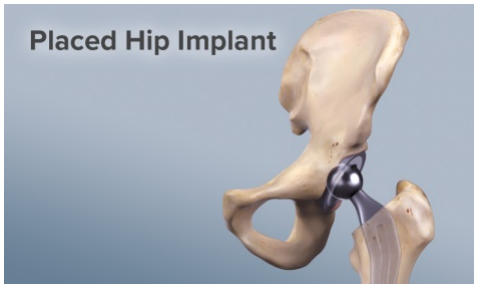


Figure 4.2: Hip prosthesis placement [6].

## 4.2. Clinical interest

Dislocation is a significant concern in total hip arthroplasty (THA) [99]. Bozic et al. [23] previously reported that instability had surpassed mechanical aseptic loosening as the most common cause of revision surgery. A patient who undergoes hip dislocations has reduced mobility, which directly affects the quality of life and increases the costs to the health system [24]. Management of THA instability remains a surgical challenge and represents a multifactorial problem that includes the patient condition, surgical technique, implant component design and orientation, bone quality, and surrounding soft tissues [16, 24, 59, 76, 82, 109, 155]. Guo et al. [59] remarked that many risk factors were identified for the dislocation following revision THA and that these factors were still undergoing controversial.

Many biomechanical studies based on the finite element (FE) method have evaluated the dislocation stability of different implant designs [27, 44, 45, 46, 49, 59, 77, 104, 137, 159]. All previous studies showed an added value with respect to a rigid body dynamics analysis. Elkins et al. [45] performed a dynamic FE analysis to clarify the different consequences of bone-on-bone versus implant femoral neck and acetabular cup impingement (hardware impingement), and they concluded that bone-on-bone impingement was less prone to dislocation than hardware impingement. Large head diameters have been shown to prevent dislocation [49, 77]. Scifert et al. [137] described the relationship between range of movement (ROM) and dislocation and showed that increasing the femoral head size increased the ROM. Terrier et al. [159] performed a FE biomechanical analysis to compare a standard implant, a constraint implant and a dual mobility implant. Compared with the standard and constant implants, the dual mobility implants showed excellent performance in extending the ROM [44, 59, 159]. Several previous works established a *safe zone* with an optimal implant position and head size that reduced the risk of dislocation [49, 77]. Although, different reviews on this topic claimed that the establishment of a *safe zone* was not enough to prevent THA dislocation [103, 138, 160]. Many different approaches can be tested using the FE method. Although FE analyses present the disadvantage of high computational cost, when a real-time response is required. The main objective of this work is to use a machine learning technique, artificial neural network (ANN) to rapidly and effectively predict the impingement and dislocation of THA. ANNs have been previously been used to predict atheroma plaque rupture [30]; femur [61] and tibia [62] loads; and damage accumulation in cancellous bone [68]. Therefore, the ultimate goal of this work is to develop a real-time computational tool to predict the ROM allowed after THA before impingement and dislocation. The tool will quantify the risk of dislocation for certain positions of the acetabular cup and for various designs of the prosthetic head. The methodology used to create this computational tool combines a 3D parametric FE model of the THA [49] and a machine learning technique (ANN). A parametric tool based on machine learning techniques that is used to predict the ROM after THA has not been previously conducted. The tool may provide to the clinicians with optimal prosthesis design and acetabular cup position to reduce post-op risk of dislocation. Additionally, the tool may allow to compare different position alternatives prior to the surgery process showing results of the suitability of each position considered by the surgeon.

## 4.3. Material and Methods

### 4.3.1. 3D Parametric finite element model

A parametric FE model of a hip prosthesis was previously developed [49] to simulate impingement and dislocation for different femoral head sizes, acetabulum abduction ($\alpha$) and anteversion ($\beta$) angles (*Figure 4.3*). Impingement is the instant when the acetabulum and the femoral bone get in contact and the dislocation is produced when the femoral head gets out of its position inside the acetabulum. The FE model was developed with Abaqus/CAE v6.16 (Dassault Systemes, Suresnes, France) and consisted of two parts: the acetabulum and the femoral head and stem. The dimensions and geometry of the implant were obtained from a standard 37.5 mm-offset Exeter®cemented prosthesis (Stryker Ltd., Newbury, United Kingdom) with a collarless, smooth, polished and tapered stem [28]. The acetabulum was modelled as a deformable solid with material properties that correspond to ultra-high-molecular-weight polyethylene (UHMWPE) (elastic modulus ($E$) of 940 MPa, Poisson's ratio of $\mu$=0.3 and yield strength of 26.26 MPa to simulate the plastic properties of polyethylene) [49, 77, 167]. Due to the stiffness differences between the metal components of the femoral head and stem and the polyethylene of the acetabulum, the femoral head and stem were modelled as rigid parts and their deformations were not considered. The mesh size was approximately 1.5 mm. A sensibility analysis was conducted by Ezquerra et al. [49]. Bone and soft tissue were not considered in the simulation. A tangential isotropic contact model was defined between the femoral head and neck (master surfaces) and the inner hemisphere of the acetabulum componentand the outer ring (slave surface). A friction coefficient of 0.038 was defined [49, 114]. Two types of movements were simulated until impingement and dislocation of the components occurred (*Figure 4.3*): external extension (EE) and internal flexion (IF). EE corresponds to the standing position of the patient with an external rotation of the hip joint, whereas IF represents the seated position of the patient with an internal rotation of the hip joint (typical leg crossing manoeuvre) [104]. The nodes of the external acetabulum component were fixed to simulate its complete fixation. All rotations were applied with respect to the reference point in the centre of the head (*Figure 4.3*). The reader is referred to Ezquerra et al. [49] for further details.

### 4.3.2. Source data

Using the parametric FE model (*Section 4.3.1*) different simulations were run. The inputs for each simulation were the femoral head sizes (22, 28, 32, 36 and 44 mm), acetabulum abduction angles (a) (20, 30, 40, 50, 60 and 70º) and acetabular anteversion angles (b) (0, 5, 10, 20, 30 and 40º) (*Figure 4.3*). Therefore, 216 simulations were run for each type of movement (EE and IF). From each simulation, we obtained the maximum ROM allowed before impingement or dislocation.

### 4.3.3. Artificial Neural Networks ANNs

ANNs are mathematical algorithms based on brain functioning that try to mimic the behaviour of the neurons [95]. A particular ANN is the multilayer perceptron (MLP). The main structure of the MLP includes an input layer, a hidden layer and an output layer (*Figure 4.4*). Each one of these layers consists of a set of basic units called neurons. ANNs also include a training algorithm that adjusts the weights and other parameters based on the input and output data provided to the network as well as the values that the network predicts (*Figure 4.4*). A commonly used training

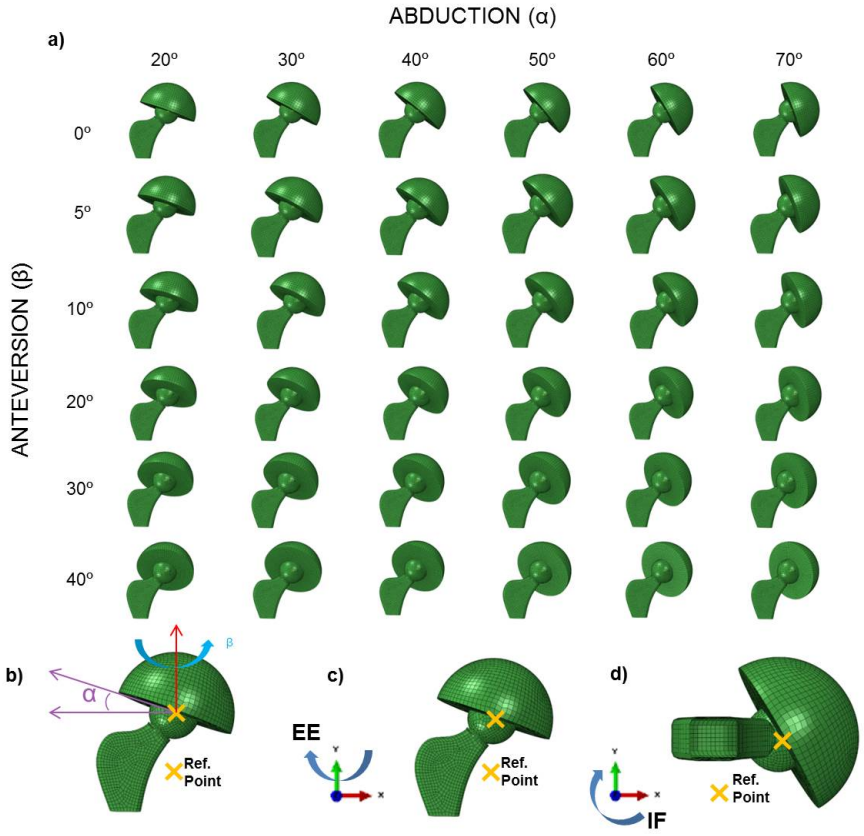


Figure 4.3: (a) Positions considered in the FE analysis to obtain the training data, (b) reference angles, (c) external extension (EE) rotation, and (d) internal flexion (IF) rotation.

algorithm in the MLP is the back-propagation algorithm [20], which was chosen for training our network. The back-propagation algorithm uses supervised learning, which means that we provide the algorithm with examples of the inputs and outputs that we want the network to compute, and then the error (the difference between actual and expected results) is calculated. The main goal of the back-propagation algorithm is to minimise this error. The training begins with random weights, and the goal is to adjust them so that the error will be minimal.

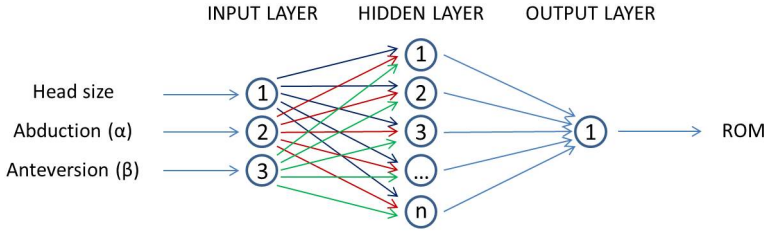


Figure 4.4: ANNs configuration in the study.

The size of the input layer was determined by the number of input variables considered (*Figure 4.4*). These input variables were the femoral head size, abduction angle (a) and anteversion angle (b) (*Section 4.3.2*), which resulted in a three-neuron layer. The hidden layer was analysed and defined independently for each case. The output layer consisted of a single neuron that determined the maximum angle of the movement predicted, which is what delimits the ROM of the hip joint (*Section 4.3.2*). Several input connections along with the corresponding weights regulate the input signal intensities. An activation function that focuses on the input signals is needed. Additionally, a transfer function should be chosen for the output of the neuron as a function of the input signals. ANNs can be configured with different transfer functions on each layer to generate their outputs. Laudani et al. [81] performed a comprehensive review on the problem of choosing a suitable function for the hidden layer. Among the different transfer functions, the most usual transfer functions are logistic sigmoid (logsig), tangent sigmoid (tansig) and linear (purelin) (*Figure 4.5*). These functions as well as $a$ and $n$ as the output and the input data, respectively, are explained below.

- *Logistic sigmoid (logsig)*

  The logistic sigmoid generates an output between 0 and 1 according to equation 4.1 , and input data range from negative to positive values.

$$a = \frac{1}{1 + e^{-n}} \tag{4.1}$$

- *Tangent sigmoid (tansig)*

  The tangent sigmoid, which is an alternative to logsig in multilayer networks, generates an output between -1 and 1 (*eq 4.2*).

$$a = \frac{e^{n} - e^{-n}}{e^{n} + e^{-n}} \tag{4.2}$$

- *Linear transfer function (purelin)*

  The linear transfer function (purelin) generates an output with a correlation of $a = n$.

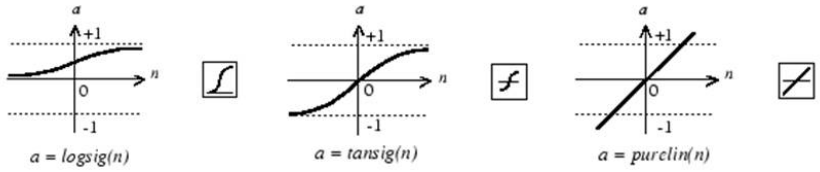


Figure 4.5: Transfer functions considered in the study.

A 10-fold cross-validation process was implemented to minimise the influence of the test set selection. In this chapter, we randomly divided the data into two groups: 90% of the data were used to train the model and 10% of the data were used to test the model [61].

Four independent ANNs were configured for impingement (i.e., the first collision between the acetabulum and femoral head/neck) and the dislocation (maximum ROM allowed) of the EE and IF movements. Different combinations of the previously defined transfer functions were tested to find the optimal configuration for each ANN (*Section 4.4*). The ANNs were implemented in MATLAB R2018b (MathWorks, Massachusetts, USA).

## 4.4. Method performance and validation

To choose the best ANN configurations (transfer functions- *section 4.3.3*) and then validate our proposed ANNs, different analyses were performed.

**ANN performance and transfer function selection**

The optimal configuration for each ANN was determined through an analysis of the performances of different transfer functions (*Figure 4.5*) and a different number of neurons in the hidden layer (between 2 and 70 neurons) (*Figure 4.4*). For this section, the results of the 216 simulations for each type of movement (EE and IF) (*Section 4.3.3*) were used. The configuration for each case was selected based on the absolute error (AE) (*Equation4.3*), the correlation coefficient (RSQ) (*Equation 4.4*) and the time required to complete the training [61]. Five independent analyses were performed for each option. These repetitions ensure the stability of the selected configuration (standard deviation).

$$AE = \hat{\theta} - \theta \tag{4.3}$$

$$RSQ = \frac{\sigma_{\hat{\theta}\theta}}{\sigma_{\hat{\theta}}\sigma_{\theta}} \tag{4.4}$$

where $\hat{\theta}$ is the predicted ROM, $\theta$ is the real ROM, $\sigma_{\hat{\theta}\theta}$ is the covariance, and $\sigma_{\hat{\theta}}$ and $\sigma_{\theta}$ are the standard deviations. Results obtained for each configuration were summarised in Section 4.5.1.

**$1^{st}$ Validation: Parametric FE cases**

Once the ANNs were configured, how accurate were ANN predictions compare with the values obtained in FE simulations was measured. From the work of Ezquerra et al. [49], different combinations (23 cases) of femoral head sizes (28, 32 and 35 mm), acetabulum abduction angles (a) (25, 40 and 60º) and acetabular anteversion angles (b) (0, 15, 25º) were considered. These input value combinations were different from the source data (*Section 4.3.2*) used to train the ANNs. Results obtained were summarised in Section 4.5.2. Additionally, a paired sample T-test was performed for each analysed case to verify the ANN prediction with respect to the FE simulation results. The statistics (p-value and Pearson correlation coefficient) were calculated using the data analysis module in Excel (Microsoft Corporation, Washington, USA).

**$2^{nd}$ Validation: Patient-specific cases**

After the computational validation with FE data, ANNs were also used to predict the ROM before impingement and dislocation in five patients who already had suffered hip dislocation after THA. The data for these five patients are shown in *Table 4.1*. The abduction and anteversion angles were measured from their corresponding computed tomography (CT) scans after the THA surgical procedure, where the position of the prosthesis was analysed.

| Patient | Age (Yr) | Gender | Mass (Kg) | Head Size (mm) | $\alpha$ (°) | $\beta$ (°) |
|---|---|---|---|---|---|---|
| *PS1* | 86 | M | 70 | 28 | 46,69 | 18,99 |
| *PS2* | 91 | F | 60 | 28 | 38,8 | 20,81 |
| *PS3* | 66 | F | 86 | 32 | 62 | 42 |
| *PS4* | 72 | F | 95 | 32 | 31,77 | 22 |
| *PS5* | 80 | M | 96 | 32 | 48,59 | 0 |

Table 4.1: Patient-Specific data included for the ANN final validation. F=Female; M=Male; $\alpha$=abduction angle; $\beta$=anteversion angle.

## 4.5. Results

### 4.5.1. ANN performance and transfer function selection

Based on an analysis of the different possible combinations of transfer functions and the number of neurons in the hidden layer (*Section 4.3.2*), the final configuration for each of the ANNs was established (*Table 4.2*). The time required for completing the training and testing of each ANN is also indicated in Table 4.2. The absolute error of the selected combinations was lower than 6.5°, and the RSQ was close to 1 for all combinations. The mean time required for their training was less than 30 seconds.

| Case | Ext-Ext Imp. | Ext-Ext Lux. | Int-Flex Imp. | Int-Flex Lux. |
|---|---|---|---|---|
| *HL Transfer Function* | Hyper. Tangent Sigmoid | Log-Sigmoid | Hyper. Tangent Sigmoid | Hyper. Tangent Sigmoid |
| *HL Neurons* | 3 | 8 | 7 | 9 |
| *OL Transfer Function* | Log-Sigmoid | Linear | Linear | Hyper. Tangent Sigmoid |
| *Abs. Error* | 4.57 | 6.12 | 3.67 | 4.41 |
| $\sigma$ *(Abs Err.)* | 4.733 | 6.043 | 2.907 | 2.576 |
| *RSQ* | 0.930 | 0.823 | 0.946 | 0.900 |
| $\sigma$ *(RSQ)* | 0.043 | 0.101 | 0.031 | 0.031 |
| *Time (s)* | 8.69 | 25.61 | 24.70 | 26.89 |
| $\sigma$ *(Time)* | 0.66 | 1.23 | 1.33 | 3.46 |

Table 4.2: Summary of the absolute error (AE) and the correlation coefficient (RSQ) of the different ANNs (EE=External extension; IF=Internal flexion; Imp=Impingement; Dis=Dislocation; and $\sigma$=Standard deviation).

### 4.5.2. $1^{st}$ Validation: Parametric FE cases

Results from the parametric FE model simulations [49] and the ANN predictions (*Section 4.4*) were detailed in Table 4.3. A summary was showed in Table 4.4. The mean error obtained for the ANNs was lower than 5.5° (*Table 4.4*), and the approximated maximum standard deviation was 5°.

The statistics show a significant difference ($p<0.05$ – *Table 4.4*) for both the impingement and luxation IF cases; nevertheless, considering the mean error and the standard deviation for these cases, the stability of the tool predictions can be assured (*Table 4.4*). The EE cases had a slightly higher standard deviation but significant differences were not observed ($p>0.05$), which implies a good correlation between the simulated ROM and the ANNs prediction.

### 4.5.3. $2^{nd}$ Validation: Patient-specific cases

Based on previously developed ANNs, the predicted ROMs for the five patients (*Table 4.1*) are presented in *Table 4.5*. Considering that all patients had already suffered hip prosthesis dislocation before the study development, the ROM limitation of each patient was determined by the lowest value obtained between the EE and IF results. Impingement of PS3 was predicted for an ROM of 33.74º and dislocation was predicted for an ROM of 43.64º under EE. PS1, 2, 4 and 5 predicted impingement and dislocation for IF (*Table 4.5*).

| Case | Mean error | $\sigma$ | P-value | Pearson Coefficient |
|---|---|---|---|---|
| *EE Imp.* | 4.547 | 4.714 | 0.9750 | 0.9770 |
| *EE Lux.* | 5.177 | 5.112 | 0.7665 | 0.9661 |
| *IF Imp.* | 3.667 | 2.906 | 0.0007 | 0.9834 |
| *IF Lux.* | 4.408 | 2.576 | 0.0141 | 0.9726 |

Table 4.4: Summary of the results and statistics obtained for the $1^{st}$ validation with 23 computational cases (EE=External extension; IF=Internal flexion; Imp=Impingement; Dis=Dislocation; and $\sigma$=Standard deviation).

| | EE Imp. | | EE Lux. | | IF Imp. | | IF Lux. | |
|---|---|---|---|---|---|---|---|---|
| **Patient** | **ROM** | **Angle (º)** | **ROM** | **Angle (º)** | **ROM** | **Angle (º)** | **ROM** | **Angle (º)** |
| *PS1* | 0.365 | 65.71 | 0.414 | 74.44 | 0.168 | 30.30 | 0.242 | 43.54 |
| *PS2* | 0.362 | 65.18 | 0.402 | 72.35 | 0.128 | 22.97 | 0.204 | 36.65 |
| *PS3* | 0.187 | 33.74 | 0.242 | 43.64 | 0.366 | 65.89 | 0.396 | 71.23 |
| *PS4* | 0.379 | 68.25 | 0.408 | 73.42 | 0.113 | 20.40 | 0.177 | 31.79 |
| *PS5* | 0.516 | 92.91 | 0.556 | 100.09 | 0.085 | 15.38 | 0.155 | 27.89 |

Table 4.5: Predicted ROM for each patient-specific analysis. Imp=Impingement; Dis=Dislocation.

| | | | | External-Extension Impingement | | | External-Extension Luxation | | | Internal-Flexion Impingement | | | Internal-Flexion Luxation | | |
|---|---|---|---|---|---|---|---|---|---|---|---|---|---|---|---|
| **Case** | **Head Size (mm)** | $\alpha$(º) | $\beta$(º) | **Real ROM(º)** | **Predicted ROM(º)** | **Abs. Error(º)** | **Real ROM(º)** | **Predicted ROM(º)** | **AE(º)** | **Real ROM(º)** | **Predicted ROM(º)** | **Abs. Error(º)** | **Real ROM(º)** | **Predicted ROM(º)** | **AE(º)** |
| *1* | 28 | 60 | 25 | 86.400 | 77.796 | 8.604 | 92.448 | 96.383 | 3.935 | 18.000 | 22.898 | 4.898 | 54.000 | 61.595 | 7.595 |
| *2* | 28 | 25 | 0 | 61.200 | 62.150 | 0.950 | 96.210 | 103.507 | 7.297 | 19.800 | 28.043 | 8.243 | 0.000 | 1.701 | 1.701 |
| *3* | 36 | 25 | 25 | 93.600 | 81.477 | 12.123 | 78.696 | 64.224 | 14.472 | 0.000 | 1.519 | 1.519 | 21.780 | 26.809 | 5.029 |
| *4* | 28 | 25 | 15 | 54.000 | 56.330 | 2.330 | 77.940 | 75.754 | 2.186 | 0.000 | 0.001 | 0.001 | 24.336 | 17.445 | 6.891 |
| *5* | 28 | 25 | 25 | 145.116 | 152.674 | 7.558 | 62.658 | 62.932 | 0.274 | 37.800 | 42.100 | 4.300 | 26.568 | 25.179 | 1.389 |
| *6* | 28 | 40 | 25 | 86.400 | 85.672 | 0.728 | 91.710 | 83.274 | 8.436 | 41.400 | 45.829 | 4.429 | 35.784 | 40.877 | 5.093 |
| *7* | 36 | 40 | 15 | 100.800 | 100.637 | 0.163 | 97.272 | 103.176 | 5.904 | 9.000 | 8.927 | 0.073 | 30.600 | 34.802 | 4.202 |
| *8* | 36 | 25 | 15 | 59.850 | 63.893 | 4.043 | 97.272 | 83.094 | 14.178 | 0.000 | 0.000 | 0.000 | 23.418 | 19.631 | 3.787 |
| *9* | 36 | 25 | 0 | 96.210 | 92.878 | 3.332 | 76.428 | 76.460 | 0.032 | 45.000 | 48.363 | 3.363 | 0.000 | 3.849 | 3.849 |
| *10* | 32 | 60 | 25 | 64.800 | 66.627 | 1.827 | 94.626 | 84.522 | 10.104 | 3.600 | 11.316 | 7.716 | 53.964 | 62.630 | 8.666 |
| *11* | 32 | 25 | 0 | 70.200 | 67.038 | 3.162 | 68.508 | 68.525 | 0.017 | 44.334 | 54.583 | 10.249 | 0.000 | 4.010 | 4.010 |
| *12* | 36 | 40 | 25 | 68.400 | 68.048 | 0.352 | 65.628 | 64.560 | 1.068 | 12.600 | 19.198 | 6.598 | 36.000 | 42.176 | 6.176 |
| *13* | 32 | 40 | 15 | 73.134 | 70.141 | 2.993 | 128.718 | 148.058 | 19.340 | 30.600 | 32.127 | 1.527 | 33.282 | 34.926 | 1.644 |
| *14* | 36 | 60 | 25 | 77.400 | 78.795 | 1.395 | 113.670 | 115.701 | 2.031 | 9.000 | 8.636 | 0.364 | 59.742 | 62.157 | 2.415 |
| *15* | 28 | 60 | 15 | 81.000 | 73.952 | 7.048 | 101.898 | 103.957 | 2.059 | 18.000 | 15.948 | 2.052 | 48.114 | 54.043 | 5.929 |
| *16* | 28 | 45 | 0 | 54.000 | 53.893 | 0.107 | 74.088 | 69.076 | 5.012 | 3.600 | 5.723 | 2.123 | 25.344 | 22.273 | 3.071 |
| *17* | 32 | 25 | 25 | 128.718 | 143.118 | 14.400 | 69.030 | 75.014 | 5.984 | 30.600 | 35.637 | 5.037 | 25.956 | 26.689 | 0.733 |
| *18* | 32 | 60 | 15 | 54.000 | 50.822 | 3.178 | 145.116 | 149.049 | 3.933 | 21.600 | 26.156 | 4.556 | 51.390 | 55.422 | 4.032 |
| *19* | 32 | 40 | 25 | 59.400 | 62.544 | 3.144 | 145.350 | 141.158 | 4.192 | 18.000 | 12.591 | 5.409 | 38.934 | 42.262 | 3.328 |
| *20* | 36 | 60 | 15 | 57.942 | 56.986 | 0.956 | 61.020 | 63.779 | 2.759 | 55.800 | 57.340 | 1.540 | 51.534 | 54.851 | 3.317 |
| *21* | 28 | 40 | 15 | 68.400 | 58.349 | 10.051 | 64.296 | 61.949 | 2.347 | 14.400 | 18.909 | 4.509 | 35.694 | 33.091 | 2.603 |
| *22* | 28 | 35 | 0 | 117.000 | 132.766 | 15.766 | 65.700 | 66.375 | 0.675 | 0.000 | 0.000 | 0.000 | 0.000 | 11.835 | 11.835 |
| *23* | 32 | 25 | 15 | 91.800 | 92.177 | 0.377 | 69.318 | 66.483 | 2.835 | 45.000 | 50.835 | 5.835 | 23.580 | 19.492 | 4.088 |
| ***Med. Error*** | | | | | | 4.547 | | | 5.177 | | | 3.667 | | | 4.408 |
| $\sigma$ | | | | | | 4.714 | | | 5.112 | | | 2.906 | | | 2.576 |

Table 4.3: Results obtained for the 23 finite element validation cases simulated. $\alpha$ = Abduction angle; $\beta$ = Anteversion angle; AE=Absolute error; $\sigma$ = Standard deviation.

## 4.6. Discussion

The results show that using a 3D parametric FE model with an ANN represents a powerful tool for estimating the ROM after THA under different prosthesis designs (head size and acetabular cup orientation) and for different clinical manoeuvre.

The ANN performance AEs (for training and testing) were lower than 6.5º (*Table 4.2*). A comparison of the ANN estimations with the results of previous FE simulations [49] showed that the calculated AEs were less than 5.5º (*Tables 4.3* and *4.4*). Several experimental and clinical studies have analysed the ROM after THA under different manoeuvres. Kouyoumdjian et al. [78] determined that the standard ROM for EE could be set to 37.9 ± 8.4º. Our computational tool estimated that a ROM of 33.74º for PS3 was predictive of impingement, and this result could justify why PS3 suffered THA dislocation. A ROM of 37.9º was not observed [78]. Nadzadi et al. [104] determined that the standard ROM for IF could be set to approximately 50º. Therefore, our computational tool for the other patients (PS1, PS2, PS4 and PS5) estimated an ROM lower than 50º for impingement and subsequent dislocation (see *Table 4.5*). These results justified the utility of the proposed computational tool.

In previous studies, Ezquerra et al. [49] found a *safe zone* when the acetabulum component was placed at a 40-60º abduction angle and a 15-25º anteversion angle. These values were similar to those reported by Kluess et al. [77] (45º abduction and 15-30º anteversion), Pedersen et al. [114] (at least 40º abduction and 10º anteversion), Lewinnek et al.[84] (40º±10 abduction and 15º±10 anteversion), Biedermann et al. [19] (45º±10 abduction and 15º±10 anteversion) or Reina et al. ([124]) (40-50º abduction and 15-30º anteversion). Fessy et al. [52] found evidence that implanting the cup in 30º to 50º inclination has a major impact on preventing dislocation. The position of the acetabulum component in the 5 patients analysed (*Table 4.1*) showed that the prosthesis was placed between the values of this predefined *safe zone* only in the case of PS1. Seagrave et al. [138] performed a systematic reviewed to describe the different methods for measuring cup placement, target zones for cup positioning and the association between cup positioning and dislocation following primary THA. They concluded that the establishment of a safe zone based on the cup positioning and orientation was not enough to prevent THA dislocation (Seagrave et al. [138]; Murphy et al. [103]; Tezuka et al. [160]). Additionally, Tezuka et al. [160] established that standard *safe zones* were outside the functional safe zone, identifying a potential reason hips dislocate despite leaving *safe zone* cup angles. Therefore, our computational tool could be a complementary tool to traditional *safe zone* theories. PS1 could be one of this *safe zone* failures.

The proposed computational tool based on an ANN trained and tested with data obtained from FE simulations has the potential for use in predicting the ROM in real patients with an error lower than 5.5º, which may help clinicians when identifying the most suitable position of the prosthesis prior to the surgical intervention. Easiness for ANNs training and low time required for obtaining results allow the revision of multiple options (design and cup orientations) with low computational cost, which could lead to a light implementation within minimum technical requirements.

Although the results obtained in this work were quite promising, the computational tool is based on several simplifications. The evaluation of more patient-specific cases could help to improve the accuracy of the tool and its validation. Additionally, acetabular polyethylene wear was not considered in the simulations, because instability created by prosthesis deterioration was not the main goal in this initial study but the direct consequences of the movement that a patient can carry

out. In the future, acetabular polyethylene wear could be simulated by incorporating a formulation based on the Archard wear law (Kruger et al. [79]). Elkins et al. [44] incorporated in their simulations the capsule's contribution to THA stability. In our study, this factor was neglected. A parametric model that considers the capsule could be implemented and its parameters could be incorporated in the ANNs. Another limitation was the neglect of bone-on-bone impingement [44], although impingement between the implant femoral neck and the acetabular cup remains the most common dislocation failure [44]. This study has not considered pelvic tilt factor, which relevance could be analysed and considered as a parameter for future developments of the predictive tool [103, 71]. Finally, the outer acetabulum component had a constant size (52 mm), and this consistency could be easily incorporated in a future parametric model and then into the computational tool based on the ANN.

## 4.7. Study Conclusions

The combination of a 3D parametric FE model of a THA and an ANN is a useful computational tool to predict the ROM after THA and to prevent dislocation. Using these kind of methodologies, complex processes can be simplified through ANNs configurations achieving low errors in the prediction. Clinically, the computational tool will allow the analysis of different alternatives for the prosthesis placement prior to the surgery. This methodology could be implemented in clinical practice to avoid time-consuming 3D FE analyses and it could be a complementary tool to well-defined *safe zones* previously established.

# Chapter 5

# Preoperative planning for syndesmotic injury correction

This chapter will study the surgical procedure for tibia-fibula bone fixation in the ankle joint when syndesmotic injury occurs. This injury is one of the most difficult to diagnose and its surgery implies the inclusion of a fixation element going though both bones and preventing their separation.

With this aim, an anatomical finite element model of an injured ankle joint taken from a real patient will be used for the inclusion of the different surgical solutions. The models will be simulated using finite element analysis (FEA) and compared with the healthy and injured state in order to stablish the influence of each solution in the patient recovery.

## 5.1. Biomechanics of the ankle joint

In chapter 2 the anatomy of the knee was analysed showing its role in the stability of the biomechanical structure of the body and the weight bearing. Ankle, as the following joint in the leg for the loads transmission, continues the role of knee in both aspects.

Ankle is also a complex joint that stands the load of the whole body while providing stability and being the first point of loads transmission when walking. This transmission can be affected not only by the load of the body but also by the surface where the foot is set, what affects the whole stability of the anatomy.

Its main structure is formed by three bones: tibia, fibula and talus (*Figure 5.1*). Inside this joint, and due to the loads distribution in the human anatomy, tibia-talus articulation bears most of the weight transmission. The lower region of the tibia presents a cavity that helps in the inclusion of the talus bone and facilitates the joint stability. Both tibia and talus contact surfaces are covered by cartilage avoiding the bone-to-bone contact. In contrast to the knee cartilage seen in chapter 2, this cartilage is thinner and more uniform. Fibula has a similar length to the tibia and its main role is the stabilisation of the ankle joint. It is in contact with both tibia and talus, but the weight transmitted through it is low compared with the tibia. Fibula and tibia articulation lacks cartilage and its strongly connected by fibrocartilage, what makes it a joint with very limited motion.

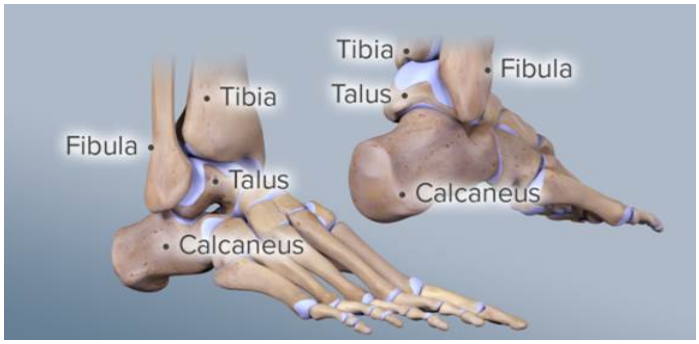


Figure 5.1: Bones in the ankle joint [7].

These bones, as occurs in all joints in the human body, are connected through ligaments (*Figure 5.2*). The main ligaments that help in the union of these three bones are the following:

- Anterior Tibiotalar Ligament (ATTL) and Posterior Tibiotalar Ligament (PTTL). These two ligaments connect the tibia and the talus in the anterior and posterior regions respectively.
- Anterior Talofibular Ligament (ATFL) and Posterior Talofibular Ligament (PTFL). These two ligaments have the same role than the previous ones but in this case connecting the fibula and the talus.
- Anterior Tibiofibular Ligament (ATL) and Posterior Tibiofibular Ligament (PTL). As in the prior cases, these two ligaments connect in the anterior and posterior regions of the tibia and the fibula.
- Interosseous Membrane (IM). This membrane connects the fibula and the tibia along their whole extension and provides stability to this joint.


Figure 5.2: Ligaments in the ankle articulation [8].

Anterior Tibiofibular Ligament (ATL), Posterior Tibiofibular Ligament (PTL) and Interosseous Membrane (IM) form what is denominated the ankle syndesmosis, that refers to the connection between tibia and fibula. ATL restricts the external rotation of the fibula while PTL prevents the posterior displacement. As mentioned before, IM stabilises this structure. These are the affected elements when a syndesmosis injury occurs.

## 5.2. Clinical Interest

Recent studies show that tibiofibular syndesmosis injuries are an underdiagnosed issue usually camouflaged by the habitual symptoms of ankle sprains [55]. Between 1 and 11% of these sprains are actually tibiofibular syndesmosis injuries, being especially significant in sports activities that imply high impact [146, 164]. This kind of injuries can be caused along with a fibular fracture or just as a consequence of an external rotation of the ankle where the talus expands the cavity where is located and leading the tibiofibular syndesmosis to a stress situation that may worsen by the foot external rotation [55, 178]. Among the regions susceptible to suffer any damage when an isolated syndesmotic injury occurs, anterior tibiofibular ligament and intraosseous membrane are the most usually affected ligaments by the injuries leading to a partial or, in the case of the anterior ligament, total rupture of the ligament [55, 121, 133].

Different surgical procedures can be considered when instability occurs in the syndesmosis sprain [35, 55]. Traditionally, screws inclusion has been the most common solution [121, 150]. In this procedure, screws are placed as a union between the fibula and the tibia drilling through the complete fibular bone and partially (tricortical fixation) or totally (quatricortical fixation) the tibial bone [133]. As stability element for the screw inclusion, a plate is also fixed with sorter screws to the fibular bone. This fixation is usually performed including one or two screws in the tibiofibular union. The type of screws used in this fixation uses to be titanium, with the subsequent surgical procedure for being removed; but in the last years has also appeared the option of including bioabsorbable screws, to avoid the second surgical procedure [121]. Suture button procedure has gained relevance as an alternative for the screws inclusion [126, 174]. In the suture button process the fixation rope or ropes, depending on the selected solution, are also placed by drilling both bones, and are placed with the use of small plates where the ropes are tied. When placed in the desired position, the ropes are tightened; partially restraining the relative displacement of the bones [174]. This surgical procedure allows a less limited motion of the joint and in most cases is not removed after the surgery unless the patient reports any issue derived from its use [113]. Also, the absence of titanium in the intraosseous fixation allows obtaining better results in posterior scans required in the affected region [174]. The comparison between these two techniques has been previously analysed in several clinical or cadaveric studies [31, 80, 105, 107, 120, 133, 136, 175, 180], but there is not a clinical consensus about the higher reliability of one technique over the other.

Previous biomechanical studies in cadaveric specimens gave a good overview of syndesmotic injuries and the different surgical procedures. Although, it is difficult to compare their findings among studies and quantify stresses, displacements, etc. Additionally, they are costly, time-consuming and some cases inefficient. To solve this problem, computational tools based on the finite element method may help to predict the biomechanical behaviour of the joint. The usefulness of Finite element (FE) models in biomechanical analyses has been widely proof for the simulation of patient-specific ankle joints or the prediction of mechanical function [86]. This methodology has been also used for analysing surgical solutions for the tibiofibular syndesmosis injuries [47, 48, 88, 89, 165]. Liu et al. [88, 89] demonstrated that a transverse syndesmotic screw can effectively control excessive abnormal activity of the distal tibia and fibula after tibiofibular syndesmosis injury. Screw fixation also affected to the physiological normality of the joint, leading to decreased magnitude of motion at the lower extremes of the tibia and fibula, reduced contact forces be-

tween bones and increased stress on the crural interosseous membrane. Serhan et al. [47] compared different screw sizes, number of cortices and number of screws needed. They concluded that quatricortical application of 3.5-mm single screws and tricortical application of 3.5-mm double cortical screws were not good choices for syndesmosis fixation. Verim et al. [165] observed that syndesmosis fixation at the level of 30-40 mm above tibiotalar joint had advantages with regard to stress in screws in comparison with other evaluated levels. Finally, Serhan et al. [48] investigated which geometric screw parameters played key roles in stresses that occur in screws used for syndesmotic fixation. None of previous FE studies compare the performance of screws against suture buttons which are growing in popularity [113]. Additionally, the performance of suture buttons using a finite element analysis has not been previously studied.

Therefore, the main goal of this study is to compare the biomechanical behaviour of different syndesmotic fixations: screws (diameter, number of cortices, number of screws and distance between screws) versus suture buttons (single, double parallel and double divergent) with different pretension forces. Titanium screws will be considered. Suture button with the characteristics of the Tightrope® implant (Arthrex) will be simulated. For a better comparison between the surgical solutions and the effect of this injury, the study will include the analysis of the healthy and injured states of the joint. With this aim, a Finite Element Analysis (FEA) will be developed based in the anatomical model of an ankle joint from a real patient. The present study will analyse these procedures from a biomechanical perspective using computational tools.

## 5.3. Material and Methods

A three-dimensional solid model of the left ankle of a male patient (56 years old, 80 kg) was reconstructed. The model consists of bones, cartilage and ligaments, muscles have not been simulated. Bones were modelled following the 3D reconstruction obtained from a computed tomography (CT) scan (*Figure 5.3 a*). The images were acquired using a 64-detector multidetector computerized tomography (MDCT) system (Brilliance 64, Philips Healthcare, Amsterdam, The Netherlands) using a tube current of 257 mA and a voltage of 120 kV. The spatial resolution was 0.65 x 0.65 mm, with a reconstructed matrix of 768 x 768. The slice thickness was 2 mm. CT images were imported in the software Mimics v20.0 (Materialise NV, Leuven, Belgium) and processed in order to get an .stl file containing the structure of the 3 bones required for this study: tibia, fibula and talus. This file was loaded in 3-Matic 12.0 (Materialise NV, Leuven, Belgium) in order to generate the mesh for the FE analysis. Bones mesh size was selected to be as accurate as possible with the same size in all three bones. After performing a mesh sensitivity analysis with values between 2 and 3 mm for edge lengths, mesh size was set to 3 mm (*Figure 5.3 b*). Cortical bone was considered as a shell with an average thickness of 3mm. Trabecular bone was created using lineal tetrahedral elements. Edge size for these elements was also set to 3 mm. (*Figure 5.3*).

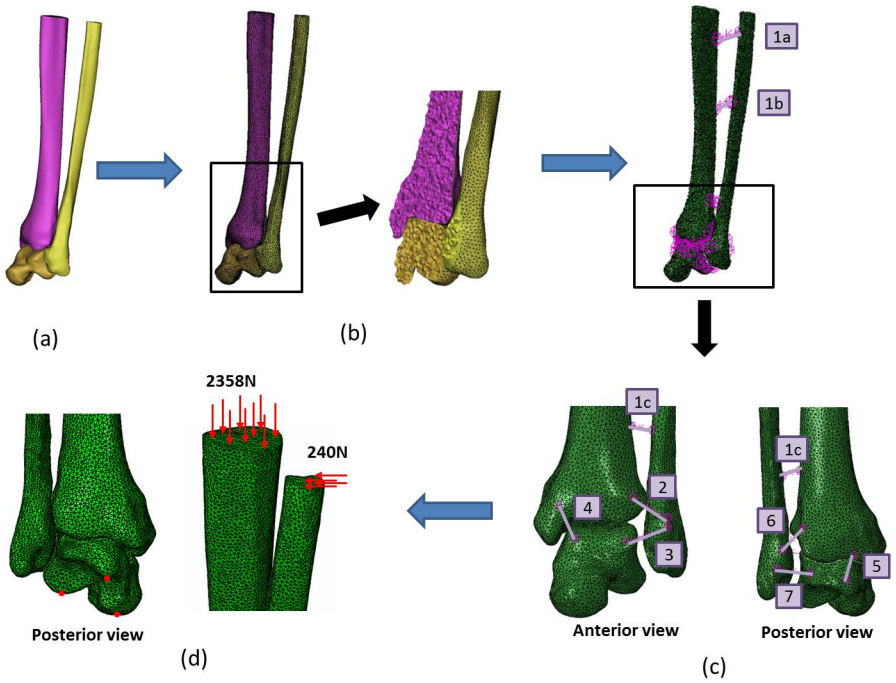


Figure 5.3: Workflow for the finite element simulations of the syndesmotic injury: (a) 3D bone reconstruction; (b) finite element mesh generated; (c) final model including the ankle joint ligaments using springs: (1a, 1b, 1c) Interosseous Membrane (IM), (2) Anterior Tibiofibular Ligament (ATL), (3) Anterior Talofibular Ligament (ATFL), (4) Anterior Tibiotalar Ligament (ATTL), (5) Posterior Tibiotalar Ligament (PTTL), (6) Posterior Tibiofibular Ligament (PTL) and (7) Posterior Talofibular Ligament (PTFL); (d) Boundary and loading conditions applied to the model.

### 5.3.1. FE models

Once the structure of the model was defined, the file containing the geometry was imported in the software Abaqus/CAE 6.19 (Dassault Systèmes, France). Following, ligaments and cartilages were included and simulated as spring elements. Cartilages were included as a set of springs with a stiffness of 13.49 N/mm, obtained as the mean value of the ankle cartilage compression response defined by the study of Shepherd and Seedhom [145]. Ligaments were also included as a set of springs following a similar configuration to the one used by Liacouras and Wayne [86] in their study (*Figure 5.3 c*). The stiffness values of ligaments and number of springs used are listed in Table 5.1.

| **Ligament** | **Stiffness (N/mm)*** | **Number of Springs** |
|---|---|---|
| *Anterior Tibiofibular Ligament (ATL)* | 90 | 1 |
| *Posterior Tibiofibular Ligament (PTL)* | 90 | 2 |
| *Interosseous Membrane (IM)* | 134 | 3 |
| *Anterior Talofibular Ligament (ATFL)* | 90 | 1 |
| *Posterior Talofibular Ligament (PTFL)* | 70 | 1 |
| *Anterior Tibiotalar Ligament (ATTL)* | 70 | 1 |
| *Posterior Tibiotalar Ligament (PTTL)* | 80 | 1 |

Table 5.1: Distribution of the ligaments included in the Finite element model. *Stiffness indicates the value for every individual spring in the ligament.

Cortical and trabecular bone structures were assumed to be isotropic, homogeneous and linearly elastic. The Young modulus values and Poisson ratios of materials used in the analysis are listed in Table 5.2 [47, 48, 165].

| **Material Properties** | | |
|---|---|---|
| **Material** | **Young Modulus (MPa)** | **Poisson Ratio** |
| *Cortical Bone* | 18000 | 0,3 |
| *Trabecular Bone* | 1000 | 0,3 |
| *Titanium* | 107000 | 0,34 |
| *UHMWPE* | 928,5 | 0,35 |

Table 5.2: Mechanical properties of bones of the ankle joint and screw and suture button materials used in the different FE models.

Boundary conditions and loads were included in the model (*Figure 5.3 d*). The ankle joint was fixed to the floor through three nodes of the lower surface of the talus bone. Physiological loads during stance phase normal walking were simulated [47, 48, 165]. Compressive force (2358 N) was applied at the proximal tibia and tangential force (240 N) was applied medially at the proximal fibula.

#### Simulated cases

In this study, different simulations were performed to analyse the intact ankle, injured syndesmosis and different methods of syndesmosis fixation (*Figures 5.4 and 5.5*). First, the intact ankle was simulated (*Figure 5.4 a*). Then, the injured syndesmosis was simulated by removing the Anterior Tibiofibular Ligament (ATL) spring (*Figure 5.3 c - 6*) and the lower spring of the Intraoseous Membrane (IM) (*Figure 5.3 c - 1c*), leaving free the lower connection between tibia and fibula (*Figure 5.4 b*). Then,

two different methods of syndesmosis fixation were considered: titanium screws (*Figure 5.4 c-f*) and suture buttons (*Figure 5.5*). Screws were modelled as beam elements (B33 - Abaqus/CAE 6.19) of 3.5mm diameter and titanium material properties (*Table 5.2*) [48, 89, 161]. One (single) screw was simulated with a tricortical fixation (*Figure 5.4 c*) or with a rigid quadricortical fixation (*Figure 5.4 d*). In both cases, the screw was placed 45 mm above the tibiotalar joint. The effect of using two (double) screws (tricortical – *Figures 5.4 e* and quadricortical – *Figure 5.4 f*) for the fixation was also considered studying the effect of the distance between screws (10 mm, 15 mm and 18 mm). The top screw was always placed 45 mm above the tibiotalar joint.

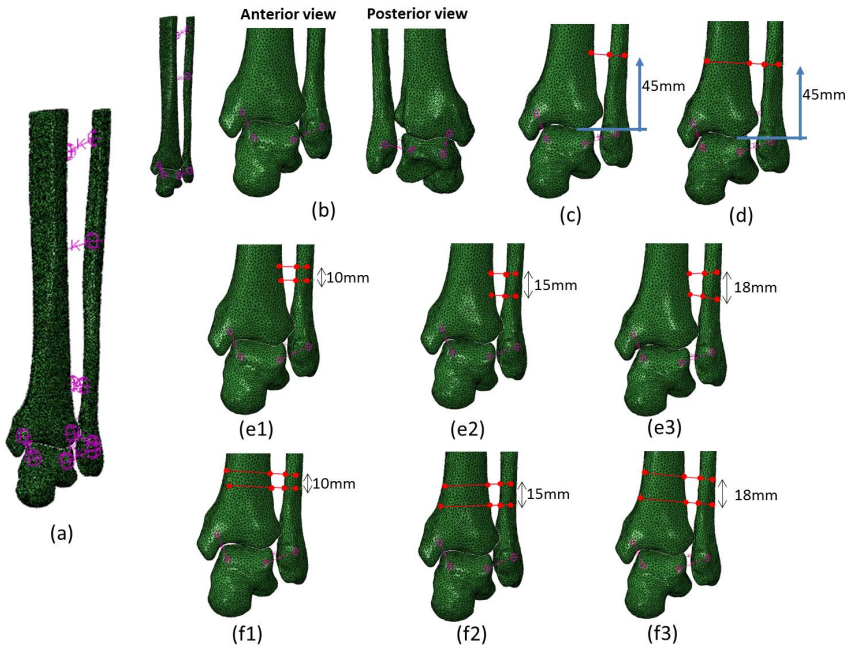


Figure 5.4: FE models analysed. (a) Intact ankle; (b) injured syndesmosis; (c) single tricortical screw; (d) single quadricortical screw; (e1) double tricortical with 10mm distance; (e2) double tricortical with 15mm distance; (e3) double tricortical with 18mm distance; (f1) double quadricortical with 10mm distance; (f2) double quadricortical with 15mm distance; (f3) double quadricortical with 18mm distance.

Suture buttons were also modelled as beam elements (B33 - Abaqus/CAE 6.19) of 3.0 mm diameter and ultra-high-molecular-weight polyethylene (UHMWPE) material properties (*Table 5.2*) (*Figure 5.5*). These properties resembled the characteristics of the Tightrope® implant (Arthrex). Three different configurations were modelled: a single suture button (*Figure 5.5 a*), two suture buttons in parallel orientation in the axial plane (*Figure 5.5 b*) and two suture buttons with approximately 20º of divergence in the axial plane (*Figure 5.5 c*). The single and top suture buttons were placed 45 mm above the tibiotalar joint. Distance between the two suture buttons was 10 mm (*Figures 5.5 b-c*). In the clinical practice, a tensiometer is used to tension each strand of the knotless kit to approximately 80 N [174, 180]. This technique was simulated applying a pretension to the beam elements simulating the suture buttons. A sensitivity analysis with different pretension forces was carried out: 20 N, 30 N, 40 N, 80 N and 100 N.

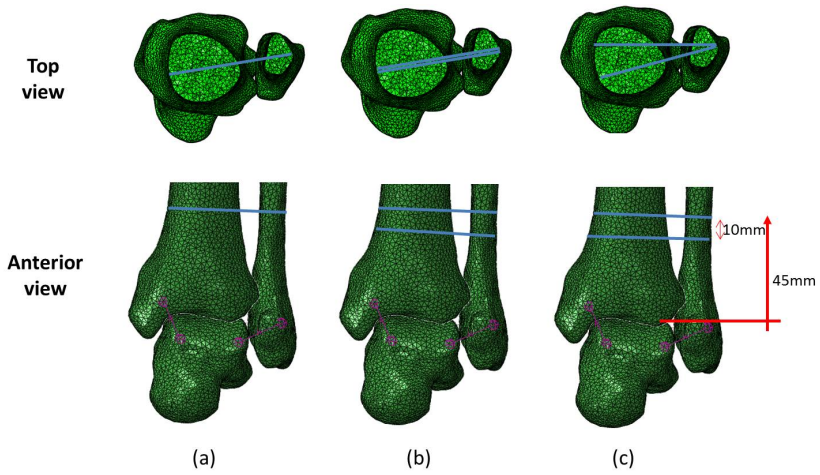


Figure 5.5: Orientation of the fixation for the single, parallel, and divergent configurations using suture buttons from the top and anterior view.

As the main goal of the syndesmotic fixation is to maintain the distal tibiofibular joint in a reduced position during healing, the syndesmosis widening was evaluated in every case (healthy, injured and with screw/suture button fixation). At the end of the FEA, the syndesmosis widening was calculated subtracting the distance between the tibia and fibula at the level of the screw/suture button location after and before loading. Additionally, von Mises stresses on the screws and suture buttons were evaluated.

## 5.4. Results

*Syndesmosis widening*

Syndesmosis widening in the injured configuration tripled intact ankle syndesmosis widening (2.06 mm vs. 0.57 mm, respectively), which compromises the joint stability (*Table 5.3*). Any of the proposed fixations importantly reduced the syndesmosis widening. The minimum syndesmosis widening was determined using a single quadricortical screw (0.18 mm), whereas the maximum was estimated when using a single suture button with a pretension force of 20 N (1.11 mm) (*Table 5.3*). Several syndesmotic fixations computed a syndesmosis widening very close to the intact ankle: one single tricortical screw (0.91 mm), double quadricortical with 18mm distance (1.02 mm), all the fixations using a single suture button, and several fixations with double parallel (20-40 N pretension force) and divergent buttons (20-30N pretension force) (*Table 5.3*). Using one single tricortical screw predicted a closer syndesmosis widening (0.91 mm) to the intact ankle value (0.97 mm) than using one single quadricortical screw (0.18 mm). The contrary effect was observed when double tricortical and quadricortical was analysed. Increasing the distance between the screws increased the syndesmosis widening. In general, assuming suture buttons for the syndesmotic fixation estimated similar syndesmosis widening values than for the intact ankle. When the pretension increased the syndesmosis widening was reduced. Increasing the number of suture buttons slightly reduced the syndesmosis widening (*Table 5.3*).

| | | **Syndesmosis widening (mm)** | **Screw/Suture Button Maximum von Mises Stress (MPa)** |
|---|---|---|---|
| ***Healthy*** | | 0.97 | |
| ***Injured*** | | 2.06 | |
| ***1 screw*** | *Tricortical* | 0.91 | 407 |
| | *Cuadricortical* | 0.18 | 382.6 |
| ***2 screws*** | *Tricortical: 10 mm distance* | 0.22 | 206.2 |
| | *Tricortical: 15 mm distance* | 0.13 | 336.1 |
| | *Tricortical: 18 mm distance* | 0.32 | 190.5 |
| | *Quadricortical: 10 mm distance* | 0.68 | 162.8 |
| | *Quadricortical: 15 mm distance* | 0.69 | 298.9 |
| | *Quadricortical: 18 mm distance* | 1.02 | 272.5 |
| ***1 suture button*** | *Pretension 20N* | 1.11 | 11.37 |
| | *Pretension 30N* | 1.10 | 12.43 |
| | *Pretension 40N* | 1.09 | 13.49 |
| | *Pretension 80N* | 1.04 | 17.74 |
| | *Pretension 100N* | 1.01 | 19.86 |
| ***2 parallel buttons*** | *Pretension 20N* | 1.02 | 11.69 |
| | *Pretension 30N* | 0.99 | 12.46 |
| | *Pretension 40N* | 0.97 | 13.25 |
| | *Pretension 80N* | 0.88 | 16.41 |
| | *Pretension 100N* | 0.83 | 17.96 |
| ***2 divergent buttons*** | *Pretension 20N* | 0.91 | 9.64 |
| | *Pretension 30N* | 0.90 | 10.73 |
| | *Pretension 40N* | 0.88 | 11.83 |
| | *Pretension 80N* | 0.84 | 16.22 |
| | *Pretension 100N* | 0.81 | 18.42 |

Table 5.3: Syndesmosis widening (mm) and maximum Von Mises stresses (MPa) at the screws/suture buttons for the different configurations simulated.

*Stress values*

Von Mises stresses were higher for the titanium screws than for the suture buttons (*Table 5.3*). The maximum von Mises stress was determined for the single tricortical screw fixation (407 MPa). Using double screws reduced the von Mises stresses. The minimum von Mises stress was determined for the double quadricortical with 10 mm distance (162.8 MPa). For the suture buttons, the von Mises stresses increased when the pretension force increased.

## 5.5. Discussion

The main objective of this study was to provide a computational tool to biomechanically compare different syndesmotic fixations. In the literature, there are several FEA of screw fixation for the syndesmotic injuries [88, 89, 47, 48, 165]. This is the first work performing a biomechanical FEA of suture buttons for syndesmotic fixations. Normally, screw diameters vary between 3.5 mm or 4.5 mm. Here we only considered a screw diameter of 3.5 mm [48, 89, 161]. Although, there is still no consensus regarding the number of screws, screw diameter or the number of cortices [47, 48, 88, 89, 165]. Our study showed similar results to previous works, however, the numerical results are not comparable due to different patient ankle models, anatomical characteristics, simulation of the screws, and results quantification. Syndesmotic fixation at the level of 20-40 mm above the tibiotalar joint showed enough stability and similar syndesmosis widening to the intact ankle configuration. Verim et al. [165] compared different positions for a single screw. They concluded that the screw fixation at the level 30-40 mm above the tibiotalar joint has advantages with other evaluated levels. In our study, we analysed this effect but using double screws and similar differences were also estimated (*Table 5.3*). One tricortical screw estimated a comparable syndesmotic widening to the intact ankle configuration (0.91 mm vs. 0.97 mm, respectively), whereas using a quadricortical screw importantly reduced the syndesmotic widening. Serhan et al. [47] reported important differences in the behaviour of tricortical and quadricortical fixations when a single screw inclusion was modelled. When using double screws, the sysndesmotic widening reversed its behaviour (*Table 5.3*). Using suture buttons, the syndesmotic widening was closer to the intact ankle configuration (*Table 5.3*). In this surgical procedure, a flexible rope is used to substitute the damaged ligament. This flexible rope could have a behaviour similar to the undamaged element. In fact, screw fixation stiffens the tibiofibular joint reducing the syndesmotic widening (*Table 5.3*). Using different pretension forces slightly varies the syndesmosis widening (*Table 5.3*). There is no clinical or cadaveric analysis where the effect of the pretension force is studied. Only Westermann et al. [174] explained how the tension was applied to the suture button construct (82 N). Laflamme et al. [80] concluded a better performance of dynamic fixation (suture button) over static fixation (screws) after 12 months follow up. Naqvi et al. [105] found no significant difference between suture button and screw fixation, but they observed cases of malreduction and risk of suffer it in the future for several patients in the group treated with screw fixation. Neary et al. [107] included a cost analysis in their study comparing suture button and screw fixations determining the better cost/effective result for suture button when single or double ropes are included versus single or double screws inclusions. Zhang et al. [180] determined that suture button could lead to better objective range of motion measurements and earlier return to work [133]. Raeder et al. [120] performed a five-year follow-up of patients treated with suture buttons or syndesmotic screws. Their long-term results favoured the use of suture buttons when treating syndesmotic injury. Xie et al. [175] suggested that suture button fixation could achieve significant higher America Orthopaedic Foot and Ankle (AOFAS) scores with a lower rate of postoperative complications. In our study, three different configurations using suture buttons were analysed. Increasing the number of suture buttons slightly reduce syndesmotic widening. The divergent technique was the most stable (*Table 5.3*) [113]. Although the results obtained in this work were quite promising, the computational model was based on several assumptions. The evaluation of more patient-specific cases could help to improve the accuracy of the model and its val-

idation. Additionally, material properties for soft tissues were obtained from the literature [165]. Only three elements distributed in the upper, middle and lower regions were used to simulate the syndesmosis which is anatomically distributed along the whole bone [86]. A unique loading case was simulated, no other loading cases or cyclic configurations were assumed. Finally, screws were modelled as beam elements neglecting their real geometry, this could affect to their stress distribution.

## 5.6. Study Conclusions

A detailed biomechanical comparison among different syndesmotic fixation was here performed. Screws provided a more rigid syndesmotic fixation than suture buttons. This computational study showed that suture buttons as syndesmotic fixation has advantages with regard to syndesmosis widening in comparison with screw fixation. This could support the good long-term clinical results obtained with dynamic syndesmotic fixation. Additionally, the computational methodology here proposed could be used as a preoperative planning tool incorporating patient-specific characteristics.

# Chapter 6

# General conclusions and future work

## 6.1. General conclusions

The main goal of this thesis was analysing the possibilities for the application of computational methods to the preoperative planning of orthopaedic surgical procedures in the lower body with the objective of avoiding long-term issues. This way, subsequent surgeries for the correction of problems derived from this initial surgeries or even the appearance of chronic damages without an actual solution could be avoided.

The inclusion of computational methods for clinical use in the orthopaedic field is far from the use made of these technologies in other medical specialities, and remains as an area in which its full potential is not yet exploited. With the purpose of showing some of their applications and capabilities for biomechanical studies, four independent surgical procedures of clinical interest affecting the four main joints in the lower body (ankle, knee, hip and lumbosacral spine) were taken for their analysis.

This work has shown how computational tools can be used as a support in making decisions for surgical alternatives, specially for those cases where the surgical technique is relatively novel or new, or in those situations where multiple factors are responsible of future issues and require a thorough analysis.

**Parametric FE model development**

As exposed in chapter 2, despite the reconstruction of a patient-specific model based in medical images is the most suitable option for the analysis of individualised patient pathologies, this process is very time consuming and requires a dedication that in some occasions is not affordable; specially when working in a clinical environment. Also, in absence of MRI images, the reconstruction of soft tissue implies geometrical approximations that affect to the accuracy of the study.

Thus, the development of a parametric model has demonstrated being a functional solution that allows the simplification of the analysed problem reducing the time required for obtaining acceptable results. Its inclusion in the study performed in chapter 2 provided good results in the comparison between the different surgical techniques analysed and was also validated with the analyses of some real patients,

whose real state fitted with the results showed by the computational model. Novel techniques belonging to the dynamic surgeries group have obtained good initial results in patients. These same results were shown in the simulations performed in this work, specially the posterior insertion that suggests the use of the AMT as a pole. Due to the lack of evidences in the long-term, this kind of analysis can support the clinicians proposal. The patient-specific analysis performed for the model validation showed good results for 7 of the 10 cases analysed, and keeping the correlation with the initial analyses of the different surgical solutions.

The versatility of the parametric model and the ease for readjusting it to the anatomical patient-specific conditions reduce the time required for preparing the simulations and their computational cost. Despite the irregularity of the geometry of the analysed region, this work has shown that when the parameters are adequately defined it is possible to recreate the key points of any geometry.

Also, as showed in chapter 4, when obtaining real patients geometries is difficult due to the lack of patients data, this kind of models provide a promising alternative that can be used for generating databases and developing and testing all kind of machine learning tools. Here, a 3D parametric model of a total hip arthroplasty was developed to assist clinicians in identifying the optimal prosthesis design and position of the acetabular cup to reduce the probability of impingement and dislocation.

**Artificial neural networks (ANN)**

Artificial neural networks are one of the most used machine learning techniques worldwide. Their characteristics allow deep analyses as complex as the problem to study could require. In chapter 4 has been demonstrated how its training and posterior validation using real patients data provides a tool easy to use and able to provide a result in seconds.

The possibility of performing the training and testing of the ANNs prior to their final use makes them a quick tool that can be carefully prepared and verified prior to their implementation in the clinical environment. Also, this kind of tool can be constantly updated as new data are collected and their configuration can be adapted to new requirements as further information about the clinical issue is included.

The accuracy demonstrated by these tools in chapter 4 providing low errors (max. 6.5º), turns them in a reliable methodology. In this case, only three variables were considered as input for the networks providing as output the range of movement of the prosthesis. For this reason, the complexity of the ANNs was substantially reduced allowing the results obtaining in some seconds (less than 30 seconds). Nevertheless, although the use of more complex configurations could cause an increase of the time required for the results to be calculated, the possibility of achieving an accurate predicting in a few minutes and prior to the surgery procedure start may help in the surgery preparation.

**Anatomical patient-specific reconstruction and FE modelling**

When time and computational cost are not a limiting factor, the anatomical patient-specific reconstruction allows a detailed analysis.

The real images reconstruction helps to have a complete overview of the affected regions and the possible issues that can be found along the analysis, even it is possible to detect additional procedures that may help in the success of the surgery. Being able of including the patient-specific distribution of material properties, assigning

them based in the clinical reports, provides accurate information about the state of the patient. This information provides a base model for testing any kind of surgical or non-invasive modification that is initially deemed as appropriated for solving the medical issue and which can be compared with other possible alternatives.

As showed in chapter 3, this model can be as accurate as the situation requires. Simplifications can be easily performed in order to isolate the region of interest and reducing the complexity of the analysis. Also, the use of patient-specific model belonging to patients who have already suffer any kind of injury can help in the analysis of future surgical techniques prior to their inclusion. As seen in chapters 3 and 5, the FEA of this reconstructions can provide useful information about the loads distribution in the desired analysis conditions and focus in deep detail in the behaviour of the biomechanical elements that form the affected regions. Generally, all the surgical alternatives considered have some pros and cons that are contemplated inherent to the procedure and are left to the surgeon to decide whether to choose. When it is not clear the significance of the procedure in the posterior recovery, computational analyses have demonstrated their capability for providing support in making a decision. Syndesmotic and lumbosacral injuries have been analysed in this work obtaining results that support the more recent alternatives proposed by clinicians that try to improve the long-term state and recovery of the patients.

Lumbosacral FE analysis has shown that the inclusion of bone augmentation using cement, that also allows the screw fixation, can improve the stiffness of the affected vertebrae helping in the loads distribution. This solution does also raise some alternatives for the screws placement angles, but this point has not shown a clear influence in the final result. When the cement volume is increased the results slightly improve; so, due to the consequences that its inclusion can cause in the bone, clinical evaluation would be crucial in making a decision about this option.

Syndesmotic analysis has proven how the inclusion of less restrictive elements (suture button) helps in reducing the syndesmosis widening between tibia and fibula, specially when the divergent ropes disposition is selected. This technique also reduces the bone stress that supposes the inclusion of a rigid body inside its structure. Also, the pre-tension that is included in the ropes has shown the von Mises stress generated decreases when the applied tension is lower.

## 6.2. Original contributions

### 6.2.1. Publications in peer reviewed journals

1. D. Alastruey-López, L. Ezquerra, B. Seral, M. A. Pérez. Using artificial neural networks to predict impingement and dislocation in total hip arthroplasty. *Computer Methods in Biomechanics and Biomedical Engineering*. (2020) 23(10): 649-657.

2. V. Sanchis-Alfonso, G. Ginovart, D. Alastruey-López, E. Montesinos-Berry, J. C. Monllau, A. Alberich-Bayarri and M. A. Pérez. Evaluation of Patellar Contact Pressure Changes after Static versus Dynamic Medial Patellofemoral Ligament Reconstructions Using a Finite Element Model. *Journal of Clinical Medicine*. (2019) 8 (12): 2093.

3. V. Sanchis-Alfonso, D. Alastruey-López, G. Ginovart, E. Montesinos-Berry, F. García-Castro, C. Ramírez-Fuentes, J. C. Monllau, A. Alberich-Bayarri and M. A. Pérez. Parametric finite element model of medial patellofemoral ligament reconstruction model development and clinical validation. *Journal of Experimental Orthopaedics*. (2019) 6(1):32.

4. D. Alastruey-López, B. Seral, M. A. Pérez. Biomechanical evaluation of syndesmotic fixation techniques via finite element analysis: screw vs. suture button. *Computer Methods and Programs in Biomedicine* (Under review).

5. D. Alastruey-López, L. Alvarez-Galovich, A. Alberich-Bayarri and M. A. Pérez. Cement augmentation of pedicle screws in lumbosacral vertebrae: a biomechanical finite element analysis (Under Preparation)

### 6.2.2. Conference and congress presentations

1. D. Alastruey-López, V. Sanchís-Alfonso, A. Alberich-Bayarri, M. A. Pérez. Computer-aided surgery for the medial patellofemoral ligament reconstruction: a parametric finite element model. Oral presentation. $15^{th}$ *International Symposium on Computer Methods in Biomechanics and Biomedical Engineering (CMBBE)*. Lisbon (Portugal) 26-29 March 2018

2. D. Alastruey-López, M. A. Pérez, L. Ezquerra-Hernando, B. Seral-García. Desarrollo de una herramienta computacional para su aplicación clínica en la predicción de luxaciones en cadera. Oral presentation. $6^{th}$ *Congreso conjunto AEA-SEROD*. Zaragoza (Spain) 24-26 May 2018

3. D. Alastruey-López, F. García-Castro, A. Alberich-Bayarri, M. A. Pérez. Biomechanical Analysis of the Pedicle Screws and Cement Injection Influence in the Sacral Region Stiffness - A Finite Element Analysis. Oral presentation. *Virtual Physiological Human Conference (VPH)*. Zaragoza (Spain) 5-7 September 2018

## 6.3. Future lines

In the development of this work some points have not been considered due to assumed as not essential for the studies development or following clinical indications. Also, due to the scope of each study, some analyses have been delimited. Including all these elements would require a deep analysis of all the exposed situations. A list of the main considerations that should be included for future works is shown below.

**Preoperative planning for Medial Patellofemoral Ligament (MPFL) reconstruction**

Future lines for developing this work would include some variations in the analysed models:

- *Soft tissue characterisation*

  Soft tissue, in this case cartilages, has been assumed to be homogeneous. For an initial approximation this helps in obtaining good results reducing the time required for finishing the simulations. The characterisation of this material including anatomical properties would provide more accurate results and probably clearly differences in the pressure maps.

- *Ligaments and tendons modelling*

  Beam and truss elements have been included for ligaments and tendons definition. This simplification along with the impossibility of obtaining an anatomical geometry of these elements without an MRI image has comply with the requirements of this study, but it has important limitations. The geometry is not considered in the loads distribution, nor is the geometrical shape influence in bones displacements. A deeper development of these elements would improve the model.

- *Elements inclusion*

  Bones, ligaments and muscles that are not directly involved in the analysis were removed. Its influence in the model and the surgical techniques simulated could be verified if these elements were included. This would require their reconstruction and inclusion as parametric elements.

- *Patient-specific models analysis*

  For this work only six patients models were included. This was used for model validation but it would be necessary the inclusion of more patients for both refining the model validation and testing its viability for using it prior to future surgeries. The use of complex geometries would help in defining the limitations of the model and solving them.

- *Surgeries in different knee joint geometries*

  As an interesting point for the analysis of the surgeries proposed in the study, using several different knee joint geometries for repeating the general analysis and comparing the behaviour of all of them would provide a more reliable overview of the viability of each reconstruction technique

- *Reconstruction techniques*

  It has been reported that some new clinically interesting techniques belonging to the dynamic solutions are still being evaluated and could be included for their analysis along with the ones already simulated.

**Preoperative planning for spine fusion**

- *Screws and cement inclusion*

  Screws were included as beam elements, while cement was included by changing the material properties of the region where it was incorporated. Based in the post-surgical images from surgeries in patients, real geometry of the screws and cement can be extracted and included in the model as full geometrical elements that better simulate the real situation.

- *Tendon, ligament and other bones*

  As in the analysis of the MPFL reconstruction, this model has been developed without the inclusion of muscles and ligaments that have influenced in the spine stability. Also, iliac bones (where sacrum articulates) and upper vertebrae have not been included. The inclusion of all these elements would improve the accuracy of the model.

- *Intervertebral discs*

  Intervertebral discs were reconstructed based in CT images. In these images soft tissues are not easy to distinguish, so, the geometry is approximated. Also, their properties were defined, as in the MPFL case, as homogeneous, due to the interest of the study was focused in their load transmission, not their internal behaviour. Using more appropriated material properties would improve the model performance.

- *Number of patients*

  The study was performed including only five patients. The inclusion of more patients with spine injuries would be key for the comparison of the surgical alternatives, specially the comparison in the screws angle positioning.

- *Surgical alternatives*

  Not only rods and screws are included in this kind of surgeries. In some occasions is necessary the incorporation of additional elements between vertebrae or inside them when are fractured. This elements do also have a role in the loads transmission that could be analysed along with the spine fusion itself.

**Preoperative planing for preventing hip prosthesis dislocation**

- *Input and output parameters*

  This study was performed considering just three input options as variables for the range of movement (ROM) prediction. This approximation included the main factors influencing the success of this surgical procedure; however, there are more parameters that can be included and can allow obtaining a more accurate prediction, such as neck prosthesis length and shape or the size of the acetabular cup.

- *Training and testing data*

  Databases for testing and training, along with the first validation, were obtained from the simulations performed using the geometrical adaptation of a parametric model. This model includes several simplifications that affect to the reliability of these data. Obtaining a database from real patients surgeries and posterior state will generate a stronger tool.

- *Parametric model*

  In case of not being possible the inclusion of real patients data, the parametric model can be improved by including some of the elements that were not considered and that have a key role in the prosthesis behaviour (such as muscles and ligaments).

- *Validation with real patients*

  This study was validated using data from only five patients. It is necessary repeat the validation with a larger file of data from patients who suffered impingement or dislocation in order to improve the obtained results.

- *ANNs configuration*

  Transfer functions for the ANNs were selected from the most commonly used due to their proven good performance. However, it would be necessary to perform an analysis including all the possible transfer functions in such way that the configuration of the ANNS is optimal.

**Preoperative planning for syndesmotic injury correction**

- *Soft tissues inclusion*

  Ligaments and cartilages have been included as spring elements. Their substitution by real geometrical reconstruction with accurate material properties inclusion would help in achieving more accurate simulations.

- *Additional bones*

  The model has been limited to the bones affected by the injury, but the inclusion of further bones could help in obtaining a better overview of the surgical procedures performance.

- *Pre-tension force*

  Pre-tension force has shown to have little influence in the results but affects in different ways depending on the suture button selected configuration. An optimisation analysis should be carried out in order to define the optimal load for obtaining the best results in the different configurations.

# Capítulo 7

# Conclusiones generales y líneas futuras de trabajo

## 7.1. Conclusiones generales

El principal objetivo de esta tesis era analizar las posibilidades para la aplicación de métodos computacionales en la planificación previa de procesos quirúrgicos ortopédicos en el tren inferior del cuerpo con el objetivo de evitar lesiones a largo plazo. De esta forma, se podrían prevenir las sucesivas intervenciones para la corrección de problemas derivados de la cirugía inicial o incluso la aparición de daños crónicos que carecen de una solución efectiva actualmente.

La inclusión de métodos computacionales para uso clínico en el campo de las intervenciones del aparato locomotor está lejos del uso que se hace de estas tecnologías en otras especialidades médicas, y sigue siendo un área donde aún no se explota todo su potencial. Con el propósito de mostrar algunas de sus aplicaciones y capacidades para su uso en estudios biomecánicos, cuatro procedimientos quirúrgicos independientes y de interés clínico que afectan a cuatro de las principales articulaciones en el tren inferior (tobillo, rodilla, cadera y región sacrolumbar) feuron seleccionadas para su análisis.

Este trabajo ha mostrado cómo las herramientas computacionales puedes usarse como apoyo a la hora de tomar decisiones sobre la solución quirúrgca a aplicar, especialmente en aquellas situaciones donde la técnica quirúrgica es relativamente novedosa, o en las situaciones donde múltiples factores pueden ser responsables de futuras lesiones y requieren un estudio exhaustivo.

**Desarrollo de un modelo paramétrico de EF**

A pesar de que la reconstrución de un modelo específico del paciente basado en imágenes médicas es la opción ideal para el análisis de patalogías individualizadas para cada paciente, este proceso requiere mucho tiempo y dedicación que en algunas ocasiones no son asumibles; especialmente cuando se trabaja en un entorno clínico.

Por tanto, el desarrollo de un modelo paramétrico ha demostrado ser una solución funcional que permite la simplificación del problema analizado reduciendo el tiempo necesario para obtener resultados aceptables. Su inclusión en el estudio sobre la reconstrucción de MPFL proporcionó buenos resultados para realizar la comparación de las diferentes técnicas quirúrgicas analizadas. Además, fue validado con el

análsis de algunos pacientes reales, cuya situación real encajó con los resultados obtenidos mediante este modelo. De esta forma, técnicas novedosas pertenecientes al grupo de las cirugías dinámicas que habían obtenido buenos resultados iniciales en pacientes mostraron estos mismos resultados en las simulaciones realizadas en este trabajo, especialmente la inserción posterior que sugiere el uso del Aductor Mayor como poste.

Debido a la falta de evidencias a largo plazo, este tipo de análisis pueden apoyar las propuestas de los cirujanos. El análisis paciente-específico realizado para la validación del modelo muestra buenos resultados para 7 de los 10 casos analizados, y mantiene la correlación con en análisis inicial de las diferentes soluciones quirúrgicas.

La versatilidad del modelo paramétrico y la facilidad para reajustarlo a las condiciones anatómicas que es necesario analizar hace posible reducir el tiempo requerido para preparar las simulaciones y su coste computacional. A pesar de la irregularidad de la geometría de la zona analizada, este trabajo ha demostrado que cuando los parámetros se definen de forma adecuada es posible recrear los puntos clave de cualquier geometría.

Además, en el capítulo 4 se ha desarrollado un modelo paramétrico de la artroplastia total de cadera que se ha combinado con redes neuronales para la predicción de dislocación de cadera. Cuando obtener datos de pacientes reales es difícil debido a la falta de pacientes o la ausencia de informes almacenados y cedidos para estudios, este tipo de modelos proporcionan una prometedora alternativa que puede usarse para la genereación de bases de datos con las que desarrollar y testear todo tipo de herramientas de *machine learning*.

**Redes neuronales artificiales (ANNs)**

Las redes neuronales artificiales son una de las técnicas de *machine learning* más utilizadas. Sus características permiten realizar análisis en detalle tan complejos como requiera el problema a estudiar. En el capítulo 4 se ha demostrado cómo su entrenamiento y posterior validación usando datos de pacientes reales proporciona una herramienta fácil de usar y capaz de dar resultados en segundos.

La posibilidad de realizar el entrenamiento y el test de estas redes neuronales antes de su uso final las convierte en una herramienta rápida que puede ser preparada y verificada cuidadosamente antes de su implementación en el entorno clínico. Además, este tipo de herramientas puede ser actualizado constantemente conforme se recopilan nuevos datos y su configuración puede adaptarse a nuevos requerimientos según se vaya incluyendo nueva informción sobre el problema clínico.

La precisión demostrada estas herramientas en el capítulo 4 proporcionando errores pequeños (máx. 6.5º) las combierte en una metodología fiable. En este caso, solo tres variables fueron consideradas como entrada de las redes, proporcionando como salida el rango de movimiento de la prótesis. Por esta razón, la complejidad de las ANNs utilizadas se redujo sustanciamente permitiendo obtener resultados en unos pocos segundos (menos de 30 segundos). Aún así, aunque el uso de configuraciones más complejas podría causar un incremento del tiempo requerido para el cálculo de los resultados, la posibilidad de obtener una predicción precisa en unos pocos minutos y antes de comenzar el proceso quirúrico puede ayudar considerablemente en la preparación de la cirugía.

**Reconstrucción anatómica paciente-específica y modelado en EF**

Cuando el tiempo y el coste computacional no son un factor limitante, la reconstrucción anatómica paciente-específica permite un análisis más detallado.

La reconstrucción de de imágenes reales ayuda a obtener una visión global completa de las regiones afectadas y los posibles problemas que pueden encontrarse durante el análisis, incluso es posible detectar procedimientos adicionales que puedan ayudar en el éxito de la cirugía. La posibilidad de incluir la distribución específica de las propiedades del material, asignándolas en base a los informes clínicos, proporciona información precisa sobre el estado del paciente y un modelo base para poder analizar cualquier tipo de técnica quirúrgica o intervención no invasiva que incialmente puede ser considerada como apropiada para solucionar la lesión y puede compararse con otras posibles alternativas. Como se muestra en el capítulo 3, este modelo puede ser tan preciso como la situación lo requiera. En caso de ser necesario, el modelo puede simplicarse con facilidad permitiendo aislar la región de interés y reduciendo la complejidad del análisis. Además, el uso de modelos paciente-específicos pertenecientes a pacientes que ya han sufrido algún tipo de lesión puede ayudar en el análisis de futuras técnicas quirúrgicas antes de ser empleadas. Como se ha visto en los capítulos 3 y 5, el análisis mediante elementos finitos de estas reconstrucciones puede proporcionar información útil sobre la distribución de las cargas en las condiciones de interés para el análisis y centrarse con gran detalle en el comportamiento de los elementos biomecánicos que forman las regiones afectadas. Generalmente, todas las soluciones quirúrgicas propuestas como posibles alternativas tienen pros y contras que son considerados inherentes al procedimiento y deja en manos de los cirujanos la elección de cuál utilizar.Los análisis computacionales han demostrado su capacidad para proporcionar apoyo en la toma de decisiones uando no está clara la influencia del procedimiento en la recuperación posterior. En los análisis realizados en esta tesis sobre las lesiones de sindesmosis del tobillo y de la región sacrolumbar se han obtenido resultados que apoyan las alternativas quirúrgicas propuestas más recientemente por cirujanos que intentan mejorar la recuperación y el estado a largo plazo de los pacientes. El análisis por elementos finitos de la región sacrolumbar ha mostrado que el aumento de hueso usando PMMA como cemento, el cual permite además la fijación de los tornillos, puede mejorar la rigidez de las vértebras afectadas ayudando en la distribución de sus cargas. Esta solución también proporciona algunas alternativas en el ángulo de colocación de los tornillos, sin embargo este punto no ha mostrado una influencia clara en los resultados finales. Cuando se incrementa el volumen de cemento los resultados mejoran ligeramente; por tanto, dadas las consecuencias que la inclusión de cemnto puede tener en el propio hueso, la evaluación clínica es crucial al tomar una decisión sobre esta opción.

El análisis de la sindesmosis ha servido para probar cómo la inclusión de una fijación menos restrictiva (botón de sutura) ayuda a reducir el ensanchamiento de la sindesmosis entre la tibia y el peroné. Esta técnica también reduce la tensión en el hueso que supone la inclusión de elementos rígidos dentro de su estructura. Además, la pretensión que se aplica en los cordones cuando se realiza esta fijación no ha mostrado que la tensión de Von Mises generada disminuye cuando la tensión aplicada es menor.

## 7.2. Contribuciones originales

### 7.2.1. Publicaciones en revistas

1. D. Alastruey-López, L. Ezquerra, B. Seral, M. A. Pérez. Using artificial neural networks to predict impingement and dislocation in total hip arthroplasty. *Computer Methods in Biomechanics and Biomedical Engineering*. (2020) 23(10): 649-657.

2. V. Sanchis-Alfonso, G. Ginovart, D. Alastruey-López, E. Montesinos-Berry, J. C. Monllau, A. Alberich-Bayarri and M. A. Pérez. Evaluation of Patellar Contact Pressure Changes after Static versus Dynamic Medial Patellofemoral Ligament Reconstructions Using a Finite Element Model. *Journal of Clinical Medicine*. (2019) 8 (12): 2093.

3. V. Sanchis-Alfonso, D. Alastruey-López, G. Ginovart, E. Montesinos-Berry, F. García-Castro, C. Ramírez-Fuentes, J. C. Monllau, A. Alberich-Bayarri and M. A. Pérez. Parametric finite element model of medial patellofemoral ligament reconstruction model development and clinical validation. *Journal of Experimental Orthopaedics*. (2019) 6(1):32.

4. D. Alastruey-López, B. Seral, M. A. Pérez. Biomechanical evaluation of syndesmotic fixation techniques via finite element analysis: screw vs. suture button. *Computer Methods and Programs in Biomedicine* (Under review).

5. D. Alastruey-López, L. Alvarez-Galovich, A. Alberich-Bayarri and M. A. Pérez. Cement augmentation of pedicle screws in lumbosacral vertebrae: a biomechanical finite element analysis (Under Preparation)

### 7.2.2. Presentaciones en congresos y conferencias

1. D. Alastruey-López, V. Sanchís-Alfonso, A. Alberich-Bayarri, M. A. Pérez. Computer-aided surgery for the medial patellofemoral ligament reconstruction: a parametric finite element model. Presentación Oral. $15^{th}$ *International Symposium on Computer Methods in Biomechanics and Biomedical Engineering (CMBBE)*. Lisboa (Portugal) 26-29 Marzo 2018

2. D. Alastruey-López, M. A. Pérez, L. Ezquerra-Hernando, B. Seral-García. Desarrollo de una herramienta computacional para su aplicación clínica en la predicción de luxaciones en cadera. Presentación Oral. $6^{th}$ *Congreso conjunto AEA-SEROD*. Zaragoza (España) 24-26 Mayo 2018

3. D. Alastruey-López, F. García-Castro, A. Alberich-Bayarri, M. A. Pérez. Biomechanical Analysis of the Pedicle Screws and Cement Injection Influence in the Sacral Region Stiffness - A Finite Element Analysis. Presentación Oral. *Virtual Physiological Human Conference (VPH)*. Zaragoza (España) 5-7 Septiembre 2018

## 7.3. Líneas de trabajo futuras

En el desarrollo de este trabajo algunos puntos no han sido considerados debido a que se ha supuesto que no eran esenciales para el dessarrollo de los estudios o a indicaciones de los propios clínicos. Además, debido al alcance de cada estudio, algunos análisis han sido delimitados. La inclusión de todos estos elementos requeriría un análisis en detalle de todas las situaciones expuestas anteriormente. A continuación se muestra una relación de las principales consideraciones que deberían incluirse para las futuros trabajo que pudieran continuar con estos estudios.

**Planificación preoperatoria para la reconstrucción del Ligamento Medial Femoropatelar (MPFL)**

Las líneas futuras de desarrollo de este trabajo deberían incluir algunas variaciones en los modelos analizados

- *Caracterización de los tejidos blandos*

  Los tejidos blandos, en este caso el cartílago, han sido asumidos como homogéneos. Para una primera aproximación esta simplificación ayuda en la obtención de buenos resultados reduciendo el tiempo requerido para finalizar las simulaciones. La caracterización de este material incluyendo sus propiedades anatómicas proporcionaría resulatdos más precisos y probablemente diferencias más claras en los mapas de presiones.

- *Modelado de los ligamentos y tendones*

  Los tendones y ligamentos han sido incluidos haciendo uso de elementos *beam* y *truss*. Esta simplificación junto con la imposibilidad de obtener una geometría anatómica de estos elementos sin disponer de imagenes de MRI ha cumplido con los requerimientos de este estudio, pero tiene limitaciones. No se ha considerado su geometría en la distribución de las cargas ni cómo su colocación sobre la geometría propia de los huesos influye en los desplazamientos de los huesos. Un desarrollo más detallado de estos elementos mejoraría el modelo.

- *Inclusión de elementos*

  Los huesos, ligamentos y músculos que no estaban implicados directamente en el análisis se eliminaron. Su influencia en el modelo y las técnicas quirúrgicas simuladas podría comprobarse si estos elementos fueran incluídos. Esto requeriría su reconstrcción 3D e inclusión como partes paramétricas.

- *Análisis de modelos paciente-específico*

  Para este estudio solo se incluyeron modelos de seis pacientes. Fueron utilizados para la validación del modelo, pero sería necesaria la inclusión de más pacientes para tanto refinar la validación del modelo como para testear su viabilidad para su uso previo a futuras cirugías. El uso de geometrías complejas ayudaría a definir las limitaciones del modelo y solventarlas.

- *Cirugías en diferentes geometrías*

  Como punto interesante para el análisis de las cirugías propuestas en el estudio, el uso de varias geometrías diferentes para repetir el análsis general y comparar el comportamiento de todas ellas proporcionaría una vista general más fiable de cada técnica de reconstrucción.

- *Técnicas de reconstrucción*

  Existen artículos en los que se mencionan otras técnicas de reconstrucción de interés clínico pertenecientes al conjunto de las soluciones dinámicas. Estas soluciones están siendo evaluadas y podrían ser incluidas para su análisis junto con las ya simuladas en este estudio.

**Planificación preoperatoria de la fusión vertebral**

- *Inclusión de tornillos y cemento*

  Los tornillos fueron incluidos como elementos *beam*, mientras que el cemento se incluyó variando las propiedades del material en la región donde se inyectaría. Basándose en imágenes postoperatorias de cirugías en pacientes, la geometría real de los tornillos y el cemento podría extraerse e incluirse en el modelo como elemento geométricos completos que simulen mejor la situación real.

- *Tendones, ligamentos y otros huesos*

  Como ocurre en el anĺisis de la reconsrucción del MPFL, este modelo se ha desarrollado sin la inclusión de músculos y ligamentos que influyen en la estabilidad de la columna vertebral. Además, los huesos ilíacos (donde articula el sacro) y las vértebras superiores no se han considerado. La inclusión de estos elementos mejorarían la precisión del modelo.

- *Discos intervertebrales*

  Los discos interverterales fueron reconstruidos en base a imágenes de tomografía axial computerizada. En estas imágenes no es sencillo distinguir los tejidos blandos, y por tanto, su geometría es aproximada.

- *Número de pacientes*

  El estudio se desarrolló incluyendo únicamente cinco pacientes. La inclusión de más pacientes con daños vertebrales sería clave para la comparación de las alternativas quirúrgicas, especialmente en la comparación del ángulo de inclusión de los tornillos.

- *Alternativas quirúrgicas*

  En este tipo de cirugías no solo se incluyen barras y tornillos. En ocasiones es necesaria la inclusión de elementos adicionales entre las vértebras o dentro de ellas cuando hay fractura. Estos elementos también tienen su papel en la transmisión de las cargas que podría ser analizado junto con la propia fusión espinal.

**Planificación preoperatoria para la prevención de la dislocación de prótesis de cadera**

- *Parámetros de entrada y salida*

  Este estudio se ha realizado considerando únicamente tres opciones de entrada como variables para la predicción del rango de movimiento. Esta aproximación incluye los principales factores que influyen en el éxito de este proceso

quirúrgico; sin embargo, hay más parámetros que pueden incluirse y que pueden ayudar para obtener una predicción más precisa, tales como la longitud y la forma del cuello de la prótesis o el tamaño de la copa acetabular.

- *Datos de entrenamiento y testeo*

  Las bases de datos para el entrenamiento y testeo, junto con la primera validación, se obtuvieron de simulaciones realizadas usando diferentes adaptaciones geométricas de un modelo paramétrico. Este modelo incluye varias simplificaciones que afectan a la fiabilidad de estos datos. La obtención de una base de datos procedentes de cirugías en pacientes reales y su estado posterior proporcionaría herramientas más potentes.

- *Modelo paramétrico*

  En caso de no ser posible la inclusión de datos procedentes de pacientes reales, el modelo paramétrico podría mejorarse incluyendo algunos de los elementos que no fueron considerados inicialmente y que tienen un papel clave en el comportamiento de la prótesis (como músculos y ligamentos).

- *Validación con pacientes reales*

  Este estudio fue validado usando datos de solo cinco pacientes. Es necesario repetir esta validación con un mayor archivo de datos de pacientes que hayan padecido impacto o dislocación de prótesis para poder mejorar los resultados obtenidos.

- *Configuración de las redes neuronales*

  Las funciones de transferencia de las redes neronales se han seleccionado entre las usadas más comunmente debido a su probada eficiencia. Sin embargo, sería necesario realizar un anaálisis que incluyera todas las posibles funciones de transferencia de tal modo que se obtuviera la configuración óptima de las redes.

**Planificación preoperatoria para la corrección de lesiones de la sindesmosis**

- *Inclusión de tejidos blandos*

  Los ligamentos y cartílagos han sido incluidos como elementos muelle. Su sustitución por reconstrucciones geométricas reales con inclusión de propiedades de los materiales precisas ayudaría a obtener simulaciones más precisas.

- *Huesos adicionales*

  El modelo ha estado limitado a los huesos afectados por la lesión, pero la inclusión de más huesos podría ayudar a obtener una mejor visión general de la ejecución del proceso quirúrgico.

- F*uerza de pretensión*

  La fuerza de pretensión aplicada en el botón de sutura ha demostrado tener poca influencia en los resultados pero afecta de diferente forma según la configuración seleccionada para la colocación de los cordones. Debería realizarse una optimización del análisis con el fin de definir la carga óptima para obtener los mejores resultados en las diferentes configuraciones.

# Bibliography


[1] https://www.arthritis-health.com/types/joint-anatomy/knee-anatomy.

[2] https://stanfordhealthcare.org/medical-conditions/bones-joints-and-muscles/knee-ligament-injury/types.html.

[3] http://www.sydneyknee.com.au/medial-patellofemoral-ligament-\\reconstruction/.

[4] https://www.perfectbalanceclinic.com/blog/injury-and-treatment-advice/twisted-pelvic-torsion/.

[5] https://www.arthritis-health.com/types/joint-anatomy/hip-anatomy.

[6] https://www.arthritis-health.com/surgery/hip-surgery/total-hip-replacement-hip-arthritis.

[7] https://www.arthritis-health.com/types/osteoarthritis/ankle-joint-anatomy-and-osteoarthritis.

[8] https://www.sports-health.com/sports-injuries/ankle-and-foot-injuries/ankle-anatomy-muscles-and-ligaments.

[9] https://www.globenewswire.com/news-release/2019/08/13/1901268/0/en/Global-Orthopedic-Surgery-Market-Report-2017-to-2022-\\Procedure-Volume-Trends-by-Type-Country-and-Region.html.

[10] https://www.ncdc.noaa.gov/data-access/model-data/model-datasets/numerical-weather-prediction.

[11] L. Alm, M. Krause, C. Mull, K.-H. Frosch, and R. Akoto. Modified adductor sling technique: a surgical therapy for patellar instability in skeletally immature patients. *The Knee*, 24(6):1282–1288, 2017.

[12] E. A. Arendt. Mpfl reconstruction: the adductor sling approach. In *Patellofemoral Pain, Instability, and Arthritis*, pages 175–179. Springer, 2010.

[13] S. M. Bah and F. Ming. An improved face recognition algorithm and its application in attendance management system. *Array*, 5:100014, 2020.

[14] C. G. Bailey. *Simulation of the structural behaviour of steel-framed buildings in fire.* PhD thesis, University of Sheffield, 1995.

[15] L. Barazzetti, F. Banfi, R. Brumana, G. Gusmeroli, M. Previtali, and G. Schiantarelli. Cloud-to-bim-to-fem: Structural simulation with accurate historic bim from laser scans. *Simulation Modelling Practice and Theory*, 57:71–87, 2015.

[16] R. L. Barrack. Dislocation after total hip arthroplasty: implant design and orientation. *JAAOS-Journal of the American Academy of Orthopaedic Surgeons*, 11(2):89–99, 2003.

[17] T. F. Besier, G. E. Gold, S. L. Delp, M. Fredericson, and G. S. Beaupré. The influence of femoral internal and external rotation on cartilage stresses within the patellofemoral joint. *Journal of Orthopaedic Research*, 26(12):1627–1635, 2008.

[18] A. Betts. Sacral vertebral augmentation: confirmation of fluoroscopic landmarks by open dissection. *Pain Physician*, 11(1):57–65, 2008.

[19] R. Biedermann, A. Tonin, M. Krismer, F. Rachbauer, G. Eibl, and B. Stöckl. Reducing the risk of dislocation after total hip arthroplasty: the effect of orientation of the acetabular component. *The Journal of Bone and Joint Surgery. British volume*, 87(6):762–769, 2005.

[20] C. M. Bishop et al. *Neural networks for pattern recognition*. Oxford university press, 1995.

[21] L. Blankevoort and R. Huiskes. Ligament-bone interaction in a three-dimensional model of the knee. 1991.

[22] M. J. Boytim, D. A. Fischer, and L. Neumann. Syndesmotic ankle sprains. *The American Journal of Sports Medicine*, 19(3):294–298, 1991. PMID: 1907807.

[23] K. J. Bozic, S. M. Kurtz, E. Lau, K. Ong, T. P. Vail, and D. J. Berry. The epidemiology of revision total hip arthroplasty in the united states. *Journal of Bone and Joint Surgery*, 91(1):128–133, 2009.

[24] T. D. Brown and J. J. Callaghan. Impingement in total hip replacement: mechanisms and consequences. *Current Orthopaedics*, 22(6):376–391, 2008.

[25] G. Casalino, F. Facchini, M. Mortello, and G. Mummolo. Ann modelling to optimize manufacturing processes: The case of laser welding. *IFAC-PapersOnLine*, 49(12):378–383, 2016.

[26] S.-H. Chen, S.-C. Lin, W.-C. Tsai, C.-W. Wang, and S.-H. Chao. Biomechanical comparison of unilateral and bilateral pedicle screws fixation for transforaminal lumbar interbody fusion after decompressive surgery–a finite element analysis. *BMC Musculoskeletal Disorders*, 13(1):72, 2012.

[27] W.-M. Chi, C.-C. Lin, Y.-J. Ho, H.-C. Lin, and J.-H. Chen. Using nonlinear finite element models to analyse stress distribution during subluxation and torque required for dislocation of newly developed total hip structure after prosthetic impingement. *Medical & Biological Engineering & Computing*, 56(1):37–47, 2018.

[28] G. G. Choy, J. A. Roe, S. L. Whitehouse, K. S. Cashman, and R. W. Crawford. Exeter short stems compared with standard length exeter stems: experience from the australian orthopaedic association national joint replacement registry. *The Journal of Arthroplasty*, 28(1):103–109, 2013.

[29] W. J. Ciccone, D. R. Bratton, D. M. Weinstein, J. J. Elias, et al. Viscoelasticity and temperature variations decrease tension and stiffness of hamstring tendon grafts following anterior cruciate ligament reconstruction. *Journal of Bone and Joint Surgery*, 88(5):1071–1078, 2006.

[30] M. Cilla, J. Martinez, E. Peña, and M. Á. Martínez. Machine learning techniques as a helpful tool toward determination of plaque vulnerability. *IEEE Transactions on Biomedical Engineering*, 59(4):1155–1161, 2012.

[31] T. O. Clanton, S. R. Whitlow, B. T. Williams, D. J. Liechti, J. D. Backus, G. J. Dornan, A. J. Saroki, T. L. Turnbull, and R. F. LaPrade. Biomechanical comparison of 3 current ankle syndesmosis repair techniques. *Foot & Ankle International*, 38(2):200–207, 2017.

[32] Z. A. Cohen, V. Mow, J. Henry, W. Levine, and G. A. Ateshian. Templates of the cartilage layers of the patellofemoral joint and their use in the assessment of osteoarthritic cartilage damage. *Osteoarthritis and Cartilage*, 11(8):569–579, 2003.

[33] T. Conlan, W. Garth Jr, and J. E. Lemons. Evaluation of the medial soft-tissue restraints of the extensor mechanism of the knee. *Journal of Bone and Joint Surgery*, 75(5):682–693, 1993.

[34] F. Costa, A. Ortolina, F. Galbusera, A. Cardia, G. Sala, F. Ronchi, C. Uccelli, R. Grosso, and M. Fornari. Pedicle screw cement augmentation. a mechanical pullout study on different cement augmentation techniques. *Medical Engineering & Physics*, 38(2):181–186, 2016.

[35] J. de-las Heras Romero, A. M. L. Alvarez, F. M. Sanchez, A. P. Garcia, P. A. G. Porcel, R. V. Sarabia, and M. H. Torralba. Management of syndesmotic injuries of the ankle. *EFORT Open Reviews*, 2(9):403–409, 2017.

[36] S. M. Desio, R. T. Burks, and K. N. Bachus. Soft tissue restraints to lateral patellar translation in the human knee. *The American Journal of Sports Medicine*, 26(1):59–65, 1998.

[37] C. J. DeWald and T. Stanley. Instrumentation-related complications of multilevel fusions for adult spinal deformity patients over age 65: surgical considerations and treatment options in patients with poor bone quality. *Spine*, 31(19S):S144–S151, 2006.

[38] D. Drez Jr, T. B. Edwards, and C. S. Williams. Results of medial patellofemoral ligament reconstruction in the treatment of patellar dislocation. *Arthroscopy: The Journal of Arthroscopic & Related Surgery*, 17(3):298–306, 2001.

[39] B. D. Elder, S.-F. L. Lo, C. Holmes, C. R. Goodwin, T. A. Kosztowski, I. A. Lina, J. E. Locke, and T. F. Witham. The biomechanics of pedicle screw augmentation with cement. *The Spine Journal*, 15(6):1432–1445, 2015.

[40] J. J. Elias, D. R. Bratton, D. M. Weinstein, and A. J. Cosgarea. Comparing two estimations of the quadriceps force distribution for use during patellofemoral simulation. *Journal of Biomechanics*, 39(5):865–872, 2006.

[41] J. J. Elias, J. A. Cech, D. M. Weinstein, and A. J. Cosgrea. Reducing the lateral force acting on the patella does not consistently decrease patellofemoral pressures. *The American Journal of Sports Medicine*, 32(5):1202–1208, 2004.

[42] J. J. Elias and A. J. Cosgarea. Technical errors during medial patellofemoral ligament reconstruction could overload medial patellofemoral cartilage: a computational analysis. *The American Journal of Sports Medicine*, 34(9):1478–1485, 2006.

[43] J. J. Elias, M. J. Kelly, K. E. Smith, K. A. Gall, and J. Farr. Dynamic simulation of the effects of graft fixation errors during medial patellofemoral ligament reconstruction. *Orthopaedic Journal of Sports Medicine*, 4(9):2325967116665080, 2016.

[44] J. M. Elkins, J. J. Callaghan, and T. D. Brown. The 2014 frank stinchfield award: The 'landing zone'for wear and stability in total hip arthroplasty is smaller than we thought: a computational analysis. *Clinical Orthopaedics and Related Research®*, 473(2):441–452, 2015.

[45] J. M. Elkins, D. R. Pedersen, J. J. Callaghan, and T. D. Brown. Bone-on-bone versus hardware impingement in total hips: a biomechanical study. *The Iowa Orthopaedic Journal*, 32:17, 2012.

[46] J. M. Elkins, N. J. Stroud, M. J. Rudert, Y. Tochigi, D. R. Pedersen, B. J. Ellis, J. J. Callaghan, J. A. Weiss, and T. D. Brown. The capsule's contribution to total hip construct stability–a finite element analysis. *Journal of Orthopaedic Research*, 29(11):1642–1648, 2011.

[47] M. S. Er, O. Verim, L. Altinel, and S. Tasgetiren. Three-dimensional finite element analysis used to compare six different methods of syndesmosis fixation with 3.5-or 4.5-mm titanium screws: a biomechanical study. *Journal of the American Podiatric Medical Association*, 103(3):174–180, 2013.

[48] M. S. Er, O. Verim, M. Eroglu, L. Altinel, B. Gokce, and S. Tasgetiren. Biomechanical evaluation of syndesmotic screw design via finite element analysis and taguchi's method. *Journal of the American Podiatric Medical Association*, 105(1):14–21, 2015.

[49] L. Ezquerra, M. P. Quilez, M. Á. Pérez, J. Albareda, and B. Seral. Range of movement for impingement and dislocation avoidance in total hip replacement predicted by finite element model. *Journal of Medical and Biological Engineering*, 37(1):26–34, 2017.

[50] F. Farahmand, W. Sejiavongse, and A. A. Amis. Quantitative study of the quadriceps muscles and trochlear groove geometry related to instability of the patellofemoral joint. *Journal of Orthopaedic Research*, 16(1):136–143, 1998.

[51] J. Fernandez, P. Hunter, V. Shim, and K. Mithraratne. A subject-specific framework to inform musculoskeletal modeling: outcomes from the iups physiome project. In *Patient-Specific Computational Modeling*, pages 39–60. Springer, 2012.

[52] M.-H. Fessy, S. Putman, A. Viste, R. Isida, N. Ramdane, A. Ferreira, A. Leglise, B. Rubens-Duval, N. Bonin, F. Bonnomet, et al. What are the risk factors for dislocation in primary total hip arthroplasty? a multicenter case-control study of 128 unstable and 438 stable hips. *Orthopaedics & Traumatology: Surgery & Research*, 103(5):663–668, 2017.

[53] C. Fink, M. Veselko, M. Herbort, and C. Hoser. Mpfl reconstruction using a quadriceps tendon graft: part 2: operative technique and short term clinical results. *The Knee*, 21(6):1175–1179, 2014.

[54] C. R. Fischer, E. Vasudeva, B. Beaubrun, Z. Messer, A. Cazzullino, and R. Lehman. Osteoporosis knowledge among spine surgery patients. *International Journal of Spine Surgery*, 12(6):689–694, 2018.

[55] N. M. Fort, A. A. Aiyer, J. R. Kaplan, N. A. Smyth, and A. R. Kadakia. Management of acute injuries of the tibiofibular syndesmosis. *European Journal of Orthopaedic Surgery & Traumatology*, 27(4):449–459, 2017.

[56] B. M. Frankel, S. D. Agostino, and C. Wang. Laboratory investigations: A biomechanical cadaveric analysis of polymethylmethacrylate-augmented pedicle screw fixation. *Journal of Neurosurgery-Spine*, 7(1):47–53, 2007.

[57] J. P. Fulkerson and C. Edgar. Medial quadriceps tendon–femoral ligament: Surgical anatomy and reconstruction technique to prevent patella instability. *Arthroscopy Techniques*, 2(2):e125–e128, 2013.

[58] F. Galbusera, D. Volkheimer, S. Reitmaier, N. Berger-Roscher, A. Kienle, and H.-J. Wilke. Pedicle screw loosening: a clinically relevant complication? *European Spine Journal*, 24(5):1005–1016, 2015.

[59] Y. Gao, Z. Chen, Z. Zhang, S. Chen, and Z. Jin. Effect of inclination and anteversion angles on kinematics and contact mechanics of dual mobility hip implants. *Clinical Biomechanics*, 57:48–55, 2018.

[60] N. Garijo, J. R. Fernández, M. A. Pérez, and J. M. García-Aznar. Numerical stability and convergence analysis of bone remodeling model. *Computer Methods in Applied Mechanics and Engineering*, 271:253–268, 2014.

[61] N. Garijo, J. Martínez, J. M. García-Aznar, and M. A. Pérez. Computational evaluation of different numerical tools for the prediction of proximal femur loads from bone morphology. *Computer Methods in Applied Mechanics and Engineering*, 268:437–450, 2014.

[62] N. Garijo, N. Verdonschot, K. Engelborghs, J. M. García-Aznar, and M. A. Pérez. Subject-specific musculoskeletal loading of the tibia: Computational load estimation. *Journal of the Mechanical Behavior of Biomedical Materials*, 65:334–343, 2017.

[63] B. Georgy. Percutaneous cement augmentations of malignant lesions of the sacrum and pelvis. *American Journal of Neuroradiology*, 30(7):1357–1359, 2009.

[64] Z. Gong, Z. Chen, Z. Feng, Y. Cao, C. Jiang, and X. Jiang. Finite element analysis of 3 posterior fixation techniques in the lumbar spine. *Orthopedics*, 37(5):e441–e448, 2014.

[65] S. G. González, G. C. Bastida, M. D. Vlad, J. L. López, P. B. Caballero, L. Alvarez-Galovich, M. Rodríguez-Arguisjuela, and E. F. Aguado. Analysis of bone cement distribution around fenestrated pedicle screws in low bone quality lumbosacral vertebrae. *International Orthopaedics*, 43(8):1873–1882, 2019.

[66] I. González-Valverde and J. M. García-Aznar. Mechanical modeling of collective cell migration: An agent-based and continuum material approach. *Computer Methods in Applied Mechanics and Engineering*, 337:246–262, 2018.

[67] L. Good. In-vitro correlation between tension and length change in an anterior cruciate ligament substitute. *Clinical Biomechanics*, 10(4):200–207, 1995.

[68] R. Hambli. Apparent damage accumulation in cancellous bone using neural networks. *Journal of the Mechanical Behavior of Biomedical Materials*, 4(6):868–878, 2011.

[69] D. L. Hamner, C. H. Brown, M. E. Steiner, A. T. Hecker, and W. C. Hayes. Hamstring tendon grafts for reconstruction of the anterior cruciate ligament: biomechanical evaluation of the use of multiple strands and tensioning techniques. *Journal of Bone and Joint Surgery*, 81(4):549–57, 1999.

[70] P. V. Hautamaa, D. C. Fithian, K. R. Kaufman, D. M. Daniel, and A. M. Pohlmeyer. Medial soft tissue restraints in lateral patellar instability and repair. *Clinical Orthopaedics and Related Research (1976-2007)*, 349:174–182, 1998.

[71] J. Hsu, M. de la Fuente, and K. Radermacher. Calculation of impingement-free combined cup and stem alignments based on the patient-specific pelvic tilt. *Journal of Biomechanics*, 82:193–203, 2019.

[72] P. Hu, T. Wu, H.-z. Wang, X.-z. Qi, J. Yao, X.-d. Cheng, W. Chen, and Y.-z. Zhang. Influence of different boundary conditions in finite element analysis on pelvic biomechanical load transmission. *Orthopaedic Surgery*, 9(1):115–122, 2017.

[73] N. Jain and E. Yu. Intraoperative radiographic technique for visualization of bicortical or tricortical anteromedial sacral screw placement. *Clinical Spine Surgery*, 31(3):108–111, 2018.

[74] B. K. Jones, C. T. Hung, and G. A. Ateshian. Biphasic analysis of cartilage stresses in the patellofemoral joint. *The Journal of Knee Surgery*, 29(2):92, 2016.

[75] S. Khan, R. Warkhedkar, and A. Shyam. Analysis of hounsfield unit of human bones for strength evaluation. *Procedia Materials Science*, 6:512–519, 2014.

[76] Y.-H. Kim, Y. Choi, and J.-S. Kim. Influence of patient-, design-, and surgery-related factors on rate of dislocation after primary cementless total hip arthroplasty. *The Journal of Arthroplasty*, 24(8):1258–1263, 2009.

[77] D. Kluess, H. Martin, W. Mittelmeier, K.-P. Schmitz, and R. Bader. Influence of femoral head size on impingement, dislocation and stress distribution in total hip replacement. *Medical Engineering & Physics*, 29(4):465–471, 2007.

[78] P. Kouyoumdjian, R. Coulomb, T. Sanchez, and G. Asencio. Clinical evaluation of hip joint rotation range of motion in adults. *Orthopaedics & Traumatology: Surgery & Research*, 98(1):17–23, 2012.

[79] K. M. Kruger, N. M. Tikekar, A. D. Heiner, T. E. Baer, J. J. Lannutti, J. J. Callaghan, and T. D. Brown. A novel formulation for scratch-based wear modelling in total hip arthroplasty. *Computer Methods in Biomechanics and Biomedical Engineering*, 17(11):1227–1236, 2014.

[80] M. Laflamme, E. L. Belzile, L. Bédard, M. P. Van Den Bekerom, M. Glazebrook, and S. Pelet. A prospective randomized multicenter trial comparing clinical outcomes of patients treated surgically with a static or dynamic implant for acute ankle syndesmosis rupture. *Journal of Orthopaedic Trauma*, 29(5):216–223, 2015.

[81] A. Laudani, G. M. Lozito, F. Riganti Fulginei, and A. Salvini. On training efficiency and computational costs of a feed forward neural network: a review. *Computational Intelligence and Neuroscience*, 2015, 2015.

[82] R. Lawton and B. Morrey. Dislocation after long-necked total hip arthroplasty. *Clinical Orthopaedics and Related Research (1976-2007)*, 422:164–166, 2004.

[83] R. A. Lehman Jr, D. G. Kang, and S. C. Wagner. Management of osteoporosis in spine surgery. *JAAOS-Journal of the American Academy of Orthopaedic Surgeons*, 23(4):253–263, 2015.

[84] G. E. Lewinnek, J. Lewis, R. Tarr, C. Compere, and J. Zimmerman. Dislocations after total hip-replacement arthroplasties. *Journal of Bone and Joint Surgery. American Volume*, 60(2):217–220, 1978.

[85] X. Li, F. He, and L. Ma. Thermal management of cylindrical batteries investigated using wind tunnel testing and computational fluid dynamics simulation. *Journal of Power Sources*, 238:395–402, 2013.

[86] P. C. Liacouras and J. S. Wayne. Computational modeling to predict mechanical function of joints: application to the lower leg with simulation of two cadaver studies. *Journal of Boimechanical Engineering*, 129(6):811–817, 2007.

[87] M. Lind, D. Enderlein, T. Nielsen, S. E. Christiansen, and P. Faunø. Clinical outcome after reconstruction of the medial patellofemoral ligament in paediatric patients with recurrent patella instability. *Knee Surgery, Sports Traumatology, Arthroscopy*, 24(3):666–671, 2016.

[88] Q. Liu, K. Zhang, Y. Zhuang, Z. Li, B. Yu, and G. Pei. Analysis of the stress and displacement distribution of inferior tibiofibular syndesmosis injuries repaired with screw fixation: a finite element study. *PloS One*, 8(12):e80236, 2013.

[89] Q. Liu, G. Zhao, B. Yu, J. Ma, Z. Li, and K. Zhang. Effects of inferior tibiofibular syndesmosis injury and screw stabilization on motion of the ankle: a finite element study. *Knee Surgery, Sports Traumatology, Arthroscopy*, 24(4):1228–1235, 2016.

[90] R. López-González, J. Sánchez-García, and F. García-Castro. Artificial intelligence in respiratory diseases. *Archivos de Bronconeumologia*, 2020.

[91] J. Mackerle. Finite element modeling and simulations in orthopedics: a bibliography 1998–2005. *Computer methods in biomechanics and biomedical engineering*, 9(3):149–199, 2006.

[92] L. Martí-Bonmatí, R. Sanz-Requena, and A. Alberich-Bayarri. Pharmacokinetic mr analysis of the cartilage is influenced by field strength. *European Journal of Radiology*, 67(3):448–452, 2008.

[93] M. Martín-Fernández, A. López-Herradón, A. Piñera, F. Tomé-Bermejo, J. Duart, M. Vlad, M. Rodríguez-Arguisjuela, and L. Alvarez-Galovich. Potential risks of using cement-augmented screws for spinal fusion in patients with low bone quality. *The Spine Journal*, 17(8):1192–1199, 2017.

[94] S. McCoy, F. Tundo, S. Chidambaram, and A. Baaj. Clinical considerations for spinal surgery in the osteoporotic patient: a comprehensive review. *Clinical Neurology and Neurosurgery*, 180:40–47, 2019.

[95] W. S. McCulloch and W. Pitts. A logical calculus of the ideas immanent in nervous activity. *The Bulletin of Mathematical Biophysics*, 5(4):115–133, 1943.

[96] K. McLaren, S. Tullis, and S. Ziada. Computational fluid dynamics simulation of the aerodynamics of a high solidity, small-scale vertical axis wind turbine. *Wind Energy*, 15(3):349–361, 2012.

[97] R. J. McNeilan, J. S. Everhart, P. K. Mescher, M. Abouljoud, R. A. Magnussen, and D. C. Flanigan. Graft choice in isolated medial patellofemoral ligament reconstruction: a systematic review with meta-analysis of rates of recurrent instability and patient-reported outcomes for autograft, allograft, and synthetic options. *Arthroscopy: The Journal of Arthroscopic & Related Surgery*, 34(4):1340–1354, 2018.

[98] S. Mehta, A. Tyler, and M. Hast. Understanding the basics of computational models in orthopaedics: A nonnumeric review for surgeons. *JAAOS-Journal of the American Academy of Orthopaedic Surgeons*, 25(10):684–692, 2017.

[99] H. Miki, N. Sugano, K. Yonenobu, K. Tsuda, M. Hattori, and N. Suzuki. Detecting cause of dislocation after total hip arthroplasty by patient-specific four-dimensional motion analysis. *Clinical Biomechanics*, 28(2):182–186, 2013.

[100] J. C. Monllau, À. Masferrer-Pino, G. Ginovart, D. Pérez-Prieto, P. E. Gelber, and V. Sanchis-Alfonso. Clinical and radiological outcomes after a quasi-anatomical reconstruction of medial patellofemoral ligament with gracilis tendon autograft. *Knee Surgery, Sports Traumatology, Arthroscopy*, 25(8):2453–2459, 2017.

[101] H. Moritomo, K. Noda, A. Goto, T. Murase, H. Yoshikawa, and K. Sugamoto. Interosseous membrane of the forearm: length change of ligaments during forearm rotation. *The Journal of Hand Surgery*, 34(4):685–691, 2009.

[102] J. Mountney, W. Senavongse, A. Amis, and N. Thomas. Tensile strength of the medial patellofemoral ligament before and after repair or reconstruction. *The Journal of Bone and Joint Surgery. British volume*, 87(1):36–40, 2005.

[103] W. S. Murphy, H. H. Yun, B. Hayden, J. H. Kowal, and S. B. Murphy. The safe zone range for cup anteversion is narrower than for inclination in tha. *Clinical Orthopaedics and Related Research*, 476(2):325, 2018.

[104] M. E. Nadzadi, D. R. Pedersen, H. J. Yack, J. J. Callaghan, and T. D. Brown. Kinematics, kinetics, and finite element analysis of commonplace maneuvers at risk for total hip dislocation. *Journal of Biomechanics*, 36(4):577–591, 2003.

[105] G. A. Naqvi, P. Cunningham, B. Lynch, R. Galvin, and N. Awan. Fixation of ankle syndesmotic injuries: comparison of tightrope fixation and syndesmotic screw fixation for accuracy of syndesmotic reduction. *The American Journal of Sports Medicine*, 40(12):2828–2835, 2012.

[106] S. Naserkhaki and M. El-Rich. Sensitivity of lumbar spine response to follower load and flexion moment: finite element study. *Computer Methods in Biomechanics and Biomedical Engineering*, 20(5):550–557, 2017.

[107] K. C. Neary, M. A. Mormino, and H. Wang. Suture button fixation versus syndesmotic screws in supination–external rotation type 4 injuries: A cost-effectiveness analysis. *The American Journal of Sports Medicine*, 45(1):210–217, 2017.

[108] A. G. Newcomb, S. Baek, B. P. Kelly, and N. R. Crawford. Effect of screw position on load transfer in lumbar pedicle screws: a non-idealized finite element analysis. *Computer Methods in Biomechanics and Biomedical Engineering*, 20(2):182–192, 2017.

[109] D. E. Padgett and H. Warashina. The unstable total hip replacement. *Clinical Orthopaedics and Related Research®*, 420:72–79, 2004.

[110] M. Papadrakakis, C. Apostolopoulou, A. Zacharopoulos, and S. Bitzarakis. Three-dimensional simulation of structural pounding during earthquakes. *Journal of Engineering Mechanics*, 122(5):423–431, 1996.

[111] S. N. Parikh, S. T. Nathan, E. J. Wall, and E. A. Eismann. Complications of medial patellofemoral ligament reconstruction in young patients. *The American Journal of Sports Medicine*, 41(5):1030–1038, 2013.

[112] Y.-S. Park, S.-J. Hyun, H. Y. Choi, K.-J. Kim, and T.-A. Jahng. Association between bicortical screw fixation at upper instrumented vertebra and risk for upper instrumented vertebra fracture. *Journal of Neurosurgery: Spine*, 26(5):638–644, 2017.

[113] A. S. Parker, D. P. Beason, J. S. Slowik, J. B. Sabatini, and N. E. Waldrop III. Biomechanical comparison of 3 syndesmosis repair techniques with suture button implants. *Orthopaedic Journal of Sports Medicine*, 6(10):2325967118804204, 2018.

[114] D. Pedersen, J. Callaghan, and T. Brown. Activity-dependence of the "safe zone" for impingement versus dislocation avoidance. *Medical Engineering & Physics*, 27(4):323–328, 2005.

[115] M. Perez and J. Palacios. Comparative finite element analysis of the debonding process in different concepts of cemented hip implants. *Annals of Biomedical Engineering*, 38(6):2093–2106, 2010.

[116] M. A. Pérez, N. Nuño, A. Madrala, J. M. García-Aznar, and M. Doblaré. Computational modelling of bone cement polymerization: temperature and residual stresses. *Computers in Biology and Medicine*, 39(9):751–759, 2009.

[117] M. A. Pérez, P.-A. Vendittoli, M. Lavigne, and N. Nuño. Bone remodeling in the resurfaced femoral head: Effect of cement mantle thickness and interface characteristics. *Medical Engineering & Physics*, 36(2):185–195, 2014.

[118] D. Pérez-Prieto, B. Capurro, P. E. Gelber, G. Ginovart, F. Reina, V. Sanchis-Alfonso, and J. C. Monllau. The anatomy and isometry of a quasi-anatomical reconstruction of the medial patellofemoral ligament. *Knee Surgery, Sports Traumatology, Arthroscopy*, 25(8):2420–2423, 2017.

[119] A. Phillips, P. Pankaj, C. Howie, A. Usmani, and A. Simpson. Finite element modelling of the pelvis: inclusion of muscular and ligamentous boundary conditions. *Medical Engineering & Physics*, 29(7):739–748, 2007.

[120] B. W. Ræder, W. Figved, J. E. Madsen, F. Frihagen, S. B. Jacobsen, and M. R. Andersen. Better outcome for suture button compared with single syndesmotic screw for syndesmosis injury: five-year results of a randomized controlled trial. *The Bone & Joint Journal*, 102(2):212–219, 2020.

[121] S. Rammelt and P. Obruba. An update on the evaluation and treatment of syndesmotic injuries. *European Journal of Trauma and Emergency Surgery*, 41(6):601–614, 2015.

[122] S. J. Ramos-Infante and M. A. Pérez. High-and low-viscosity cement for osteoporotic femoral augmentation: A computational subject-specific approach. *Engineering Fracture Mechanics*, 219:106647, 2019.

[123] S. J. Ramos-Infante, A. Ten-Esteve, A. Alberich-Bayarri, and M. A. Pérez. Discrete particle model for cement infiltration within open-cell structures: Prevention of osteoporotic fracture. *Plos One*, 13(6):e0199035, 2018.

[124] N. Reina, S. Putman, R. Desmarchelier, E. S. Ali, P. Chiron, M. Ollivier, J. Jenny, D. Waast, C. Mabit, E. de Thomasson, et al. Can a target zone safer than lewinnek's safe zone be defined to prevent instability of total hip arthroplasties? case-control study of 56 dislocated tha and 93 matched controls. *Orthopaedics & Traumatology: Surgery & Research*, 103(5):657–661, 2017.

[125] W.-T. Rhee, S.-H. You, Y.-G. Jang, and S.-Y. Lee. Lumbo-sacro-pelvic fixation using iliac screws for the complex lumbo-sacral fractures. *Journal of Korean Neurosurgical Society*, 42(6):495, 2007.

[126] R. B. Rigby and J. M. Cottom. Does the arthrex tightrope® provide maintenance of the distal tibiofibular syndesmosis? a 2-year follow-up of 64 tightropes® in 37 patients. *The Journal of Foot and Ankle Surgery*, 52(5):563–567, 2013.

[127] A. Rohlmann, N. K. Burra, T. Zander, and G. Bergmann. Comparison of the effects of bilateral posterior dynamic and rigid fixation devices on the loads in the lumbar spine: a finite element analysis. *European Spine Journal*, 16(8):1223–1231, 2007.

[128] A. Rohlmann, S. Lauterborn, M. Dreischarf, H. Schmidt, M. Putzier, P. Strube, and T. Zander. Parameters influencing the outcome after total disc replacement at the lumbosacral junction. part 1: misalignment of the vertebrae adjacent to a total disc replacement affects the facet joint and facet capsule forces in a probabilistic finite element analysis. *European Spine Journal*, 22(10):2271–2278, 2013.

[129] A. Rohlmann, T. Zander, M. Rao, and G. Bergmann. Applying a follower load delivers realistic results for simulating standing. *Journal of Biomechanics*, 42(10):1520–1526, 2009.

[130] A. Rood, G. Hannink, A. Lenting, K. Groenen, S. Koëter, N. Verdonschot, and A. van Kampen. Patellofemoral pressure changes after static and dynamic medial patellofemoral ligament reconstructions. *The American Journal of Sports Medicine*, 43(10):2538–2544, 2015.

[131] V. Sanchis-Alfonso. Guidelines for medial patellofemoral ligament reconstruction in chronic lateral patellar instability. *JAAOS-Journal of the American Academy of Orthopaedic Surgeons*, 22(3):175–182, 2014.

[132] V. Sanchis-Alfonso, C. Ramirez-Fuentes, E. Montesinos-Berry, J. Domenech, and L. Martí-Bonmatí. Femoral insertion site of the graft used to replace the medial patellofemoral ligament influences the ligament dynamic changes during knee flexion and the clinical outcome. *Knee Surgery, Sports Traumatology, Arthroscopy*, 25(8):2433–2441, 2017.

[133] T. Schepers, H. van der Linden, E. M. van Lieshout, D.-D. Niesten, and M. van der Elst. Technical aspects of the syndesmotic screw and their effect on functional outcome following acute distal tibiofibular syndesmosis injury. *Injury*, 45(4):775–779, 2014.

[134] L. Schiphouwer, A. Rood, S. Tigchelaar, and S. Koëter. Complications of medial patellofemoral ligament reconstruction using two transverse patellar tunnels. *Knee Surgery, Sports Traumatology, Arthroscopy*, 25(1):245–250, 2017.

[135] H. Schmidt, F. Galbusera, A. Rohlmann, and A. Shirazi-Adl. What have we learned from finite element model studies of lumbar intervertebral discs in the past four decades? *Journal of Biomechanics*, 46(14):2342–2355, 2013.

[136] J. M. Schon, B. T. Williams, M. B. Venderley, G. J. Dornan, J. D. Backus, T. L. Turnbull, R. F. LaPrade, and T. O. Clanton. A 3-d ct analysis of screw and suture-button fixation of the syndesmosis. *Foot & Ankle International*, 38(2):208–214, 2017.

[137] C. F. Scifert, T. D. Brown, D. R. Pedersen, and J. J. Callaghan. A finite element analysis of factors influencing total hip dislocation. *Clinical Orthopaedics and Related Research (1976-2007)*, 355:152–162, 1998.

[138] K. G. Seagrave, A. Troelsen, H. Malchau, H. Husted, and K. Gromov. Acetabular cup position and risk of dislocation in primary total hip arthroplasty: a systematic review of the literature. *Acta Orthopaedica*, 88(1):10–17, 2017.

[139] N. A. Segal, D. D. Anderson, K. S. Iyer, J. Baker, J. C. Torner, J. A. Lynch, D. T. Felson, C. E. Lewis, and T. D. Brown. Baseline articular contact stress levels predict incident symptomatic knee osteoarthritis development in the most cohort. *Journal of Orthopaedic Research*, 27(12):1562–1568, 2009.

[140] G. Seitlinger, P. Moroder, C. Fink, and G. Wierer. Acquired femoral flexion deformity due to physeal injury during medial patellofemoral ligament reconstruction. *The Knee*, 24(3):680–685, 2017.

[141] Y.-J. Seo, S. Y. Song, I. S. Kim, M. J. Seo, Y. S. Kim, and Y.-S. Yoo. Graft tension of the posterior cruciate ligament using a finite element model. *Knee Surgery, Sports Traumatology, Arthroscopy*, 22(9):2057–2063, 2014.

[142] E. Servien, B. Fritsch, S. Lustig, G. Demey, R. Debarge, C. Lapra, and P. Neyret. In vivo positioning analysis of medial patellofemoral ligament reconstruction. *The American Journal of Sports Medicine*, 39(1):134–139, 2011.

[143] K. S. Shah, A. Saranathan, B. Koya, and J. J. Elias. Finite element analysis to characterize how varying patellar loading influences pressure applied to cartilage: model evaluation. *Computer Methods in Biomechanics and Biomedical Engineering*, 18(14):1509–1515, 2015.

[144] F. H. Shen, M. Harper, W. C. Foster, I. Marks, and V. Arlet. A novel "four-rod technique" for lumbo-pelvic reconstruction: theory and technical considerations. *Spine*, 31(12):1395–1401, 2006.

[145] D. Shepherd and B. Seedhom. The'instantaneous' compressive modulus of human articular cartilage in joints of the lower limb. *Rheumatology (Oxford, England)*, 38(2):124–132, 1999.

[146] B. J. Shore and D. E. Kramer. Management of syndesmotic ankle injuries in children and adolescents. *Journal of Pediatric Orthopaedics*, 36:S11–S14, 2016.

[147] C. Smirk and H. Morris. The anatomy and reconstruction of the medial patellofemoral ligament. *The Knee*, 10(3):221–227, 2003.

[148] J. M. Stephen, D. Kaider, P. Lumpaopong, D. J. Deehan, and A. A. Amis. The effect of femoral tunnel position and graft tension on patellar contact mechanics and kinematics after medial patellofemoral ligament reconstruction. *The American Journal of Sports Medicine*, 42(2):364–372, 2014.

[149] J. M. Stephen, C. Kittl, A. Williams, S. Zaffagnini, G. M. Marcheggiani Muccioli, C. Fink, and A. A. Amis. Effect of medial patellofemoral ligament reconstruction method on patellofemoral contact pressures and kinematics. *The American Journal of Sports Medicine*, 44(5):1186–1194, 2016.

[150] K. Stuart and V. K. Panchbhavi. The fate of syndesmotic screws. *Foot & Ankle International*, 32(5):519–525, 2011.

[151] R. Sunyer, V. Conte, J. Escribano, A. Elosegui-Artola, A. Labernadie, L. Valon, D. Navajas, J. M. García-Aznar, J. J. Muñoz, P. Roca-Cusachs, et al. Collective cell durotaxis emerges from long-range intercellular force transmission. *Science*, 353(6304):1157–1161, 2016.

[152] J. Tan, J. Xu, R. G. Xie, A. D. Deng, and J. B. Tang. In vivo length and changes of ligaments stabilizing the thumb carpometacarpal joint. *The Journal of Hand Surgery*, 36(3):420–427, 2011.

[153] M. J. Tanaka, J. Chahla, J. Farr, R. F. LaPrade, E. A. Arendt, V. Sanchis-Alfonso, W. R. Post, and J. P. Fulkerson. Recognition of evolving medial patellofemoral anatomy provides insight for reconstruction. *Knee Surgery, Sports Traumatology, Arthroscopy*, 27(8):2537–2550, 2019.

[154] M. J. Tanaka, A. Voss, and J. P. Fulkerson. The anatomic midpoint of the attachment of the medial patellofemoral complex. *Journal of Bone and Joint Surgery*, 98(14):1199–1205, 2016.

[155] H. Tanino, M. K. Harman, S. A. Banks, and W. A. Hodge. Association between dislocation, impingement, and articular geometry in retrieved acetabular polyethylene cups. *Journal of Orthopaedic Research*, 25(11):1401–1407, 2007.

[156] R. A. Teitge and R. Torga-Spak. Medial patellofemoral ligament reconstruction. *Orthopedics*, 27(10):1037–1040, 2004.

[157] A. R. Teles, D. Yavin, C. P. Zafeiris, K. C. Thomas, P. Lewkonia, F. H. Nicholls, G. Swamy, and W. B. Jacobs. Fractures after removal of spinal instrumentation: revisiting the stress-shielding effect of instrumentation in spine fusion. *World Neurosurgery*, 116:e1137–e1143, 2018.

[158] A. Templier, L. Denninger, C. Mazel, F. Lavaste, and W. Skalli. Comparison between two different concepts of lumbar posterior osteosynthesis implants a finite-element analysis. *European Journal of Orthopaedic Surgery & Traumatology*, 8(1):27–36, 1998.

[159] A. Terrier, A. Latypova, M. Guillemin, V. Parvex, and O. Guyen. Dual mobility cups provide biomechanical advantages in situations at risk for dislocation: a finite element analysis. *International Orthopaedics*, 41(3):551–556, 2017.

[160] T. Tezuka, N. D. Heckmann, R. J. Bodner, and L. D. Dorr. Functional safe zone is superior to the lewinnek safe zone for total hip arthroplasty: why the lewinnek safe zone is not always predictive of stability. *The Journal of Arthroplasty*, 34(1):3–8, 2019.

[161] M. C. Thompson and D. S. Gesink. Biomechanical comparison of syndesmosis fixation with 3.5-and 4.5-millimeter stainless steel screws. *Foot & Ankle International*, 21(9):736–741, 2000.

[162] M. Tizzoni, P. Bajardi, C. Poletto, J. J. Ramasco, D. Balcan, B. Gonçalves, N. Perra, V. Colizza, and A. Vespignani. Real-time numerical forecast of global epidemic spreading: case study of 2009 a/h1n1pdm. *BMC Medicine*, 10(1):165, 2012.

[163] F. Tomé-Bermejo, A. R. Piñera, and L. Alvarez. Osteoporosis and the management of spinal degenerative disease (ii). *Archives of Bone and Joint Surgery*, 5(6):363, 2017.

[164] T. J. Van Heest and P. M. Lafferty. Injuries to the ankle syndesmosis. *Journal of Bone and Joint Surgery*, 96(7):603–613, 2014.

[165] O. Verim, M. S. Er, L. Altinel, and S. Tasgetiren. Biomechanical evaluation of syndesmotic screw position: a finite-element analysis. *Journal of Orthopaedic Trauma*, 28(4):210–215, 2014.

[166] J. Vieira, J. Amorim, L. Martí-Bonmatí, Á. Alberich-Bayarri, and M. França. Quantifying steatosis in the liver and pancreas with mri in patients with chronic liver disease. *Radiologia*, 2020.

[167] C. Voigt, C. Klöhn, R. Bader, G. von Salis-Soglio, and R. Scholz. Finite element analysis of shear stresses at the implant-bone interface of an acetabular press-fit cup during impingement/finite-elemente-berechnung der schubspannungen im implantat-knochen-interface einer acetabulären press-fit-pfanne bei impingement. *Biomedical Engineering/Biomedizinische Technik*, 52(2):208–215, 2007.

[168] M. L. Vopat, B. G. Vopat, B. Lubberts, and C. W. DiGiovanni. Current trends in the diagnosis and management of syndesmotic injury. *Current Reviews in Musculoskeletal Medicine*, 10(1):94–103, 2017.

[169] T. Wang, Z. Cai, Y. Zhao, G. Zheng, W. Wang, D. Qi, D. Song, and Y. Wang. Development of a three-dimensional finite element model of thoracolumbar kyphotic deformity following vertebral column decancellation. *Applied Bionics and Biomechanics*, 2019, 2019.

[170] W. Wang, G. R. Baran, H. Garg, R. R. Betz, M. Moumene, and P. J. Cahill. The benefits of cement augmentation of pedicle screw fixation are increased in osteoporotic bone: a finite element analysis. *Spine Deformity*, 2(4):248–259, 2014.

[171] N. A. D. Watson, K. R. Duchman, M. J. Bollier, and N. M. Grosland. A finite element analysis of medial patellofemoral ligament reconstruction. *The Iowa Orthopaedic Journal*, 35:13, 2015.

[172] J. M. Weinberger, P. D. Fabricant, S. A. Taylor, J. Y. Mei, and K. J. Jones. Influence of graft source and configuration on revision rate and patient-reported outcomes after mpfl reconstruction: a systematic review and meta-analysis. *Knee Surgery, Sports Traumatology, Arthroscopy*, 25(8):2511–2519, 2017.

[173] J. W. Wekezer, M. S. Oskard, R. W. Logan, and E. Zywicz. Vehicle impact simulation. *Journal of Transportation Engineering*, 119(4):598–617, 1993.

[174] R. W. Westermann, C. Rungprai, J. E. Goetz, J. Femino, A. Amendola, and P. Phisitkul. The effect of suture-button fixation on simulated syndesmotic malreduction: a cadaveric study. *Journal of Bone and Joint Surgery*, 96(20):1732–1738, 2014.

[175] L. Xie, H. Xie, J. Wang, C. Chen, C. Zhang, H. Chen, and W. Zheng. Comparison of suture button fixation and syndesmotic screw fixation in the treatment of distal tibiofibular syndesmosis injury: A systematic review and meta-analysis. *International Journal of Surgery*, 60:120–131, 2018.

[176] M. Xu, J. Yang, I. H. Lieberman, and R. Haddas. Lumbar spine finite element model for healthy subjects: development and validation. *Computer Methods in Biomechanics and Biomedical Engineering*, 20(1):1–15, 2017.

[177] R. Yang, N. Wang, C. Tho, J. Bobineau, and B. Wang. Metamodeling development for vehicle frontal impact simulation. *Journal of Mechanical Design*, 127(5):1014–1020, 2005.

[178] C. P. Yuen and T. H. Lui. Suppl-4, m7: Distal tibiofibular syndesmosis: Anatomy, biomechanics, injury and management. *The Open Orthopaedics Journal*, 11:670, 2017.

[179] H. Zhang and W. Zhu. The path to deliver the most realistic follower load for a lumbar spine in standing posture: A finite element study. *Journal of Biomechanical Engineering*, 141(3), 2019.

[180] P. Zhang, Y. Liang, J. He, Y. Fang, P. Chen, and J. Wang. A systematic review of suture-button versus syndesmotic screw in the treatment of distal tibiofibular syndesmosis injury. *BMC Musculoskeletal Disorders*, 18(1):1–12, 2017.

[181] Y. Zhao, S. Zhang, T. Sun, D. Wang, W. Lian, J. Tan, and D. Zou. Mechanical comparison between lengthened and short sacroiliac screws in sacral fracture fixation: a finite element analysis. *Orthopaedics & Traumatology: Surgery & Research*, 99(5):601–606, 2013.

[182] Q.-k. Zhou, F.-h. Zeng, J.-l. Tu, Z.-q. Dong, and Z.-H. Ding. Influence of cement-augmented pedicle screw instrumentation in an osteoporotic lumbosacral spine over the adjacent segments: a 3d finite element study. *Journal of Orthopaedic Surgery and Research*, 15:1–8, 2020.